Jonas Tøgersen Kjellstadli

Local versus Equal Load Sharing in the Fiber Bundle Model

Jonas Tøgersen Kjellstadli

Doctoral Thesis

NTNU
Norwegian University of
Science and Technology
Faculty of Natural Sciences
Department of Physics

NTNU
Norwegian University of
Science and Technology

NTNU

NTNU
Norwegian University of
Science and Technology

Jonas Tøgersen Kjellstadli

Local versus Equal Load Sharing in the Fiber Bundle Model

Thesis for the degree of Philosophiae Doctor

Trondheim, December 2019

Norwegian University of Science and Technology
Faculty of Natural Sciences
Department of Physics

NTNU
Norwegian University of
Science and Technology

Abstract

This thesis studies fracture phenomena with the fiber bundle model, a heavily simplified model used to analyze various aspects of fracture processes. In the equal load sharing variant of the model, energy concepts are introduced and an exact result and asymptotic series expansion of the burst size distribution is calculated. In the local load sharing variant of the model, we investigate two different effects related to the stability of the model.

In addition, I present a generalization of an earlier result for the first burst in the equal load sharing model, and a possible generalization of the local load sharing model. Both of these results are previously unpublished.

Article I: We consider the Equal-Load-Sharing Fiber Bundle Model as a model for composite materials under stress and derive elastic energy and damage energy as a function of strain. With gradual increase of stress (or strain) the bundle approaches a catastrophic failure point where the elastic energy is always larger than the damage energy. We observe that elastic energy has a maximum that appears after the catastrophic failure point is passed, i.e., in the unstable phase of the system. However, the slope of elastic energy vs. strain curve has a maximum which always appears before the catastrophic failure point and therefore this can be used as a reliable signal of upcoming catastrophic failure. We study this behavior analytically for power-law type and Weibull type distributions of fiber thresholds and compare the results with numerical simulations on a single bundle with large number of fibers.

Article II: We derive an asymptotic series expansion for the burst size distribution in the equal load sharing fiber bundle model, a predominant model for breakdown in disordered media. Earlier calculations give expressions with correct asymptotic behavior for large bursts, but low accuracy for small bursts, up to an order of magnitude off. The approximations from the expansion we present here give relative errors of only a few percent when compared with results for infinite system sizes. We also solve the burst size distribution exactly for the Weibull threshold distributions.

Article III: By comparing the evolution of the local and equal load sharing fiber bundle models, we point out the paradoxical result that stresses seem to make the local load sharing model stable when the equal load sharing model is not. We explain this behavior by demonstrating that it is only an *apparent stability* in the local load sharing model, which originates from a statistical effect due to sample averaging. Even though we use the fiber bundle model to demonstrate the apparent stability, we argue that it is a more general feature of fracture processes.

Article IV: We use the local load sharing fiber bundle model to demonstrate a shielding effect where strong fibers protect weaker ones. This effect exists due to the local stress enhancement around broken fibers in the local load sharing model, and it is therefore not present in the equal load sharing model. The shielding effect is only prominent after the initial disorder-driven part of the fracture process has finished, and if the fiber bundle has not reached catastrophic failure by this point, then the shielding increases the critical damage of the system, compared to equal load sharing. In this sense, the local stress enhancement may make the fracture process more stable, but at the cost of reduced critical force.

List of Articles

   I. S. Pradhan, J. T. Kjellstadli, and A. Hansen,
Variation of Elastic Energy Shows Reliable Signal of Upcoming Catastrophic Failure,
Frontiers in Physics **7**:106 (2019).

  II. J. T. Kjellstadli,
Burst Distribution for Small Bursts by Asymptotic Expansion in the Fiber Bundle Model,
Submitted to Frontiers in Physics.

III. J. T. Kjellstadli, E. Bering, M. Hendrick, S. Pradhan, and A. Hansen,
Can Local Stress Enhancement Induce Stability in Fracture Processes? Part I: Apparent Stability,
Frontiers in Physics **7**:105 (2019).

IV. J. T. Kjellstadli, E. Bering, S. Pradhan, and A. Hansen,
Can Local Stress Enhancement Induce Stability in Fracture Processes? Part II: The Shielding Effect,
Accepted in Frontiers in Physics.

Contribution to Articles

Article I: *Variation of Elastic Energy Shows Reliable Signal of Upcoming Catastrophic Failure*
I did the derivations for a general threshold distribution in the appendix, and contributed to writing and editing of the article.

Article II: *Burst Distribution for Small Bursts by Asymptotic Expansion in the Fiber Bundle Model*
I did the theoretical derivations, the simulations, and wrote the article. Alex Hansen suggested to look for an exact solution and assisted me in writing the abstract, introduction and conclusion.

Article III: *Can Local Stress Enhancement Induce Stability in Fracture Processes? Part I: Apparent Stability*
I contributed to the original idea and interpretation of the results. I also did the simulations and data analysis, and wrote the first draft of the manuscript.

Article IV: *Can Local Stress Enhancement Induce Stability in Fracture Processes? Part II: The Shielding Effect*
I contributed to the original idea and interpretation of the results. I also did the simulations and data analysis, and wrote the first draft of the manuscript.

Acknowledgments

"Jo mer du vet, jo mer vet du at du ikke vet."
Norwegian original

"The more you know, the more you realize how little you know."
English translation

<div align="right">TORSTEIN RIBE</div>

The above quote from my former teacher has always fascinated me. The words have rung true ever since I first heard them, through middle school, high school, the university, and, most recently, throughout my time as a PhD student. They eloquently encapsulate both the importance of acknowledging ignorance [1] and how learning is a neverending process.

As a PhD student, my knowledge has grown, and my ignorance has seemingly increased even more. For every explanation found, new (and hitherto unanswered) questions have emerged. There are many I would like to thank for supporting me through this journey of discovery:

My supervisor, Professor Alex Hansen, for embodying the scientific process. Every idea is heavily scrutinized; the bad ones are swiftly and efficiently weeded out, while the good ones prevail. There have been many bad ideas — they don't show up in this thesis — but only a few good ones. Without you I wouldn't have gotten around to the good ideas.

Everyone in PoreLab, for providing a great environment in which to work and learn. You've made me realize how little I know about fluid flow and porous media.

The fiber bundle group — Alex Hansen, Srutarshi Pradhan, Eivind Bering, Martin Hendrick, and Subhadeep Roy — for making science fun. Our meetings were immensely motivating, because the most exciting part of my research was discussing new (and sometimes old) ideas with you.

NTNUI Innebandy — my de facto family in Trondheim — for providing much-needed relief via activities besides research. When nothing was working out, there were always practices, matches and parties together with great people to look forward to.

My family, for believing in me even when I didn't. When none of your ideas

seem to work, it helps to know that someone thinks it's going to turn around soon.

You, dear reader, for spending your valuable time reading these words. Perhaps this thesis helps you learn something new. Perhaps it helps you realize how little we all know. If it does, I will consider it a success.

<div align="right">

Jonas Tøgersen Kjellstadli
Trondheim, September 2019

</div>

Contents

1   Introduction

"A metaphorical model does not attempt to precisely describe reality, nor does it necessarily rely on very plausible assumptions. Rather, it aims to illustrate a non-trivial mechanism, the scope of which goes much beyond the specifics of the model itself." [2]

<div align="right">

JEAN-PHILIPPE BOUCHAUD

</div>

The fiber bundle model is not realistic, but it is incredibly useful. This may sound contradictory to some. How can a model be both unrealistic and useful? Because its purpose is to help us understand behavior qualitatively, not to give exact results.

1.1   The importance of simplified models

The archetypical example of a metaphorical model is the Ising model [3], which describes magnetism. The simplest version of the model, with no external magnetic field, isotropic interaction strength, and interactions between neighboring pairs of spins only, manages to capture the essence of the phase transition that magnetic materials undergo as the temperature changes.

Is it a realistic model for a real magnet? Not really. But that is precisely why it is so useful.

The model is simple enough to be solved analytically, and we can study the influence of its parameters without having to infer it from numerical solutions or experiments.

By removing complicating factors, we can see what behavior stems from the bare-bones mechanics of the model. This serves as both an expected qualitative behavior of magnetic systems, and a reference that more complex models can be compared with. It is reasonably simple to determine the influence of new mechanics (e.g. an external magnetic field) when we know how the model behaves without them. Conversely, inferring the general behavior of the bare-bones mechanics from hundreds or thousands of different results from more complex models is much more difficult.

Hence the Ising model contributes with an important understanding of *why* magnetism behaves the way it does, and provides a framework and key concepts that can be used to analyze experiments and more realistic models.

This use of simplified models to understand the general principles of a highly complex field is ubiquitous in physics [4], and is not limited to the Ising model in condensed matter physics. Thermodynamics has the ideal gas [5] and quantum mechanics uses the particle in a box [6]. And fracture has (among other models) the fiber bundle model.

1.2 Fracture

Humanity uses a huge variety of different materials, and the field of fracture is therefore correspondingly broad. It comprises engineering, materials science, geology, and physics. It covers rocks [7], metals [8], concrete [9], snow avalanches [10], earthquakes [11], glasses, and ceramics [12]. A review of the field is far outside the scope of this brief introduction; if you want to learn more, you should consult one of the numerous books on the subject, e.g. Ref. [13, 14].

But precisely because fracture is a wide and complicated field, simplified models are important for serving as references for experiments and more elaborate models, and for understanding universal behavior in fracture processes. This is where the fiber bundle model excels; with only the bare minimum of mechanics, it is able to describe some of the characteristic features of fracture.

1.3 Outline

Chapter 2 gives a short introduction to the fiber bundle model, both equal and local load sharing. Chapter 3 introduces energy concepts in the equal load sharing model and describes how they can potentially be used to predict failure. Chapter 4 presents several results about the burst size distribution in the equal load sharing model, with some of the lengthy proofs relegated to Appendix A. Chapter 5 deals with stability in the local load sharing model, while Chapter 6 describes a way to generalize the model.

2 The Fiber Bundle Model

This chapter is by no means a complete account of the fiber bundle model, but rather a brief introduction that covers some history and details of interest for this thesis. For a more thorough historical perspective and more detailed descriptions of the model and its applications, see e.g. Ref. [15, 16].

2.1 History

The fiber bundle model (FBM) began when Peirce made it to describe yarns as bundles of smaller fibers with individual strengths [17]. The next big step was the statistical treatment of the FBM done by Daniels in 1945 [18], where the effects of probability distributions of fiber strengths were analyzed. These inital works described the equal load sharing version of the model.

The fiber bundle model continued to be used by the materials science community, and in 1978 the local load sharing model was introduced to describe fibrous composite materials [19].

In 1989 the fiber bundle model was introduced to the physics community by Sornette [20]. Since then much research has been done on both the equal and local load sharing FBMs, and several models — like the γ-model [21] and the soft clamp model [22] — have been suggested as more realistic FBMs with intermediate interaction ranges.

2.2 The basics

A fiber bundle consists of N elastic fibers connected in parallel between two plates, see Figure 2.1. Each fiber i behaves as a Hookean spring until its elongation x reaches a threshold t_i, where it breaks. The stress-strain relation of a single fiber is hence

$$f_i = \begin{cases} \kappa x & \text{for } x < t_i \\ 0 & \text{for } x \geq t_i, \end{cases} \tag{2.1}$$

where f_i is the force acting on the fiber and κ is the fiber's elastic constant. The fibers are usually assumed to have identical elastic constants, which is commonly
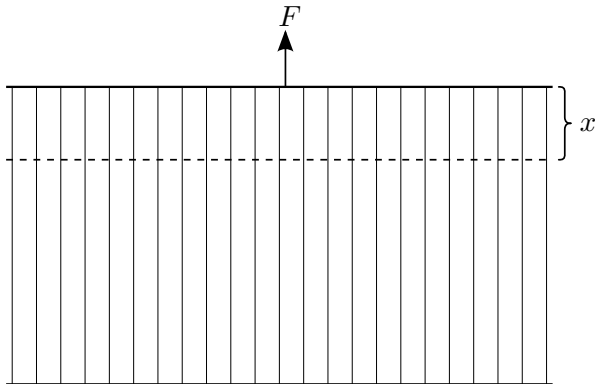
Figure 2.1: A fiber bundle: N elastic fibers are connected in parallel between two plates, and an external force F elongates the bundle a distance x.

set to $\kappa = 1$ for simplicity.

The fiber thresholds t_i are drawn from a probability distribution, denoted by the probability density $p(t)$ or the corresponding cumulative distribution $P(t) = \int_0^t \mathrm{d}t'\, p(t')$.

This threshold distribution needs experimental data to be determined for a particular application, otherwise it must be chosen somewhat arbitrarily. However, we are generally interested in studying properties and behaviors that are *universal* in the sense that they are common to large groups of threshold distributions. These universal properties are much more likely to be general features of fracture processes, which is what simplified models like the FBM excel at describing.

A fiber bundle is exposed to an externally applied force F, which is distributed on the intact fibers of the bundle. When no fibers are broken, the load is equal for all fibers, but what happens when fibers break? To determine this internal distribution of forces, a *load sharing rule* is needed.

2.3   Equal load sharing

In the equal load sharing (ELS) model, the force F is distributed equally on all intact fibers. This means that fibers fail in order of increasing thresholds t_i when the force is increased, which makes this version of the fiber bundle model amenable to analytic calculations.

The *load curve* — the macroscopic stress-strain relation for the entire fiber bundle — for the ELS model is

$$\sigma \equiv \frac{F}{N} = \kappa \left(1 - P(x)\right) x, \tag{2.2}$$

where σ is the applied force per fiber and x is the elongation of the bundle. Equivalently, this can be formulated in terms of the number of broken fibers k

or the damage $d = k/N$ as

$$\sigma = \kappa(1 - d)P^{-1}(d), \qquad (2.3)$$

since $d = P(x)$ — with an elongation x, all fibers with $t_i < x$ have broken, which gives a damage equal to the cumulative threshold distribution evaluated at x.

Equations (2.2) and (2.3) represent the behavior in the thermodynamic limit $N \to \infty$; for finite system sizes N there are fluctuations around this average behavior.

From Eq. (2.2) we can find the critical elongation x_c and the critical damage $d_c = P(x_c)$ where the bundle collapses by setting $\mathrm{d}\sigma/\mathrm{d}x|_{x=x_c} = 0$, which gives the condition

$$P(x_c) + x_c p(x_c) = 1. \qquad (2.4)$$

Once x_c is known, it is simple to calculate the critical strength σ_c of the fiber bundle via Eq. (2.2).

2.3.1   Burst size distribution

When a fiber breaks because the applied load elongates it past its threshold, the load it carried is redistributed onto other intact fibers. These additional loads can push other fibers past their breaking points, triggering an avalanche of fiber failures under a constant external force F.

The *burst size distribution* describes the distribution of these bursts of fiber ruptures. If Δ is the number of fibers that fail in a burst, we say that it is a burst of size Δ. The burst size distribution $D(\Delta)$ is the average number of bursts of size Δ that occurs when a fiber bundle breaks. Since this measure scales with the system size N, it is more convenient to work with $\bar{D}(\Delta) = D(\Delta)/N$, with the physical interpretation that $\Delta \bar{D}(\Delta)$ is the fraction of fibers that break in bursts of size Δ.

It has been shown [23] that

$$\bar{D}(\Delta) \sim C\Delta^{-5/2}\left(1 - \mathrm{e}^{-\Delta/\Delta_c}\right)$$
$$\propto \begin{cases} \Delta^{-3/2} & \text{for } \Delta \ll \Delta_c \\ \Delta^{-5/2} & \text{for } \Delta \gg \Delta_c \end{cases} \qquad (2.5)$$

in the limit $\Delta \to \infty$, where

$$C = \frac{x_c p(x_c)^2}{\sqrt{2\pi}\left[2p(x_c) + x_c p'(x_c)\right]}$$
$$\Delta_c = \frac{4\pi C^2}{p(x_c)^2\left(x_c - t_0\right)^2}, \qquad (2.6)$$

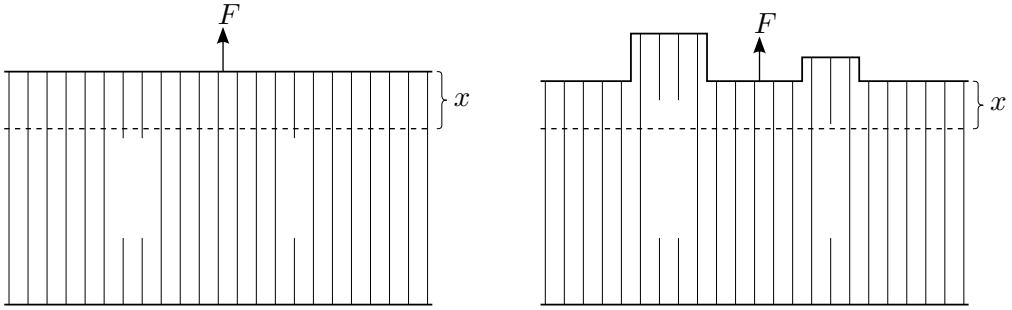and $t_0 \geq 0$ is the lower limit of the threshold distribution.

Figure 2.2: A one-dimensional fiber bundle with three broken fibers under a load F, shown with ELS (left) and LLS (right). With LLS, fibers that neighbor holes receive higher loads, but the other fibers receive smaller loads than they would have in the ELS model.

2.4   Local load sharing

In the local load sharing (LLS) model, the load that is redistributed when a fiber breaks is given to only its nearest neighbors. Since this means that fibers no longer carry the same loads (and hence no longer have the same elongations), the load curve of the LLS model cannot be represented by $\sigma(x)$ as in Eq. (2.2), and must instead be represented by $\sigma(d)$ as in Eq. (2.3).

The fact that fibers have different elongations also means that fibers no longer fail in order of increasing thresholds. This lack of orderly behavior makes the LLS model much more difficult to work with analytically than the ELS model. Most LLS results are therefore based on simulations rather than analytic calculations.

The LLS model was originally [19] defined on a one-dimensional lattice with periodic boundary conditions, see Figure 2.2 for an example. The burst distribution of this model is not a power law [24], unlike the ELS model. More importantly, the critical damage is $d_c = 0$ in the thermodynamic limit [16, 25]. However, the model can be generalized to an arbitrary lattice [26]:

Let a *hole* j be a set of h_j broken fibers joined by nearest neighbor connections of the underlying lattice. The hole has a *perimeter* of p_j intact fibers that are nearest neighbors of the hole. Every hole redistributes load — the load its fibers would have carried had they been intact — equally on the fibers in its perimeter. The force f_i on an intact fiber i is then

$$f_i = \sigma \left(1 + \sum_j \frac{h_j}{p_j} \right), \tag{2.7}$$

where the sum goes over all holes j that neighbor the fiber.

To figure out which fiber will break under the smallest load σ, we define an

effective threshold $t_{\text{eff},i}$ for each fiber i:

$$t_{\text{eff},i} = \frac{t_i}{1 + \sum_j \dfrac{h_j}{p_j}}. \tag{2.8}$$

By combining this expression with Eqs. (2.1) and (2.7) and the breaking criterion $f_i \geq \kappa t_i$ for a single fiber, we find the breaking criterion $\sigma \geq \kappa t_{\text{eff},i}$, which means that fibers break in order of increasing effective thresholds as the force increases. Unfortunately, the effective thresholds depend on the local hole structure of the fiber bundle, so the order of effective thresholds is dynamic amd changes as fibers break.

Importantly, the generalization of LLS to higher dimensions in Eq. (2.7) is stable in the sense that the critical damage is nonzero in the thermodynamic limit, which makes dimensions $D > 1$ much more interesting to study than the one-dimensional case.

This generalization of LLS to higher dimensions is not the only one possible — the soft membrane FBM [27] also reduces to LLS in one dimension — but it is the simplest one that ensures history independence of the distribution of forces.

2.4.1   History dependence

The original LLS model was *history independent* in the sense that the breaking order of the fibers doesn't affect the distribution of forces f_i on intact fibers, but not everyone has implemented LLS in this way. When a fiber breaks, some implementations (e.g. Ref. [28]) simply redistribute its load equally on its nearest intact neighbors. This is very efficient computationally, but leads to a model where the breaking order of the fibers affects how forces are distributed within the fiber bundle — the model is history dependent. (See e.g. Ref. [16, 29] for examples of how redistributing the forces in this way leads to history dependence.) Contrast this with the force distribution in Eq. (2.7), where the breaking order of fibers is irrelevant.

These two implementations of LLS give very different behavior for lattices with dimension $D > 1$. Compare, for instance, the results for the square lattice from Ref. [29] and [30], where e.g. σ_c differs greatly between the two implementations. I am not aware of any direct comparisons of history dependent and independent LLS in one dimension, but I expect the qualitative behavior to be the same, as the model has zero critical damage in both cases.

3 Energy and Predicting Failure

One of the holy grails of fracture is to predict when catastrophic failure is going to happen. For it to be useful, a prediction method must work with the limited information that is available from the system before the failure happens.

As such, Eq. (2.4) for finding x_c in the ELS model is not a useful prediction method because it requires information about the threshold distribution that cannot be measured before failure. To determine $P(t)$, we would need to measure both the force σ and the elongation x and then use Eq. (2.2). But to get the relevant information $(P(x_c))$ we would have to reach the critical point, and predicting it would be pointless.

But are there methods that can actually be used to predict when failure is going to happen in the ELS model? It turns out that the elastic energy of the fiber bundle may give a semi-accurate prediction method.

3.1   Elastic energy, damage energy, and work

The elastic energy E^e of a fiber bundle is simply the total elastic energy of all its constituent fibers. In the ELS model, they all share the same elongation x, and hence it can be written

$$\frac{E^e}{N} = \frac{\kappa}{2}(1-d)x^2, \tag{3.1}$$

where d is the damage the fiber bundle has sustained. If x is the largest elongation so far during the fracture process, the damage and elongation are connected via $d = P(x)$, and we can express the elastic energy as a function of either x or d alone.

The damage energy E^d is the dissipated energy from fiber failures, and can be calculated as

$$\frac{E^d}{N} = \frac{\kappa}{2} \int\limits_0^{P^{-1}(d)} \mathrm{d}x' \; p(x')x'^2. \tag{3.2}$$

This dissipated energy could be measured via acoustic emissions, like in rock fracturing experiments [31, 32].

The total work W done on the fiber bundle by the force F when the bundle is stretched from 0 to x can be found via Eq. (2.2):

$$\frac{W}{N} = \int\limits_0^x \mathrm{d}x' \; \sigma(x') = \kappa \int\limits_0^x \mathrm{d}x' \; x'(1 - P(x')), \tag{3.3}$$

which clearly separates into Eq. (3.1) and Eq. (3.2), i.e., $W = E^e + E^d$. This relation can be used to calculate the elastic energy if the work and damage energy are measured.

3.2   Elastic energy maximum

As seen from Eq. (3.1), the elastic energy must have a well-defined maximum at an elongation $x_m > 0$. By differentiation of Eq. (3.1) and some rewriting, we find that x_m must satisfy

$$\frac{1 - P(x_m)}{x_m p(x_m)} = \frac{1}{2}. \tag{3.4}$$

The left-hand side of this equation defines a function of the elongation, which can be rewritten as

$$\begin{aligned}
\frac{1 - P(x)}{xp(x)} &= \frac{1 - P(x)}{1 - P(x) - \frac{\mathrm{d}\sigma}{\mathrm{d}x}} \\
&= \begin{cases} > 1 & \text{for } \frac{\mathrm{d}\sigma}{\mathrm{d}x} > 0 \\ < 1 & \text{for } \frac{\mathrm{d}\sigma}{\mathrm{d}x} < 0 \end{cases}
\end{aligned} \tag{3.5}$$

by differentiation of Eq. (2.2).

If the load curve has only a single local maximum, then $\mathrm{d}\sigma/\mathrm{d}x > 0$ in the stable phase ($x < x_c$) and $\mathrm{d}\sigma/\mathrm{d}x < 0$ in the unstable phase ($x > x_c$). From the above equations we can then conclude that x_m must be in the unstable phase, i.e., $x_m > x_c$. Continuous measurements of the elastic energy to look for its maximum is hence not a suitable prediction method for failure of the fiber bundle.

3.3   Elastic energy inflection point

The maximum of E^e is not suitable for predicting failure, but what about the maximum of its derivative, located at the inflection point x_i? We know that $x_i < x_m$, but is it also smaller than x_c? If it is, and a relation between x_i and x_c can be found, then continuously measuring the elastic energy of the fiber bundle during the fracture process to look for its inflection point could be a useful prediction method for failure of the bundle.

Differentiating Eq. (3.1) twice and setting the derivative $\mathrm{d}^2 E^e/\mathrm{d}x^2 = 0$ at x_i leads to the condition

$$0 = 2(1 - P(x_i)) - 4x_i p(x_i) - x_i^2 p'(x_i), \tag{3.6}$$

or, equivalently,

$$\left.\frac{\mathrm{d}\sigma}{\mathrm{d}x}\right|_{x_i} = -\frac{x_i}{2} \left.\frac{\mathrm{d}^2\sigma}{\mathrm{d}x^2}\right|_{x_i}. \tag{3.7}$$

We have not found a general proof that $x_i < x_c$ from this condition, but it is true for all Weibull distributions $P(t) = 1 - \exp\left(-t^\beta\right)$ and power law distributions $P(t) = t^{\alpha+1}$, regardless of the shape parameters $\beta > 0$ and $\alpha \geq 0$. This indicates that x_i is commonly smaller than x_c.

Does this mean that the inflection point x_i can be used to predict failure? Unfortunately, trying to express the critical point as

$$x_c = C x_i \tag{3.8}$$

leads to a constant C that depends on the threshold distribution. However, the window $C \in [1.2, 1.5]$ covers a wide range of threshold distributions, and detecting x_i via elastic energy measurements can be seen as a precursor to failure, which is most likely to happen in the region $[1.2x_i, 1.5x_i]$.

So far we have discussed only the ELS model, but what about LLS? Here we must rely on simulations, since analytic calculations are impossible. The results so far indicate that the behavior of the LLS model depends more on the threshold distribution than the ELS model, which makes it harder to draw general conclusions.

4 Bursts

Bursts (also called avalanches) are an important part of the study of fiber bundles. They represent events of several fibers that break successively, and these events can be measured by acoustic emissions in experiments [31, 32]. Also, the distribution of these events changes when the ELS fiber bundle approaches the critical point, as shown by Eqs. (2.5) and (2.6). This transition has therefore been suggested as a possble way to predict failure of the bundle [33].

But Eq. (2.5) does not tell the whole story. It is only an asymptotic relation that is valid for very large (and hence rare) bursts. For smaller bursts, it can be very inaccurate. This is easily seen by calculating

$$\sum_{\Delta=1}^{\infty} \Delta \bar{D}(\Delta). \tag{4.1}$$

Since $\Delta \bar{D}(\Delta)$ is the fraction of fibers that break in bursts of size Δ (excluding the fatal burst when the bundle collapses), this sum should equal $P(x_c)$. For a uniform threshold distribution $P(t) = t$, we find that the sum is ≈ 0.246 via Eq. (2.5), whereas $P(x_c) = 1/2$. This discrepancy is a result of Eq. (2.5) being inaccurate for small Δ, which contribute the most to the sum in Eq. (4.1).

If the burst distribution is to be used to predict failure, it is better to rely on smaller and more common events, rather than the large and rare ones. This chapter therefore focuses on calculating small bursts more accurately for the ELS model. We do not investigate the LLS model, although it is possible to derive some analytic results about its burst distribution [24].

4.1 Exact solution

One can show that (to first order in N, i.e., in the limit $N \to \infty$) the ELS burst distribution is [34]

$$\bar{D}(\Delta) = \frac{\Delta^{\Delta-1}}{\Delta!} \int_{t_0}^{x_c} dt \left[a(t) e^{-a(t)} \right]^{\Delta} a(t)^{-1} \left[1 - a(t) \right] p(t), \tag{4.2}$$

with a lower limit $t_0 < x_c$ of the threshold distribution, and

$$a(t) = \frac{tp(t)}{1 - P(t)}.\tag{4.3}$$

Can Eq. (4.2) be solved exactly for some threshold distributions? Surprisingly, it can. For a Weibull distribution $P(t) = 1 - \mathrm{e}^{-t^\beta + t_0^\beta}$ $(t \geq t_0)$ — which gives $a(t) = \beta t^\beta$ — integration by parts and induction yields

$$\begin{aligned}
\bar{D}(\Delta) = {} & \frac{\Delta^{\Delta-1}\mathrm{e}^{t_0^\beta}}{\Delta!(\beta\Delta+1)}\left[\mathrm{e}^{-(\Delta+1/\beta)} - \left(\beta t_0^\beta\right)^\Delta \mathrm{e}^{-t_0^\beta(\beta\Delta+1)}\right] \\
& + \frac{(\beta\Delta)^{\Delta-1}\,\mathrm{e}^{-\beta\Delta t_0^\beta}}{\Delta(\beta\Delta+1)^{\Delta+1}}\sum_{i=0}^{\Delta-1}\frac{\left[(\beta\Delta+1)t_0^\beta\right]^i}{i!} \\
& - \frac{(\beta\Delta)^{\Delta-1}\,\mathrm{e}^{t_0^\beta-(\Delta+1/\beta)}}{\Delta(\beta\Delta+1)^{\Delta+1}}\sum_{i=0}^{\Delta-1}\frac{(\beta\Delta+1)^i}{i!\beta^i}.
\end{aligned}\tag{4.4}$$

This expression can easily be calculated for small Δ, which is what we want to describe accurately. For large bursts it is impractical to use, but then Eq. (2.5) is a good approximation and can be used instead. (Equation (4.4) reduces to Eq. (2.5) in the limit $\Delta \to \infty$.)

4.2 Asymptotic expansion

What about threshold distributions where the burst distribution cannot be solved exactly? Equation (4.2) can be formulated as a Laplace integral [35] where one can do an asymptotic series expansion in the limit $\Delta \to \infty$. This approach was used to derive Eq. (2.5), which is the first term of the series expansion.

But it is possible to derive a scheme for the full asymptotic expansion. The resulting series has the form

$$\begin{aligned}
\bar{D}(\Delta) \sim {} & \frac{\Delta^{\Delta-2}\mathrm{e}^{-\Delta}}{\Delta!}\Big(C_1(\Delta) + C_2(\Delta)\Delta^{-1/2} \\
& + C_3(\Delta)\Delta^{-1} + C_4(\Delta)\Delta^{-3/2} + \cdots\Big).
\end{aligned}\tag{4.5}$$

Unfortunately, the "coefficients" C_n depend on Δ because of the lower limit of integration in Eq. (4.2). Hence it is difficult to use this series to extract any general behavior of $\bar{D}(\Delta)$ as a function of Δ.

However, Eq. (4.5) can be used to calculate approximations to $\bar{D}(\Delta)$ for small Δ, where Eq. (2.5) is very inaccurate.

4.2.1 Optimal asymptotic approximation

In general, asymptotic series like Eq. (4.5) diverge for finite Δ. But one can find good approximations to the burst distribution for finite bursts by discarding the divergent part of the series expansion. The procedure for doing this summation is [35]:

Calculate the terms in the series and locate the smallest term in absolute value — let us call it m. Then sum all terms up to, but not including, the smallest term. The resulting approximation is

$$\bar{D}(\Delta) \approx \frac{\Delta^{\Delta-2}e^{-\Delta}}{\Delta!} \sum_{i=1}^{m-1} C_i(\Delta)\Delta^{-(i-1)/2}, \tag{4.6}$$

which is optimal in the sense that it gives us the smallest estimate of the error.

Equation (4.6) can hence give us approximations of the burst distribution for small bursts, even though Eq. (4.5) is valid only in the limit $\Delta \to \infty$ and (most likely) diverges for finite Δ.

In practice, one cannot calculate the entire infinite series to find the smallest term, so one must settle for calculating a certain number of terms and then finding the smallest among those. This term is not necessarily the smallest one in the entire series, in which case the accuracy of the approximation is reduced.

The exact result in Eq. (4.4) provides a perfect test case to assess the accuracy of Eq. (4.6). Both results are derived in the thermodynamic limit, and therefore do not contain finite size effects. The relative errors when using Eq. (4.6) (with 13 calculated terms for each value of Δ) to approximate the exact result is shown in Figure 4.1 for a Weibull threshold distribution with shape parameter $\beta = 1$.
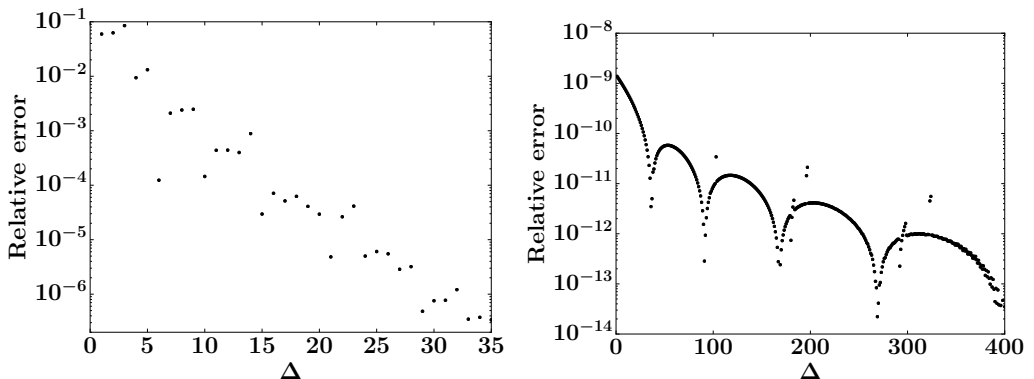

Figure 4.1: Relative errors when using Eq. (4.6) with 13 calculated terms to approximate the exact result for the ELS burst distribution with the Weibull threshold distribution. Left: $\beta = 1$ and $t_0 = 0$. Right: $\beta = 1$ and $t_0 = 0.8$.

When $t_0 = 0.8$, close to $x_c = 1$, the optimal approximation is very accurate.

The largest relative errors — for the smallest Δ, as one would intuitively expect — are of order 10^{-9}!

When $t_0 = 0$, the accuracy is much lower, with the largest relative errors of order 10%. The results indicate that the cause is that 13 terms is insufficient to find the smallest terms in the asymptotic series. However, this approximation is still much better than using Eq. (2.5), which is nearly an order of magnitude off for $\Delta = 1$.

In conclusion, the asymptotic expansion in Eq. (4.5) and the optimal approximation in Eq. (4.6) provide a framework for estimating the ELS burst distribution for small bursts when no exact results exist and Eq. (2.5) is not accurate enough.

4.3   The first burst

Instead of calculating the entire burst distribution during the breaking of a fiber bundle, we can focus on only the first burst. What is the probability $P_1(\Delta)$ that the first burst that occurs is of size Δ? For the special case $t_0 = x_c$, this has been shown [23] to be

$$P_1(\Delta) = \frac{e^{-\Delta}\Delta^{\Delta-1}}{\Delta!} \simeq \frac{1}{\sqrt{2\pi}}\Delta^{-3/2} \tag{4.7}$$

in the thermodynamic limit.

But this result can be generalized to an arbitrary lower limit t_0. The proof of this generalization is essentially identical to the original proof of Eq. (4.7), and is shown in Appendix A. The general expression is

$$P_1(\Delta) = [1 - r(t_0)]^{-1}\,e^{\Delta/\Delta_0(t_0)}\frac{e^{-\Delta}\Delta^{\Delta-1}}{\Delta!}$$
$$\simeq \frac{1}{\sqrt{2\pi}\,[1 - r(t_0)]}\Delta^{-3/2}e^{\Delta/\Delta_0(t_0)}, \tag{4.8}$$

where

$$r(t) = 1 - \frac{tp(t)}{1 - P(t)}, \tag{4.9}$$
$$1/\Delta_0(t) = r(t) + \ln\left(1 - r(t)\right).$$

For $t_0 = x_c$, we recover Eq. (4.7), since $r(x_c) = 0$ and hence $1/\Delta_0(x_c) = 0$. For other values of t_0, $\Delta_0(t_0) < 0$, and the power law observed when $t_0 = x_c$ is modified with an exponential decay. In Figure 4.2, Eq. (4.8) is compared with simulation results for a Weibull threshold distribution, with excellent agreement between the two.

Equation (4.8) should be properly normalized, and therefore one would intuitively expect that $\sum_{\Delta=1}^{\infty} P_1(\Delta) = 1$. This is indeed the case for $t_0 \le x_c$, but for $t_0 > x_c$ we find that

$$\sum_{\Delta=1}^{\infty} P_1(\Delta) = \frac{W_0\left((r(t_0) - 1)e^{r(t_0)-1}\right)}{r(t_0) - 1} < 1, \tag{4.10}$$
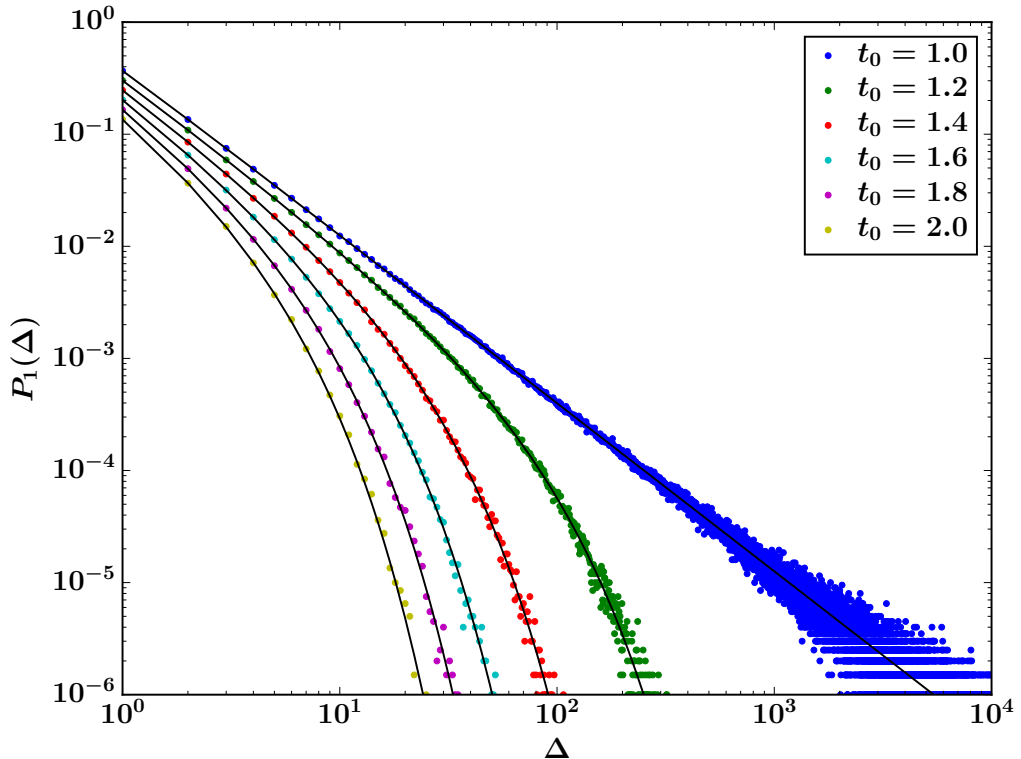
Figure 4.2: Probability distribution $P_1(\Delta)$ for the first burst with a Weibull threshold distribution with $\beta = 1$ and $t_0 \geq x_c = 1$. Colored circles are simulation results ($N = 10^6, 2 \times 10^6$ samples) and the black lines show Eq. (4.8) for the corresponding threshold distributions.

where W_0 is the principal branch of the Lambert W function, the inverse of the function $f(z) = ze^z$. When $t_0 > x_c$, we have $r(t_0) - 1 < -1$, and the principal branch W_0 provides the nontrivial, real solution of $We^W = (r(t_0) - 1)e^{r(t_0)-1}$. Calculating this normalization is rather lengthy, and the derivation is therefore relegated to Appendix A.

Why is $P_1(\Delta)$ not normalized so that it sums to one in this case? Because for $t_0 > x_c$, there is a nonzero probability that the first burst breaks the entire bundle: $P_1(\Delta = N) > 0$. The derivation of Eq. (4.8) requires that $\Delta \ll N$, which means that it does not include cases where $\Delta = N$.

This insight allows us to use Eq. (4.10) to calculate the probability of instant rupture of the fiber bundle when $t_0 > x_c$. This probability is simply the one that is "missing" from Eq. (4.10):

$$P_1(\Delta = N) = \begin{cases} 0 & \text{when } t_0 \leq x_c \\ 1 - \frac{W_0((r(t_0)-1)e^{r(t_0)-1})}{r(t_0)-1} & \text{when } t_0 > x_c. \end{cases} \tag{4.11}$$
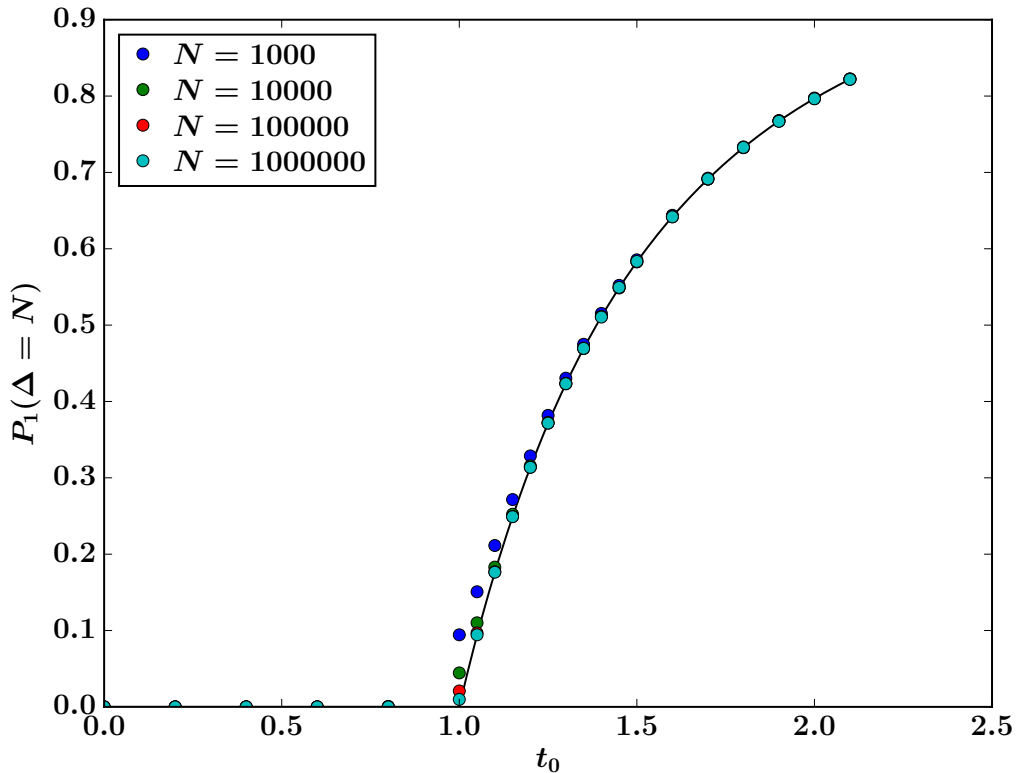
Figure 4.3: Probability $P_1(\Delta = N)$ that the first burst breaks the entire fiber bundle with a Weibull threshold distribution ($\beta = 1$, i.e., $x_c = 1$). Colored circles are simulation results, and the black line shows Eq. (4.11).

Equation (4.11) is compared with simulations for a Weibull threshold distribution in Figure 4.3. The agreement is excellent for large system sizes N, with clear finite size effects for smaller N, which indicates that Eq. (4.11) is indeed the correct expression in the thermodynamic limit.

5 Stability

Stability is easily defined for the ELS model. We can use Eq. (2.4) to find the critical elongation x_c. There is then a stable phase $x < x_c$ where the load σ must be increased to continue the fracture process, and an unstable phase $x > x_c$ where the load required to continue the fracture process decreases. (Some threshold distributions can complicate this picture [16, 24], but they are exceptions rather than the typical case.)

This simplicity is due to the lack of fluctuations in the ELS model in the thermodynamic limit. But what about the LLS model, where there are dynamics-dependent fluctuations that do not disappear in the thermodynamic limit?

The answer — but not the calculations that lead there — is relatively simple in one dimension [16, 25], where $d_c = 0$ in the thermodynamic limit. If $t_0 = 0$, Eq. (2.3) yields a critical strength $\sigma_c = 0$. The 1D LLS model is globally unstable and collapses once the elongation reaches the thresholds of the weakest fibers. But for dimensions $D > 1$ the LLS model can exhibit stable phases like the ELS model [16, 28–30], and the issue of stability is more complicated than in one dimension.

5.1 Apparent stability

An example of how fluctuations in the LLS model can seemingly affect stability is through the *apparent stability* where the LLS model looks locally stable even though it isn't. Figure 5.1 shows load curves for a Weibull threshold distribution with $\beta = t_0 = 1$. The ELS model is in this case unstable everywhere, since $t_0 = x_c$. The square lattice LLS model is also globally unstable, since the bundle breaks once the load σ reaches the thresholds of the weakest fibers. But it looks like there is a region where the LLS model is locally stable, i.e., the (sample averaged) load $\langle\sigma\rangle$ required to continue the fracture process increases.

We have previously interpreted this as a sign that the LLS model is locally stable in this region [29], and attributed this to the shielding effect [36] that is described later in this chapter. But this is wrong, because the LLS model is not locally stable in this case, it only appears to be due to how fluctuations affect the sample averaged load.

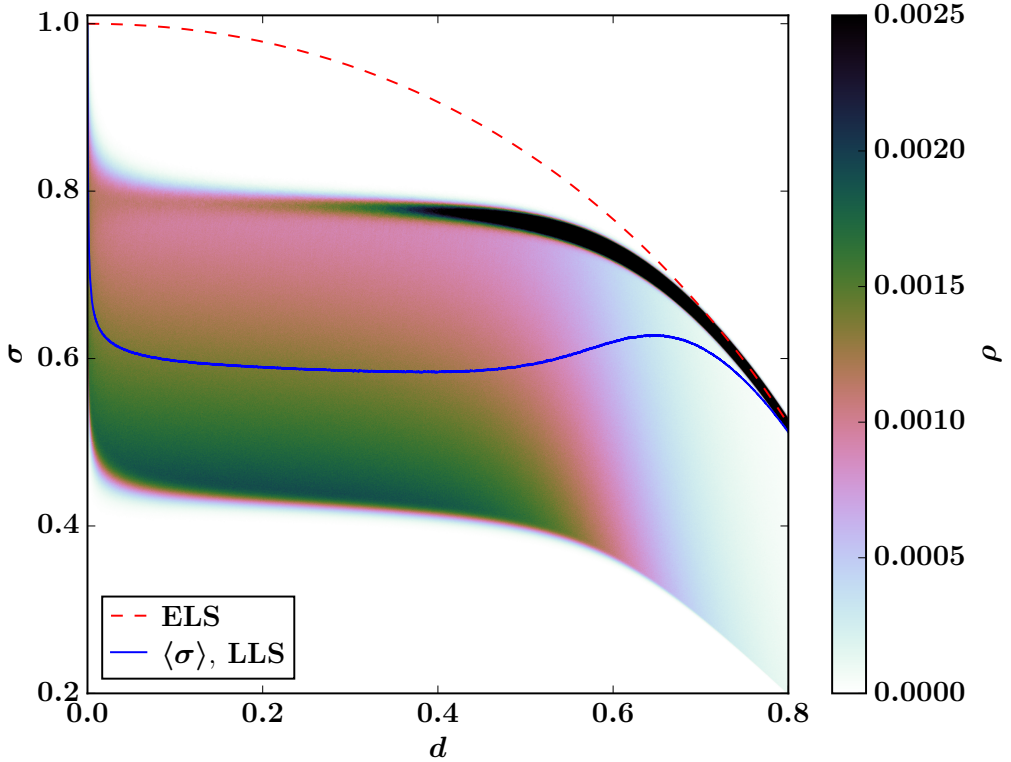The background of Figure 5.1 shows a color map of how the load curves of

Figure 5.1: Load curves for the ELS and LLS models with a Weibull threshold distribution $P(t) = 1 - \exp\left(-t + 1\right)$, $(\beta = t_0 = 1)$. The ELS curve is Eq. (2.3), whereas the LLS curve is a sample average from simulations on a square lattice $(N = 128^2)$. The background is a color map that shows the density ρ of single sample LLS load curves for the 1.5×10^5 samples that the average is based on. The color bar is capped at $\rho = 0.0025$ to highlight the fluctuations with the smallest values of σ.

individual samples are distributed for the LLS model, with big force differences between samples for the same damage d. These fluctuations (in the ensemble of individual samples) reveal that the increase in the averaged load $\langle \sigma \rangle$ as the damage increases does not happen because the LLS model is locally stable there; the average increases in a small region because the lower end of the fluctuations become much more rare there, but the upper end of the fluctuations still decreases.

The central issue is how one should define local stability in the LLS model. Because of the large fluctuations (even for forces required to break consecutive fibers in a single sample), we cannot use the approach of the ELS model. Instead, we can define small damage intervals $[d_i, d_{i+1}]$ for each sample, where $\Delta d = d_{i+1} - d_i$ is any small, but finite, number. To break the fibers in a given interval, we must break the strongest fiber there. Hence, we find the largest force $\sigma_{\max,i}$ in each

interval. If this sequence of forces increases somewhere — in the limit $N \to \infty$, where we have sufficiently many fibers in each interval for the variance of $\sigma_{\max,i}$ to be irrelevant — there is a local stability in that region. Since the upper limit of the color map in Figure 5.1, which can be used as a substitute for the sequence of maximum forces, decreases everywhere, there is no local stability in the LLS model either.

But if the LLS model is not stable, why is there an apparent stability where $\langle \sigma \rangle$ increases? The lower end of the force fluctuations happen because a fiber breaks, and the hole that grew "encounters" a new fiber with a small threshold that is added to its perimeter. The new fiber's effective threshold becomes even smaller (Eq. (2.8)), and the force required to break it is hence small. These events become much rarer when the perimeters of holes cover most of the intact fibers, which happens in a region around the percolation threshold[1] of the lattice. There is nothing special about the square lattice in this regard, and the apparent stability is visible for other lattices around their corresponding percolation thresholds, as shown in Figure 5.2.

This underlying cause is always present in the LLS model, but it doesn't necessarily result in an apparent stability. For many threshold distributions, the changing fluctuations aren't enough to make $\langle \sigma \rangle$ increase when the model is unstable.

5.2   The shielding effect

In the LLS model, intact fibers that neighbor holes carry larger forces than other fibers. Intuitively, one might expect that this local stress enhancement would make the LLS model less stable than the ELS model, but that is not always the case.

Stress enhancement somewhere also means stress *reduction* somewhere else. Figure 2.2 illustrates this for the one-dimensional LLS model; fibers that neighbor holes are loaded more than with ELS, but the other fibers are loaded slightly less. The other fibers are *shielded* from some of the load by the fibers that neighbor holes.

There are small pockets of weak fibers scattered throughout the fiber bundle, surrounded by stronger fibers that shield them from some of the external load. The shielding effect makes sure that these weak fibers survive longer in LLS than in ELS; at the same damage, the weakest intact fibers are weaker in LLS than in ELS, because slightly stronger fibers with smaller effective thresholds break in their stead. The effect is more pronounced in less connected, i.e., lower-dimensional, lattices, and its effects are therefore most easily noticed in two dimensions. (One dimension is, as usual, exceptional in the LLS model.)

The effects of shielding are significant only when the fracture process is no longer in the disorder-dominated regime — when Eq. (2.8) is dominated by the

---

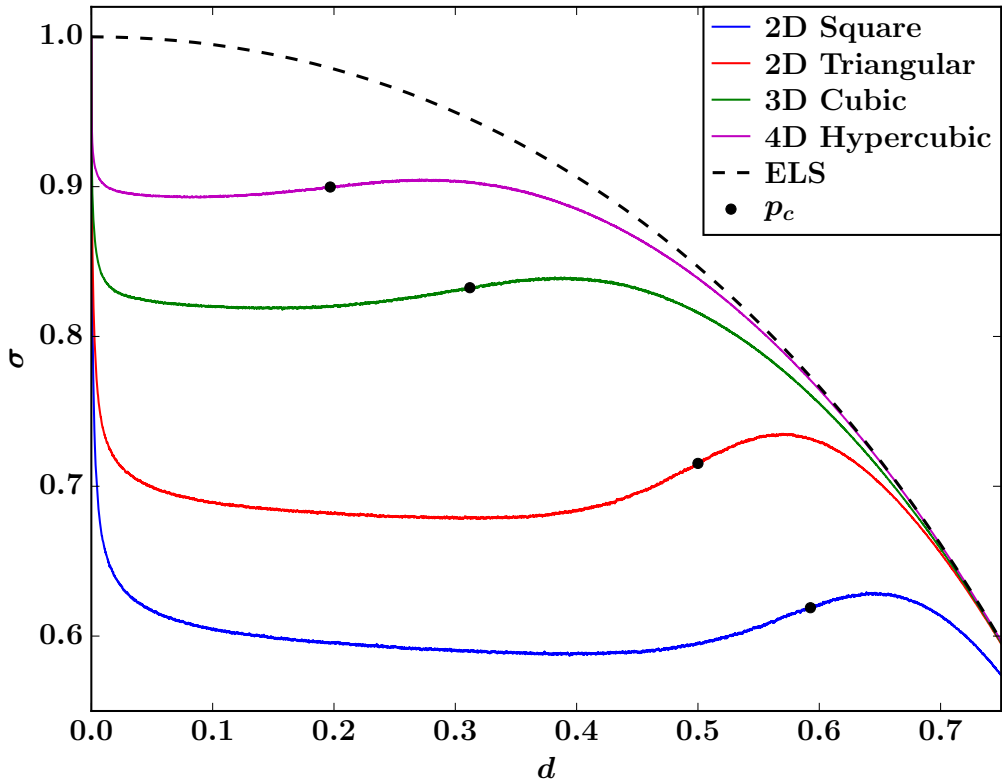[1] For more information about percolation theory, see e.g. Ref. [37].

Figure 5.2: Sample averaged LLS load curves for lattices in two to four dimensions with corresponding site percolation thresholds p_c indicated. The threshold distribution is $P(t) = 1 - \exp(1 - t)$, a Weibull distribution with $\beta = t_0 = 1$.

thresholds in the denominator — where ELS and LLS behave very similarly. In cases where the LLS model is stable long enough for the fracture process to leave the disorder-dominated regime, the shielding effect can actually make it more stable than the ELS model in terms of how much damage the fiber bundle can sustain before collapsing. However, this comes at the expense of the critical strength σ_c, which is smaller in the LLS model than in the ELS model due to the local stress enhancement.

With a uniform threshold distribution $P(t) = t$, the square lattice LLS model has a critical damage d_c that is roughly 5% larger than the corresponding ELS value $d_c = 1/2$. The critical strength is $\sigma_c \approx 0.233$, which is around 7% smaller than the ELS result $\sigma_c = 1/4$.

If the collapse happens in the disorder-dominated regime, then the local stress enhancement of LLS makes both d_c and σ_c smaller than in the ELS model. This is the case when $P(t) = t^2$, where the LLS model has $d_c < 0.2$ in the thermodynamic limit, whereas the ELS model is stable much longer, with $d_c = 1/3$.

6 Generalizing the LLS Model

The LLS model has been criticized for being unrealistic, because distributing forces equally on all perimeter fibers independently of hole shapes is not how real materials behave. As mentioned in the introduction, models that are simplified and sometimes unrealistic can be very useful, but we would like to compare them with more realistic models. Hence we want to create a generalization of the LLS model that can accomodate for more realistic ways of distributing forces on perimeter fibers.

If we insist that the model should be history independent, there are only a few things that the force distribution scheme can depend on: hole sizes, perimeter sizes and hole shapes. The first two are necessary to define an LLS model, and only the hole shapes can be used to generalize the model. But how? The shape of a hole contains a wealth of information that could potentially be used. This section will outline what I consider the simplest approach, which creates a model that can be applied to any connected network, just like regular LLS.

6.1 Link-distributed local load sharing

Let us define the link-distributed LLS model. The basics of the model are identical to regular LLS:

The model consists of N elastic fibers between two plates. A fiber i behaves as a Hookean spring with spring constant κ until its elongation x reaches its threshold t_i, where the fiber breaks. The stress-strain relation of fiber i is hence

$$f_i = \begin{cases} \kappa x & \text{while } x < t_i \\ 0 & \text{after } x \text{ reaches } t_i \end{cases}. \tag{6.1}$$

The set of thresholds $\{t_i\}$ is drawn from a probability density $p(t)$ with corresponding cumulative probability distribution $P(t) = \int_0^t \mathrm{d}u\, p(u)$. These thresholds are individual for each fiber, and the threshold distribution $P(t)$ is a parameter of the model.

A total force F can be exerted on the fiber bundle, and we define the force per

fiber as $\sigma = F/N$. The forces f_i on individual fibers must of course satisfy

$$F = N\sigma = \sum_i f_i, \tag{6.2}$$

where the sum can be restricted to intact fibers, since $f_i = 0$ for broken fibers.

Fibers are placed on a lattice in $D \geq 1$ dimensions with well-defined nearest neighbor connections. (This model will be identical to regular LLS in 1D, so $D > 1$ is the most interesting.) Let the connectivity — the number of nearest neighbors for each site — of the lattice be c.

Let a hole j be a set of broken fibers that are connected by nearest neighbor connections. The number of broken fibers that make up the hole is its size h_j, and the hole has a perimeter consisting of p_j neighboring intact fibers.

Let a *link* be a nearest neighbor connection from a hole to an intact fiber. A hole j then has L_j total links connecting it to intact fibers. Each of these fibers — which make up the perimeter of the hole — has at least one and at most (when it is completely surrounded by the hole) c links to the hole.

Denote the number of links between fiber i and hole j by l_{ij}. These numbers satisfy

$$\sum_{\langle i,j \rangle} l_{ij} = L_j, \tag{6.3}$$

where I have used the notation $\langle i, j \rangle$ for the set $\{$intact fiber $i | i$ neighbors hole $j\}$, i.e., all intact fibers i that neighbor the hole j. Similarly, $\langle j, i \rangle$ will mean the set of holes j that neighbor the intact fiber i.

With the above definitions we can now define a force distribution scheme. A hole j with size h_j has a total load σh_j (from its broken fibers) to distribute on its L_j links. We let a link between hole j and fiber i receive a fraction $g_j(l_{ij})$ of this total load. This means that the load distribution function g_j must satisfy the normalization condition

$$1 = \sum_{\langle i,j \rangle} l_{ij} g_j(l_{ij}) \tag{6.4}$$

for all holes j. The function g_j is another parameter of the link-distributed LLS model, in addition to the threshold distribution $P(t)$. For now we will keep g_j completely general, and investigate potential choices later.

A fiber i thus receives an additional load $\sigma h_j l_{ij} g_j(l_{ij})$ from a hole j, and we can write the total force acting on it as

$$f_i = \sigma \left(1 + \sum_{\langle j,i \rangle} h_j l_{ij} g_j(l_{ij}) \right), \tag{6.5}$$

This equation is similar to Eq. (2.7) for regular LLS, but it is more versatile because the function g_j can take many different forms.

With the force distribution from Eq. (6.5) in place, we define effective thresholds $t_{\text{eff},i}$ of the fibers as

$$t_{\text{eff},i} = \frac{t_i}{1 + \sum_{\langle j,i \rangle} h_j l_{ij} g_j(l_{ij})}, \tag{6.6}$$

analogous to Eq. (2.8) for regular LLS. Combining Eqs. (6.1), (6.5) and (6.6) gives the breaking criterion

$$\sigma = \kappa t_{\text{eff},i} \tag{6.7}$$

where the fiber with the smallest effective threshold breaks under the smallest load σ.

6.2 The load distribution function

The function g_j can take many different forms. Let us investigate a few possibilities.

6.2.1 Reproducing regular LLS

Is link-distributed LLS a generalization of the regular LLS model, i.e., can we find a function g_j that makes Eqs. (2.7) and (6.5) identical? Consider the function

$$g_j(l_{ij}) = (p_j l_{ij})^{-1}. \tag{6.8}$$

which satisfies the normalization condition in Eq. (6.4). Now insert this expression into Eq. (6.5). This yields

$$f_i = \sigma \left(1 + \sum_{\langle j,i \rangle} \frac{h_j}{p_j} \right), \tag{6.9}$$

which is exactly Eq. (2.7). It is therefore possible to reproduce regular LLS from link-distributed LLS by choosing the proper load distribution function g_j, and the model can be categorized as a generalization of regular LLS.

6.2.2 Equal load for each link

The simplest approach for the load distribution function would be to let each link get an equal share of the load that the hole redistributes. This would amount to a constant function

$$g_j = \frac{1}{L_j}. \tag{6.10}$$

Inserting this function into Eq. (6.5) gives the force distribution

$$f_i = \sigma \left(1 + \sum_{\langle j,i \rangle} h_j \frac{l_{ij}}{L_j} \right). \tag{6.11}$$

This model would incentivize the breaking of fibers with many links to holes, i.e., incentivize the creation of more compact holes than in regular LLS.

6.2.3   Crack tip stress enhancement

Can we use this model to mimic the stress enhancement that occurs around crack tips in real materials? (See e.g. Ref. [38] for some illustrations of how this stress enhancement can look for different crack geometries.) The best we can do would be to use a load distribution function

$$g_j(l_{ij}) = C_j l_{ij}^{-\alpha},\tag{6.12}$$

where C_j is a normalization constant and $\alpha > 1$, so that the total load given to a fiber is smaller the fewer links it has to a given hole. Inserting this into the normalization condition of Eq. (6.4) yields

$$C_j = \left(\sum_{\langle i,j \rangle} l_{ij}^{-\alpha+1} \right)^{-1}.\tag{6.13}$$

However, this would account for the number of links only, and not the general shape of holes. For instance, this model would not differentiate between a fiber at the end of a long, narrow hole and a fiber at the long edge of the hole if both of them have only one link to the hole.

A First Burst Derivations

We study the ELS model with a threshold distribution $P(t)$, $t > t_0$, with N total fibers. To derive the probability $P_1(\Delta)$ that the first burst that occurs is of size Δ, we follow the same procedure as Ref. [23], but with a general lower limit t_0 instead of the special case $t_0 = x_c$.

Let $\{t_k\}$ be the ordered sequence of fiber thresholds, so that $t_k \leq t_{k+1}$ for all allowed values of k. The force required to break fiber number k is then

$$F_k = \kappa t_k \left(N - k + 1 \right), \tag{A.1}$$

where we set $\kappa = 1$ for simplicity. From this equation we can calculate the difference between the forces required to break to consecutive fibers:

$$f_k \equiv F_{k+1} - F_k = (N - k)(t_{k+1} - t_k) - t_k. \tag{A.2}$$

Since the sequence $\{t_k\}$ is ordered, this force difference satisfies $f_k \geq -t_k$. The probability density ρ of these force differences is [16]

$$\rho\left(f_k\right) = \begin{cases} \frac{1-r(t_k)}{t_k} \exp\left[-\frac{1-r(t_k)}{t_k} \left(f_k + t_k \right) \right] & \text{for } f_k \geq -t_k \\ 0 & \text{for } f_k < -t_k, \end{cases} \tag{A.3}$$

in the limit $N - k \to \infty$, where

$$r(t) = 1 - \frac{tp(t)}{1 - P(t)}. \tag{A.4}$$

For the first burst that happens to be of size Δ, the forces F_k for $k = 2, 3, \cdots, \Delta+1$ must satisfy the following criteria: $F_1 \geq F_k$ for $2 \leq k \leq \Delta$ and $F_1 < F_{\Delta+1}$. In terms of the force differences f_k, this forward condition [34] can be written as

$$\sum_{k=1}^{j} f_k \leq 0 \qquad \text{for } j = 1, 2, \cdots, \Delta - 1$$

$$\sum_{k=1}^{\Delta} f_k > 0 \tag{A.5}$$

since $\sum_{k=1}^{j} f_k = F_{j+1} - F_1$. This can be reformulated to

$$f_1 \leq 0$$

$$f_j \leq -\sum_{k=1}^{j-1} f_k \qquad \text{for } j = 2, 3, \cdots, \Delta - 1$$

$$f_\Delta > -\sum_{k=1}^{\Delta-1} f_k \geq 0. \tag{A.6}$$

Note that $f_\Delta > 0$, as it must be when $F_{\Delta+1} > F_1 \geq F_\Delta$.

We can now express $P_1(\Delta)$ as

$$P_1(\Delta) = \int_{-\infty}^{0} \mathrm{d}f_1 \rho(f_1) \int_{-\infty}^{-f_1} \mathrm{d}f_2 \rho(f_2) \int_{-\infty}^{-f_1-f_2} \mathrm{d}f_3 \rho(f_3) \cdots$$

$$\times \int_{-\infty}^{-f_1-f_2-\cdots-f_{\Delta-2}} \mathrm{d}f_{\Delta-1} \rho(f_{\Delta-1}) \int_{-f_1-f_2-\cdots-f_{\Delta-1}}^{\infty} \mathrm{d}f_\Delta \rho(f_\Delta), \tag{A.7}$$

where the limits of the integrals come from the forward condition in Eq. (A.6). Since $\rho(f) = 0$ for $f < -t_0$, we can limit the integration limits even further,

$$P_1(\Delta) = \int_{-t_0}^{0} \mathrm{d}f_1 \rho(f_1) \int_{-t_0}^{-f_1} \mathrm{d}f_2 \rho(f_2) \int_{-t_0}^{-f_1-f_2} \mathrm{d}f_3 \rho(f_3) \cdots$$

$$\times \int_{-t_0}^{-f_1-f_2-\cdots-f_{\Delta-2}} \mathrm{d}f_{\Delta-1} \rho(f_{\Delta-1}) \int_{-f_1-f_2-\cdots-f_{\Delta-1}}^{\infty} \mathrm{d}f_\Delta \rho(f_\Delta). \tag{A.8}$$

Note that the innermost integral over f_Δ is not affected by this since the lower limit is positive, as shown in Eq. (A.6), and therefore larger than $-t_0 \leq 0$.

The probability densities for the force differences in these integrals are given by Eq. (A.3) when $N - k$ is sufficiently large. If we assume that $\Delta \ll N$, then the $\Delta + 1$ fibers with the smallest thresholds will all have thresholds very close to t_0. It is then a reasonable approximation to use Eq. (A.3) with $t_k = t_0$ as the probability density for all the differences f_k (with $k = 1, 2, \cdots, \Delta$) that are relevant for the forward condition.

With this approximation, the innermost integral is straightforward to calculate:

$$\int_{-f_1-f_2-\cdots-f_{\Delta-1}}^{\infty} \mathrm{d}f_\Delta \rho(f_\Delta) = \exp\left[r(t_0) - 1\right]$$

$$\times \exp\left[\frac{r(t_0) - 1}{t_0}(-f_1 - f_2 - \cdots - f_{\Delta-1})\right]. \tag{A.9}$$

When we insert this and Eq. (A.3) into the expression for P_1, we see that the f_k-dependence disappears from all the remaining integrands, the remainders of which can then be moved outside the integrals as common factors:

$$
P_1(\Delta) = (1 - r(t_0))^{\Delta-1} e^{\Delta(r(t_0)-1)} \int\limits_{-t_0}^{0} \frac{\mathrm{d}f_1}{t_0} \int\limits_{-t_0}^{-f_1} \frac{\mathrm{d}f_2}{t_0} \int\limits_{-t_0}^{-f_1-f_2} \frac{\mathrm{d}f_3}{t_0} \cdots
$$
$$
\times \int\limits_{-t_0}^{-f_1-f_2-\cdots-f_{\Delta-2}} \frac{\mathrm{d}f_{\Delta-1}}{t_0}.
$$

(A.10)

Now do the substitutions $z_k = f_k/t_0$, which simplifies the expression to

$$
P_1(\Delta) = (1 - r(t_0))^{\Delta-1} e^{\Delta(r(t_0)-1)} I,
$$

(A.11)

where we have designated the symbol I to represent the remaining integrals. In the appendix of Ref. [23] it is shown that

$$
I \equiv \int\limits_{-1}^{0} \mathrm{d}z_1 \int\limits_{-1}^{-z_1} \mathrm{d}z_2 \int\limits_{-1}^{-z_1-z_2} \mathrm{d}z_3 \cdots \int\limits_{-1}^{-z_1-z_2-\cdots-z_{\Delta-2}} \mathrm{d}z_{\Delta-1}
$$
$$
= \frac{\Delta^{\Delta-1}}{\Delta!},
$$

(A.12)

which we use together with Stirling's approximation $\Delta! \simeq \sqrt{2\pi\Delta}\,\Delta^{\Delta} e^{-\Delta}$ to further simplify our expression for $P_1(\Delta)$:

$$
P_1(\Delta) = [1 - r(t_0)]^{-1} e^{\Delta/\Delta_0(t_0)} \frac{e^{-\Delta}\Delta^{\Delta-1}}{\Delta!}
$$
$$
\simeq \frac{1}{\sqrt{2\pi}\,[1 - r(t_0)]} \Delta^{-3/2} e^{\Delta/\Delta_0(t_0)}.
$$

(A.13)

Here $1/\Delta_0(t) \equiv r(t) + \ln(1 - r(t))$. For $t_0 \neq x_c$ we have that $\Delta_0(t_0) < 0$, and hence there is an exponential decay with Δ that depends on the threshold distribution and t_0.

A.1 Normalization

Since P_1 is a probability, it should be properly normalized. To check the normalization, we calculate the sum

$$
S = \sum_{\Delta=1}^{\infty} P_1(\Delta)
$$
$$
= \sum_{\Delta=1}^{\infty} (1 - r(t_0))^{\Delta-1} e^{\Delta(r(t_0)-1)} \frac{\Delta^{\Delta-1}}{\Delta!}.
$$

(A.14)

We should expect that $S = 1$, but if that is not the case, then the sum could potentially depend on t_0: $S = S(t_0)$.

A.1.1 The Lagrange inversion theorem

To calculate the normalization of P_1 we will need the Lagrange inversion theorem. A special case of the theorem [39] can be stated as:

Let $g(z)$ and $\phi(z)$ be functions that are analytic on and inside a contour C in the complex plane that surrounds a point a. If λ is a number such that $|\lambda\phi(z)| < |z-a|$ for all points z on C, then the equation

$$\xi = a + \lambda\phi(\xi) \tag{A.15}$$

has a single solution ξ inside C, and one can also write

$$g(\xi) = g(a) + \sum_{k=1}^{\infty} \frac{\lambda^k}{k!} \left[\left(\frac{\partial}{\partial z}\right)^{k-1} \left(\phi(z)^k g'(z)\right) \right]_{z=a}. \tag{A.16}$$

If g is chosen to be the identity function, i.e., $g(z) = z$, then the analyticity of g is satisfied and the previous equation simplifies to

$$\xi = a + \sum_{k=1}^{\infty} \frac{\lambda^k}{k!} \left[\left(\frac{\partial}{\partial z}\right)^{k-1} \phi(z)^k \right]_{z=a}. \tag{A.17}$$

If we can show that Eq. (A.14) can be written in the form of Eq. (A.17) and that the conditions for the Lagrange theorem applies, then we can use the simpler Eq. (A.15) to calculate the normalization of P_1. We start by rewriting Eq. (A.14):

$$
\begin{aligned}
S &= \sum_{\Delta=1}^{\infty} (1 - r(t_0))^{\Delta-1} e^{\Delta(r(t_0)-1)} \frac{\Delta^{\Delta-1}}{\Delta!} \\
&= \sum_{\Delta=1}^{\infty} \frac{e^{\Delta(r(t_0)-1)}}{\Delta!} \left[\Delta\left(1 - r(t_0)\right)\right]^{\Delta-1} \\
&= \sum_{\Delta=1}^{\infty} \frac{\left(e^{r(t_0)-1}\right)^{\Delta}}{\Delta!} \left[\left(\frac{\partial}{\partial z}\right)^{\Delta-1} \left(e^{(1-r(t_0))z}\right)^{\Delta} \right]_{z=0}.
\end{aligned} \tag{A.18}
$$

This is exactly Eq. (A.17) with $\xi = S$, $a = 0$, $\lambda = e^{r(t_0)-1}$, and $\phi(z) = e^{(1-r(t_0))z}$.

Since ϕ is a simple exponential function, its analyticity is satisfied, and the only remaining criterion to satisfy is the contour C.

A.1.2 The contour condition

The contour condition from the Lagrange theorem is

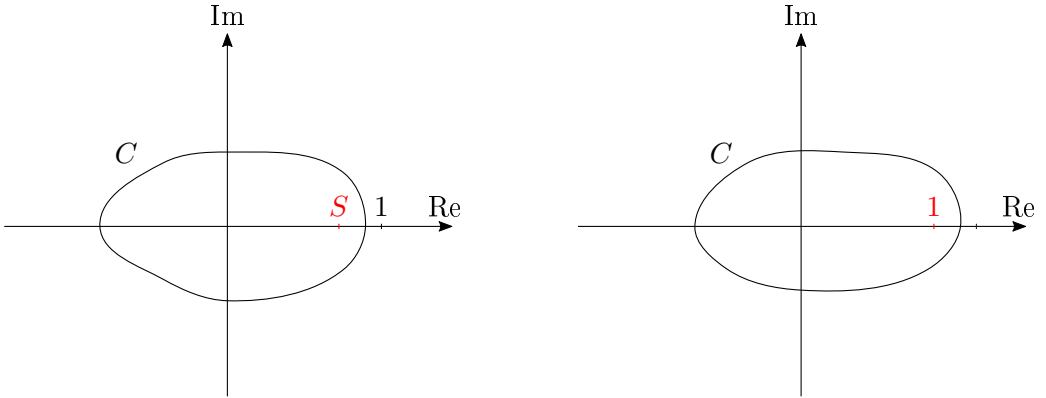$$e^{(1-r(t_0))(\mathrm{Re}(z)-1)} < |z| \tag{A.19}$$

Figure A.1: Sketches of contours C that can be used for the Lagrange theorem. The two real solutions of Eq. (A.20) are indicated on the real axis. For $t_0 > x_c$ (left) the contour contains the solution $S < 1$ (red), while for $t_0 < x_c$ (right) it contains $S = 1$ (red).

in our case. There are three different cases that we need to consider: $t_0 < x_c$, $t_0 = x_c$, and $t_0 > x_c$.

For $t_0 < x_c$, $1 \geq r(t_0) > 0$. The contour contition becomes $\exp(K(\text{Re}(z) - 1)) < |z|$, where K is a constant that satisfies $0 \leq K < 1$. (Equality when $t_0 = 0$, i.e. $r(t_0) = 1$.) For real z this is satisfied when z is sufficiently negative and slightly larger than 1. Hence, a contour C surrounding $a = 0$ can be found that crosses the real line infinitesimally higher than $z = 1$ and when z is sufficiently negative, as sketched in Figure A.1.

For $t_0 > x_c$, $r(t_0) < 0$. The contour condition becomes $\exp(K(\text{Re}(z)-1)) < |z|$ where $K > 1$ is a constant. This is satisfied for real z both when z is sufficiently negative and slightly smaller than 1. We can hence construct a contour C surrounding $a = 0$ as sketched in Figure A.1 that crosses the real line infinitesimally lower than $z = 1$ and when z is sufficiently negative.

For $t_0 = x_c$, $r(t_0) = 0$. The contour condition becomes $\exp(\text{Re}(z) - 1) < |z|$, which is not valid for nonnegative, real z. It is therefore impossible to find a contour C that encloses $a = 0$, and the Lagrange theorem cannot be applied to this case. This means that the derivation in Appendix A of Ref. [16] is incorrect, since it tries to use the Lagrange theorem in this case. However, the result is still correct. If the sum S exists (i.e., converges) in this case, it must be given by the limit $S(t_0 = x_c) = S(t_0 \to x_c^+) = S(t_0 \to x_c^-)$.

We have shown that we can apply the Lagrange theorem to our problem, and the remaining part is to solve Eq. (A.15) and find the solution that is enclosed in the contour C.

A.1.3 Calculating the sum

In our case, Eq. (A.15) becomes

$$Se^{(r(t_0)-1)S} = e^{r(t_0)-1}, \tag{A.20}$$

whose solutions S are given by the Lambert W function as

$$S = \frac{W\left((r(t_0)-1)e^{r(t_0)-1}\right)}{r(t_0)-1}. \tag{A.21}$$

There are infinitely many branches of W, but only two of them are real and candidates for our sum S. The first is the trivial $S = 1$. The other gives $S < 1$ when $t_0 > x_c$ and $S > 1$ when $t_0 < x_c$. These two branches are sketched in Figure A.1, from which we can deduce which branch is the correct one to use when calculating S.

For $t_0 < x_c$, the contour C encloses the trivial solution $S = 1$, and P_1 is properly normalized in this case.

For $t_0 > x_c$, the contour C encloses the nontrivial solution $S < 1$ given by the principal branch W_0 of the Lambert W function. Hence P_1 is not normalized so that it sums to one.

For $t_0 = x_c$ we cannot use the Lagrange theorem, but we can find the sum as the limit of the two previous cases: $S(t_0 = x_c) = S(t_0 \to x_c^+) = S(t_0 \to x_c^-) = 1$.

A.1.4 The missing probability

As we have shown, Eq. (A.13) for P_1 is nicely normalized so that $S = 1$ for $t_0 \leq x_c$. But why is that not the case for $t_0 > x_c$?

The derivation of Eq. (A.13) requires $\Delta \ll N$, meaning that it cannot account for cases where the first burst is of size N and breaks the entire fiber bundle. We can therefore interpret the missing probability in the normalization of Eq. (A.13) as the probability $P_1(\Delta = N)$, and we can calculate this probability via Eq. (A.21):

$$P_1(\Delta = N) = 1 - S = \begin{cases} 0 & \text{when } t_0 \leq x_c \\ 1 - \frac{W_0((r(t_0)-1)e^{r(t_0)-1})}{r(t_0)-1} & \text{when } t_0 > x_c. \end{cases} \tag{A.22}$$

References

[1]   Y. N. Harari. *Sapiens. A Brief History of Humankind*. 1st ed.
      New York: Harper, 2015. Chap. 14.

[2]   J.-P. Bouchaud. "Econophysics: still fringe after 30 years?"
      Europhysics News **50** (2019), pp. 24–27. DOI: 10.1051/epn/2019103.

[3]   W. Lenz. "Beiträge zum Verständnis der magnetischen Eigenschaften in
      festen Körpern". *Physikalische Zeitschrift* **21** (1920), pp. 613–615.

[4]   A. Hansen. "Grand challenges in interdisciplinary physics".
      Frontiers in Physics **2** (2014), p. 58. DOI: 10.3389/fphy.2014.00058.

[5]   C. Kittel and H. Kroemer. *Thermal Physics*. 2nd ed.
      New York: W. H. Freeman, 1980.

[6]   D. J. Griffiths. *Introduction to Quantum Mechanics*. 2nd ed.
      Harlow: Pearson, 2014.

[7]   B. K. Atkinson, T. Engelder, et al. *Fracture Mechanics of Rock*.
      Ed. by B. K. Atkinson. London: Academic Press, 1987.

[8]   B. Farahmand. *Fracture Mechanics of Metals, Composites, Welds, and
      Bolted Joints. Application of LEFM, EPFM, and FMDM Theory*.
      Boston: Springer, 2001.

[9]   A. DiTommaso, P. Jacquot, et al.
      Fracture mechanics of concrete: Material characterization and testing.
      Ed. by A. Carpinteri and A. R. Ingraffea. Dordrecht: Springer, 1984.

[10] I. Reiweger. "Failure of weak snow layers".
      PhD Thesis. Zürich: ETH Zürich, 2011.

[11] H. Kawamura, T. Hatano, et al.
      "Statistical physics of fracture, friction, and earthquakes".
      Rev. Mod. Phys. **84** (2012), pp. 839–884.
      DOI: 10.1103/RevModPhys.84.839.

[12] B. Lawn. *Fracture of brittle solids*. 2nd ed.
      Cambridge: Cambridge University Press, 1993.

[13] H. J. Herrmann, S. Roux, et al.
      Statistical Models for the Fracture of Disordered Media.
      Ed. by H. J. Herrmann and S. Roux. 1st ed.
      Amsterdam: North-Holland, 1990.

[14] S. Biswas, P. Ray, and B. K. Chakrabarti. *Statistical Physics of Fracture,
      Breakdown, and Earthquake. Effects of Disorder and Heterogeneity*. 1st ed.
      Berlin: Wiley-VCH, 2015.

[15] S. Pradhan, A. Hansen, and B. K. Chakrabarti.
      "Failure processes in elastic fiber bundles".
      Rev. Mod. Phys. **82** (2010), pp. 499–555.
      DOI: 10.1103/RevModPhys.82.499.

[16] A. Hansen, P. C. Hemmer, and S. Pradhan.
      The Fiber Bundle Model. Modeling Failure in Materials. 1st ed.
      Berlin: Wiley-VCH, 2015.

[17] F. T. Peirce. "32—X.—Tensile Tests for Cotton Yarns v.—"The Weakest
      Link" Theorems on the Strength of Long and of Composite Specimens".
      Journal of the Textile Institute Transactions **17** (1926), T355–T368.
      DOI: 10.1080/19447027.1926.10599953.

[18] H. E. Daniels.
      "The statistical theory of the strength of bundles of threads. I".
      *Proceedings of the Royal Society of London A: Mathematical, Physical and
      Engineering Sciences* **183** (1945), pp. 405–435.
      DOI: 10.1098/rspa.1945.0011.

[19] D. G. Harlow and S. L. Phoenix. "The Chain-of-Bundles Probability Model
      For the Strength of Fibrous Materials I: Analysis and Conjectures".
      Journal of Composite Materials **12** (1978), pp. 195–214.
      DOI: 10.1177/002199837801200207.

[20] D. Sornette. "Elasticity and failure of a set of elements loaded in parallel".
      Journal of Physics A: Mathematical and General **22** (1989),
      pp. L243–L250. DOI: 10.1088/0305-4470/22/6/010.

[21] R. C. Hidalgo, Y. Moreno, et al.
      "Fracture model with variable range of interaction".
      Phys. Rev. E **65** (2002), p. 046148. DOI: 10.1103/PhysRevE.65.046148.

[22] G. G. Batrouni, A. Hansen, and J. Schmittbuhl.
      "Heterogeneous interfacial failure between two elastic blocks".
      Phys. Rev. E **65** (2002), p. 036126. DOI: 10.1103/PhysRevE.65.036126.

[23] S. Pradhan, A. Hansen, and P. C. Hemmer.
      "Crossover behavior in failure avalanches".
      Phys. Rev. E **74** (2006), p. 016122. DOI: 10.1103/PhysRevE.74.016122.

[24] M. Kloster, A. Hansen, and P. C. Hemmer.
"Burst avalanches in solvable models of fibrous materials".
Phys. Rev. E **56** (1997), pp. 2615–2625. DOI: 10.1103/PhysRevE.56.2615.

[25] S. Zhang and E. Ding.
"Burst-size distribution in fiber-bundles with local load-sharing".
Physics Letters A **193** (1994), pp. 425–430.
DOI: 10.1016/0375-9601(94)90534-7.

[26] J. T. Kjellstadli. "Investigating the Local Load Sharing Fibre Bundle
Model in Higher Dimensions". Master's Thesis. Trondheim: Norwegian
University of Science and Technology, 2015.

[27] S. Patinet, D. Vandembroucq, et al. "Cracks in random brittle solids: From
fiber bundles to continuum mechanics".
The European Physical Journal Special Topics **223** (2014), pp. 2339–2351.
DOI: 10.1140/epjst/e2014-02268-9.

[28] F. Kun, S. Zapperi, and H. J. Herrmann. "Damage in fiber bundle models".
*The European Physical Journal B - Condensed Matter and Complex
Systems* **17** (2000), pp. 269–279. DOI: 10.1007/PL00011084.

[29] S. Sinha, J. T. Kjellstadli, and A. Hansen.
"Local load-sharing fiber bundle model in higher dimensions".
Phys. Rev. E **92** (2015), p. 020401. DOI: 10.1103/PhysRevE.92.020401.

[30] Z. Danku, G. Ódor, and F. Kun.
"Avalanche dynamics in higher-dimensional fiber bundle models".
Phys. Rev. E **98** (2018), p. 042126. DOI: 10.1103/PhysRevE.98.042126.

[31] D. J. Holcomb, C. M. Stone, and L. S. Costin.
"Combining acoustic emission locations and a microcrack damage model to
study development of damage in brittle materials". In: *Rock Mechanics
Contributions and Challenges. Proceedings of the 31st U.S. Symposium.*
(Golden, Colorado, June 18–20, 1990).
Ed. by W. A. Hustrulid and G. A. Johnson.
American Rock Mechanics Association. Rotterdam: A.A. Balkema, 1990,
pp. 645–652.

[32] P. Baud and P. G. Meredith. "Damage accumulation during triaxial creep
of darley dale sandstone from pore volumometry and acoustic emission".
International Journal of Rock Mechanics and Mining Sciences **34** (1997),
24.e1–24.e10. DOI: 10.1016/S1365-1609(97)00060-9.

[33] S. Pradhan, A. Hansen, and P. C. Hemmer.
"Crossover Behavior in Burst Avalanches: Signature of Imminent Failure".
Phys. Rev. Lett. **95** (2005), p. 125501.
DOI: 10.1103/PhysRevLett.95.125501.

[34] A. Hansen and P. C. Hemmer.
"The Distribution of Simultaneous Fiber Failures in Fiber Bundles".
Journal of Applied Mechanics **59** (1992), pp. 909–914.
DOI: 10.1115/1.2894060.

[35] C. M. Bender and S. A. Orszag. *Advanced Mathematical Methods for Scientists and Engineers. Asymptotic Methods and Perturbation Theory.*
New York: Springer, 1999.

[36] E. Bering.
"On the Stability of the Local Load Sharing Fiber Bundle Model". Master's Thesis. Trondheim: Norwegian University of Science and Technology, 2016.

[37] D. Stauffer and A. Aharony. *Introduction to Percolation Theory.* 2nd ed.
Boca Raton: CRC Press, 1994.

[38] M. Liu, Y. Gan, et al.
"An improved semi-analytical solution for stress at round-tip notches".
Engineering Fracture Mechanics **149** (2015), pp. 134–143.
DOI: 10.1016/j.engfracmech.2015.10.004.

[39] E. T. Whittaker and G. N. Watson. *A course of modern analysis.* 4th ed.
Cambridge: Cambridge University Press, 1996.

Articles

Article I

*Variation of Elastic Energy Shows Reliable Signal of
Upcoming Catastrophic Failure*

Article I

Variation of Elastic Energy Shows Reliable Signal of Upcoming Catastrophic Failure

Srutarshi Pradhan*, Jonas T. Kjellstadli and Alex Hansen

PoreLab, Department of Physics, Norwegian University of Science and Technology (NTNU), Trondheim, Norway

We consider the Equal-Load-Sharing Fiber Bundle Model as a model for composite materials under stress and derive elastic energy and damage energy as a function of strain. With gradual increase of stress (or strain) the bundle approaches a catastrophic failure point where the elastic energy is always larger than the damage energy. We observe that elastic energy has a maximum that appears after the catastrophic failure point is passed, i.e., in the unstable phase of the system. However, the slope of elastic energy vs. strain curve has a maximum which always appears before the catastrophic failure point and therefore this can be used as a reliable signal of upcoming catastrophic failure. We study this behavior analytically for power-law type and Weibull type distributions of fiber thresholds and compare the results with numerical simulations on a single bundle with large number of fibers.

Keywords: material failure, fiber bundle model, elastic energy, damage energy, catastrophic failure, reliable signal

1. INTRODUCTION

Accurate prediction of upcoming catastrophic failure events has important and far-reaching consequences. It is a central problem in material science in connection with the durability of composite materials under external stress [1–5]. The same problem exists at a large scale (field-scale) associated with mine and cave collapses, landslides, snow avalanches and the onset of earthquakes due to plate movements [6, 7]. In medical science, understanding fracturing of human bones exposed to a sudden stress is an important research area [8]. These phenomena belong to the class of phenomena called stress-induced fracturing, where initially micro-fractures are produced here and there in the system and at some point, due to gradual stress increase, a major fracture develops through coalescence of micro-fractures and the whole system collapses (catastrophic event). Such stress-induced failures occur also in very different domains—for example, in breakdown of social relationships and mental health [9, 10].

The central question is—when does the catastrophic failure occur? Is there any prior signature that can tell us whether catastrophic failure is imminent? The inherent heterogeneities of the systems and the stress redistribution mechanisms (inhomogeneous in most cases) make things complicated and a concrete theory of the prediction schemes, even in model systems, is still lacking.

In this article, we address this problem (prediction of catastrophic events) in the Fiber Bundle Model (FBM) which has been used as a standard model [11–14] for fracturing in composite materials under external stress. We will show theoretically that in the Equal-Load-Sharing (ELS) model: (1) At the catastrophic failure point, the elastic energy is always larger than the damage energy. (2) The elastic energy variation shows a distinct peak before the catastrophic failure point

and this is a universal feature, i.e., it does not depend on the threshold distribution of the elements in the system. (3) The energy release during final catastrophic event is much bigger than the elastic energy stored in the system at the failure point. Our numerical results show perfect agreement with the theoretical estimates.

We organize our article as follows: After the brief introduction (section 1), we define the elastic energy and the damage energy in the Fiber Bundle Model in section 2. In sections 3 and 4 we calculate the elastic and damage energies of the model in terms of strain or extension. In several subsections of sections 3 and 4 we explore the theoretical calculations for power-law type and Weibull type distribution of fiber thresholds. Simulation results are presented and numerical results are compared with the theoretical estimates in these sections. We present a general analysis of elastic energy variations and existence of an elastic-energy maximum in section 5. In section 6 we identify the warning sign of catatrophic failure by locating the inflection point. Here, in addition to uniform and Weibull distributions, we choose a mixed threshold distribution and present the numerical results, based on Monte Carlo simulation, to confirm the universality of the behavior in the ELS models. Finally, we keep some discussions in section 7.

2. THE FIBER BUNDLE MODEL

The fiber bundle model consists of N parallel fibers placed between two solid clamps (**Figure 1**). Each fiber responds linearly with a force f to a stretch or extension Δ,

$$f = \kappa \Delta \ , \tag{1}$$

where κ is the spring constant. κ is the same for all fibers. Each fiber has a threshold x assigned to it. If the stretch Δ exceeds this threshold, the fiber fails irreversibly. When the clamps are stiff, load will be redistributed equally on the surviving fibers and this is called the equal-load-sharing (ELS) scheme. Throughout this article we work with ELS models only.

The fiber thresholds are drawn from a probability density $p(x)$. The corresponding cumulative probability is:

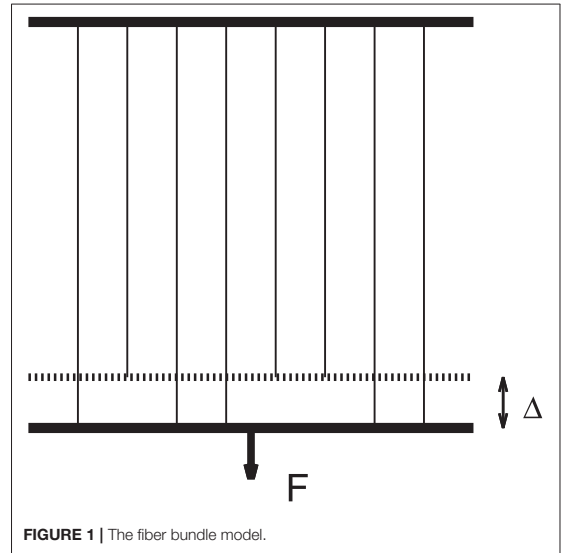$$P(x) = \int_0^x dx' p(x') \ . \tag{2}$$

When the fiber bundle is loaded, the fibers fail according to their thresholds, the weaker before the stronger. Suppose that n fibers have failed. At a stretch Δ, the fiber bundle carries a force:

$$F = \kappa(N - n)\Delta = N\kappa(1 - d)\Delta \ , \tag{3}$$

where we have defined the *damage*:

$$d = \frac{n}{N} \ . \tag{4}$$

When N is large enough, d may be treated as a continuous parameter.

FIGURE 1 | The fiber bundle model.

We will now assume that the stretch Δ is our control parameter. We can construct the energy budget according to continuous damage mechanics [1, 15]. Clearly, when we stretch the bundle with external force, work is done on the system. At a stretch Δ and damage d, the elastic energy stored by the surviving fibers is:

$$E^e(\Delta, d) = \frac{N\kappa}{2} \Delta^2 (1 - d) \ . \tag{5}$$

The damage energy of the failed fibers is given by:

$$E^d(d) = \frac{N\kappa}{2} \int_0^d d\delta \left[P^{-1}(\delta) \right]^2 \ . \tag{6}$$

The total energy at stretch Δ and damage d is, then:

$$E(\Delta, d) = E^e(\Delta, d) + E^d(d). \tag{7}$$

3. ELASTIC ENERGY AND DAMAGE ENERGY AT THE FAILURE POINT

We are going to analyze the energy relations when the bundle is in equilibrium. We know that there is a certain value, $\Delta = \Delta_c$, beyond which catastrophic failure occurs and the system collapses completely. We are particularly interested in what happens at the failure point. Is there a universal relation between elastic energy and damage energy at the failure point?

When N is large, we can reframe (Equations 5, 6) and express the energies in terms of external stretch (or extension) Δ as:

$$E^e(\Delta) = \frac{N\kappa}{2} \Delta^2 \left(1 - P(\Delta) \right) \ . \tag{8}$$

and

$$E^d(\Delta) = \frac{N\kappa}{2} \int_0^{\Delta} dx \left[p(x) x^2 \right] . \quad (9)$$

The force on the bundle at a stretch Δ can be written as:

$$F = \kappa(N - n)\Delta = N\kappa(1 - P(\Delta))\Delta. \quad (10)$$

The force must have a maximum at the failure point Δ_c, therefore setting $dF(\Delta)/d\Delta = 0$ we get:

$$1 - \Delta_c p(\Delta_c) - P(\Delta_c) = 0. \quad (11)$$

3.1. Uniform Threshold Distribution

We start with the simplest threshold distribution: the uniform distribution, which is well-known in fiber bundle research [14]. For a uniform fiber threshold distribution within the range $(0, 1)$, $p(x) = 1$ and $P(x) = x$. Therefore we get, from Equation (11),

$$\Delta_c = \frac{1}{2}. \quad (12)$$

Now putting $\Delta_c = 1/2$ in Equations (8, 9), we get:

$$E^e(\Delta_c) = \frac{N\kappa}{16} , \quad (13)$$

and

$$E^d(\Delta_c) = \frac{N\kappa}{2} \int_0^{1/2} dx \left[x^2 \right] = \frac{N\kappa}{48} . \quad (14)$$

Therefore, the ratio between damage energy and elastic energy at the failure point (Δ_c) is:

$$\frac{E^d(\Delta_c)}{E^e(\Delta_c)} = \frac{1}{3} . \quad (15)$$

3.2. Power-Law Type Threshold Distribution

Now we move to a general power law type fiber threshold distributions within the range $(0, 1)$,

$$p(x) = (1 + \alpha)x^{\alpha}. \quad (16)$$

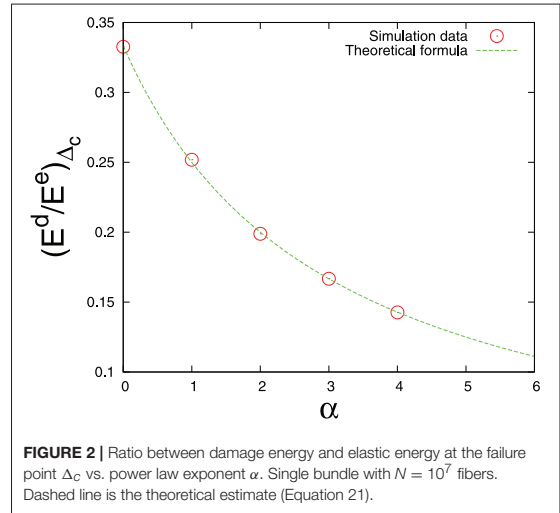The cumulative distribution takes the form:

$$P(x) = \int_0^x p(y)dy = x^{1+\alpha}. \quad (17)$$

We insert the expressions for $p(x)$ and $P(x)$ into Equation (11) and find the critical extention:

$$\Delta_c = \left(\frac{1}{2 + \alpha} \right)^{\frac{1}{1+\alpha}} . \quad (18)$$

We can calculate the elastic energy and damage energy at the failure point Δ_c:

$$E^e(\Delta_c) = \frac{N\kappa}{2} \Delta_c^2 \left(1 - P(\Delta_c) \right)$$
$$= \frac{N\kappa}{2} \Delta_c^2 \left(1 - \Delta_c^{1+\alpha} \right), \quad (19)$$

FIGURE 2 | Ratio between damage energy and elastic energy at the failure point Δ_c vs. power law exponent α. Single bundle with $N = 10^7$ fibers. Dashed line is the theoretical estimate (Equation 21).

and

$$E^d(\Delta_c) = \frac{N\kappa}{2} \int_0^{\Delta_c} dx \left[p(x) x^2 \right]$$
$$= \frac{N\kappa}{2} \frac{1+\alpha}{3+\alpha} \Delta_c^{3+\alpha} . \quad (20)$$

Plugging in the value of Δ_c (Equation 18) into the above equations for elastic energy and damage energy we end up with the following relation:

$$\frac{E^d(\Delta_c)}{E^e(\Delta_c)} = \frac{1}{3 + \alpha} . \quad (21)$$

Clearly, the ratio depends on the power factor α (**Figure 2**). When $\alpha = 0$, the threshold distribution reduces to a uniform distribution and we immediately go back to Equation (15).

3.3. Energy Balance

It is easy to show that the work done on the system up to the failure point Δ_c is equal to the sum of the energies E^e and E^d. The total work done on the system can be calculated as:

$$W(\Delta_c) = \int_0^{\Delta_c} d\Delta F(\Delta) . \quad (22)$$

Inserting the expression for $F(\Delta)$ into the integral we get, for a general power law type distribution,

$$W(\Delta_c) = Nk\Delta_c^2 \left[\frac{1}{2} - \frac{\Delta_c^{1+\alpha}}{3 + \alpha} \right] , \quad (23)$$

which is the total of elastic energy and damage energy, $W = E^e + E^d$ (see Equations 19, 20). In fact, the energy conservation here is analogous to the one in thermodynamics.

3.4. Energy Release During the Final Catastrophic Avalanche

It is known that when the extension exceeds the critical value Δ_c, the whole bundle collapses via a single avalanche called the final or catastrophic avalanche [14]. Can we calculate how much energy will be released in this final avalanche? It must be equal to the total damage energy of the fibers between threshold values Δ_c and the upper cutoff level of the fiber thresholds for the distribution in question.

We calculate the damage energy of the final avalanche for power-law type distributions as

$$
\begin{aligned}
E_{final}^d &= \frac{N\kappa}{2} \int_{\Delta_c}^{1} d\delta \left[p(\delta)\delta^2 \right] \\
&= \frac{N\kappa}{2} \frac{(1+\alpha)}{(3+\alpha)} \left(1 - \Delta_c^{3+\alpha} \right) .
\end{aligned} \tag{24}
$$

It is important to find out whether the damage energy for the catastrophic avalanche has a universal relation with the elastic or damage energies at the failure point. As already mentioned, the bundle has stable (equilibrium) states up to $\Delta \leq \Delta_c$. Therefore, if we correlate the final avalanche energy with E^e or E^d values at Δ_c, we can predict the catastrophic power of the final avalanche.

Comparing the expressions for $E_{\Delta_c}^e$, $E_{\Delta_c}^d$ and E_{final}^d we can write the following relation:

$$
\frac{E_{final}^d}{E_{\Delta_c}^d} = \left[(2+\alpha)^{\frac{3+\alpha}{1+\alpha}} - 1 \right] . \tag{25}
$$

As $E_{\Delta_c}^e = (3+\alpha)E_{\Delta_c}^d$, we can easily get the other relation:

$$
\frac{E_{final}^d}{E_{\Delta_c}^e} = \frac{1}{3+\alpha} \left[(2+\alpha)^{\frac{3+\alpha}{1+\alpha}} - 1 \right] . \tag{26}
$$

We can get the last relation (Equation 26) by comparing expressions (Equations 24 and 19) directly. These theoretical estimates are compared with numerical simulation results in **Figures 3**, **4**.

Now, if we put $\alpha = 0$, we get these energy relations for uniform fiber threshold distribution:

$$
\frac{E_{final}^d}{E_{\Delta_c}^d} = \left[(2)^3 - 1 \right] = 7. \tag{27}
$$

And

$$
\frac{E_{final}^d}{E_{\Delta_c}^e} = \frac{1}{3} \left[(2)^3 - 1 \right] = \frac{7}{3}. \tag{28}
$$

That means the energy release during final catastrophic avalanche is much bigger than the the elastic energy stored in the system just before failure (final stable state when $\Delta = \Delta_c$).

It is commonly believed that during catastrophic events like earthquakes, landslides, dam collapses etc., the accumulated elastic energy releases through avalanches [6, 7]. We observe a
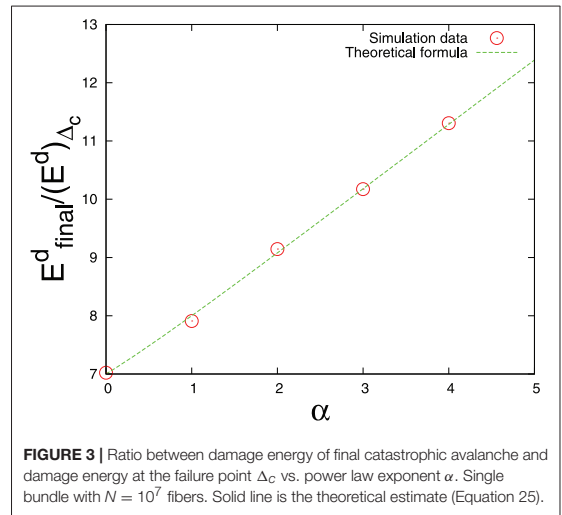
FIGURE 3 | Ratio between damage energy of final catastrophic avalanche and damage energy at the failure point Δ_c vs. power law exponent α. Single bundle with $N = 10^7$ fibers. Solid line is the theoretical estimate (Equation 25).
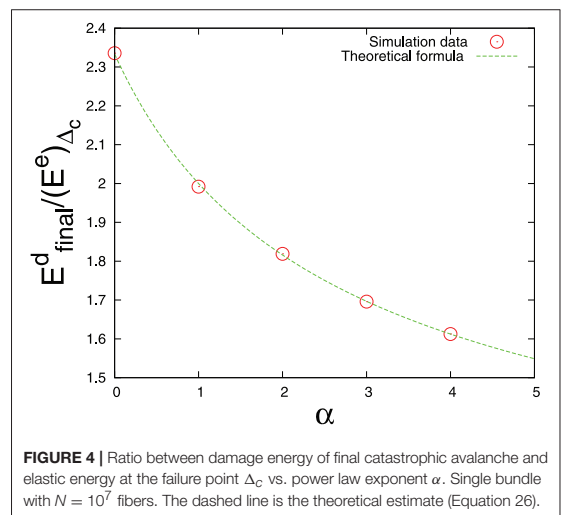
FIGURE 4 | Ratio between damage energy of final catastrophic avalanche and elastic energy at the failure point Δ_c vs. power law exponent α. Single bundle with $N = 10^7$ fibers. The dashed line is the theoretical estimate (Equation 26).

different scenario in this simple fiber bundle model where the system is doing *work* during the catastrophic failure phase as the external force is still acting on the bundle. As a result, the energy release (during catastrophic failure event) becomes much bigger than the elastic energy stored at the final stable phase.

4. ENERGY-ANALYSIS FOR WEIBULL DISTRIBUTION OF THRESHOLDS

We now consider the Weibull distribution, which has been used widely in material science [14]. The cumulative Weibull distribution has a form:

$$
P(x) = 1 - \exp(-x^k), \tag{29}
$$

where k is the Weibull index. Therefore the probability density takes the form:

$$p(x) = kx^{k-1} \exp(-x^k). \tag{30}$$

As the force has a maximum at the failure point Δ_c, inserting $P(x)$ and $p(x)$ values in expression (Equation 11) we get:

$$\exp(-\Delta_c^k) - \Delta_c k \Delta_c^{k-1} \exp(-\Delta_c^k) = 0. \tag{31}$$

From the above equation we can easily calculate the critical extension value as:

$$\Delta_c = k^{-1/k}. \tag{32}$$

The elastic energy at the critical extension Δ_c is:

$$\begin{aligned}
E^e(\Delta_c) &= \frac{N\kappa}{2} \Delta_c^2 \left(1 - P(\Delta_c)\right) \\
&= \frac{N\kappa}{2} \Delta_c^2 \exp(-\Delta_c^k),
\end{aligned} \tag{33}$$

and the damage energy is:

$$\begin{aligned}
E^d(\Delta_c) &= \frac{N\kappa}{2} \int_0^{\Delta_c} d\delta \left[p(\delta)\delta^2 \right] \\
&= \frac{N\kappa}{2} \int_0^{\Delta_c} d\delta \, k \left[\exp(-\delta^k)\delta^{k+1} \right].
\end{aligned} \tag{34}$$

Putting,

$$\delta^k = u, \tag{35}$$

we get:

$$E^d(\Delta_c) = \frac{N\kappa}{2} \int_0^{\Delta_c^k} du \left[\exp(-u)u^{2/k} \right]. \tag{36}$$

This integral is exactly calculable for $k = 1$ and $k = 2$.

4.1. Weibull Distribution With $k = 1$

For Weibull index $k = 1$, $\Delta_c = 1$ and the damage energy expression at the failure point takes the form:

$$E^d(\Delta_c) = \frac{N\kappa}{2} \int_0^1 du \exp(-u)u^2. \tag{37}$$

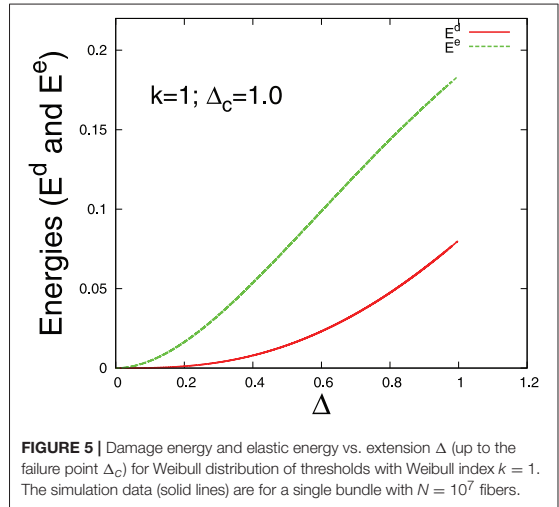Using integration by parts we arrive at the result:

$$E^d(\Delta_c = 1) = \frac{N\kappa}{2} \left(2 - 5e^{-1}\right). \tag{38}$$

We get the elastic energy at the failure point directly by putting $k = 1$ in Equation (33),
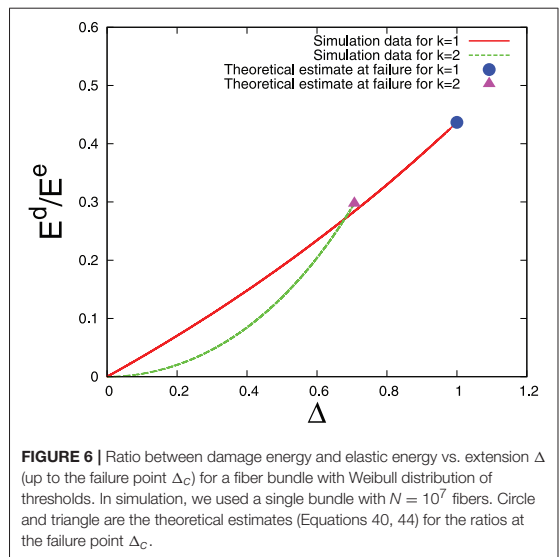
$$E^e(\Delta_c = 1) = \frac{N\kappa}{2e}; \tag{39}$$

Therefore, the ratio between damage and elastic energies at the failure point for Weibull distribution with $k = 1$ is:

$$\frac{E^d(\Delta_c)}{E^e(\Delta_c)} = 2e - 5 . \tag{40}$$

FIGURE 5 | Damage energy and elastic energy vs. extension Δ (up to the failure point Δ_c) for Weibull distribution of thresholds with Weibull index $k = 1$. The simulation data (solid lines) are for a single bundle with $N = 10^7$ fibers.

FIGURE 6 | Ratio between damage energy and elastic energy vs. extension Δ (up to the failure point Δ_c) for a fiber bundle with Weibull distribution of thresholds. In simulation, we used a single bundle with $N = 10^7$ fibers. Circle and triangle are the theoretical estimates (Equations 40, 44) for the ratios at the failure point Δ_c.

In **Figure 5**, we have shown numerical results of the variation of elastic and damage energies with strain for Weibull distribution (with $k = 1$). The theoretical estimates of the ratio between damage and elastic energies at the failure point are compared with numerical results in **Figure 6**.

4.2. Weibull Distribution With $k = 2$

For Weibull index $k = 2$, $\Delta_c = 1/\sqrt{2}$ and the damage energy expression at the failure point is:

$$E^d(\Delta_c) = \frac{N\kappa}{2} \int_0^{1/2} du \exp(-u)u. \tag{41}$$

Again, using integration by parts we arrive at the result:

$$E^d(\Delta_c = 1/\sqrt{2}) = \frac{N\kappa}{2}\left(1 - \frac{3}{2\sqrt{e}}\right). \tag{42}$$

We get the elastic energy at the failure point directly by putting $k = 2$ in Equation (33):

$$E^e(\Delta_c = 1/\sqrt{2}) = \frac{N\kappa}{2}\frac{1}{2\sqrt{e}}. \tag{43}$$

Therefore, the ratio between damage and elastic energies at the failure point for Weibull distribution with $k = 2$ is:

$$\frac{E^d(\Delta_c)}{E^e(\Delta_c)} = 2\left(\sqrt{e} - \frac{3}{2}\right). \tag{44}$$

The theoretical estimates of the ratio between damage and elastic energies at the failure point is compared with numerical results in **Figure 6**. In **Appendix A**, we give a general argument that elastic energy will be always bigger than damage energy at the critical (failure) point.

5. ELASTIC ENERGY MAXIMUM

There are two distinct phases of the system: A stable phase for $0 < \Delta \leq \Delta_c$ and an unstable phase for $\Delta > \Delta_c$. If we plot the elastic energy and damage energy vs. Δ, we see that damage energy always increases with Δ but elastic energy has a maximum at a particular value of Δ, let us call it Δ_m. Can we calculate the exact value of Δ_m for a given threshold distribution? Is it somehow connected to Δ_c? In this section we are going to answer these questions.

We recall the elastic energy expression (Equation 8). If we differentiate the elastic energy with respect to the extension Δ, we get:

$$\frac{dE^e(\Delta)}{d\Delta} = \frac{N\kappa}{2}\left[2\Delta\left(1 - P(\Delta)\right) - \Delta^2 p(\Delta)\right], \tag{45}$$

Which is 0 at Δ_m, with:

$$\Delta_m = \frac{2(1 - P(\Delta_m))}{p(\Delta_m)}. \tag{46}$$

If we consider a general power law type distribution $p(x) = (1 + \alpha)x^\alpha$, within $(0, 1)$, we can write:

$$\Delta_m = \left[\frac{2}{3 + \alpha}\right]^{\frac{1}{1+\alpha}} = \Delta_c\left[\frac{2(2 + \alpha)}{3 + \alpha}\right]^{\frac{1}{1+\alpha}} > \Delta_c. \tag{47}$$

For Weibull distribution $P(x) = 1 - \exp(-x^k)$, we can write:

$$\Delta_m = \left[\frac{2}{k}\right]^{\frac{1}{k}} = \Delta_c 2^{\frac{1}{k}} > \Delta_c. \tag{48}$$

Therefore we can conclude that Δ_m is bigger than Δ_c, i.e., elastic energy shows a maximum in the unstable phase (**Figures 7, 8**). A more general treatment for the relation between Δ_m and Δ_c is given in the **Appendix B**.
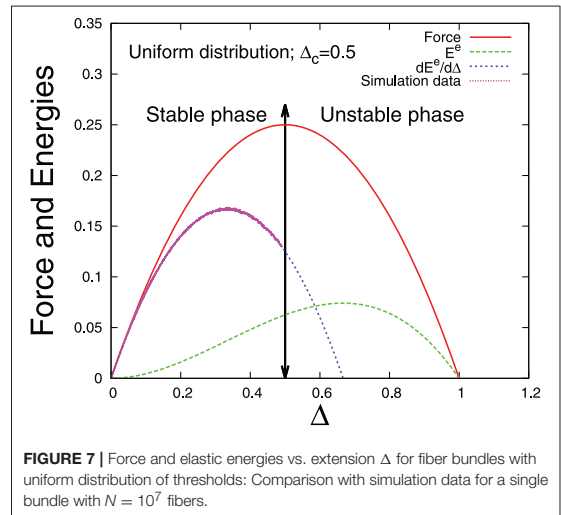
FIGURE 7 | Force and elastic energies vs. extension Δ for fiber bundles with uniform distribution of thresholds: Comparison with simulation data for a single bundle with $N = 10^7$ fibers.
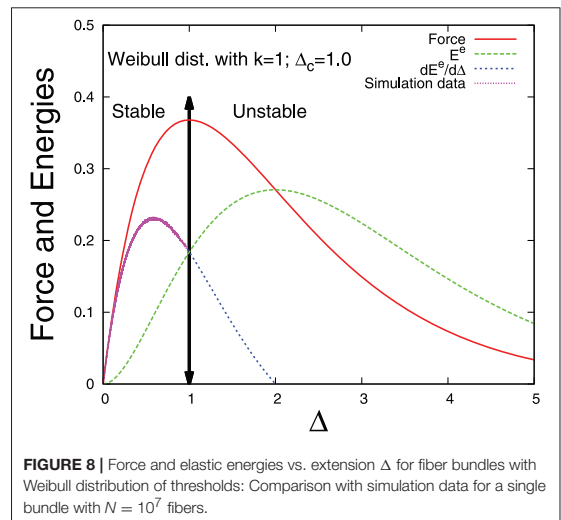
FIGURE 8 | Force and elastic energies vs. extension Δ for fiber bundles with Weibull distribution of thresholds: Comparison with simulation data for a single bundle with $N = 10^7$ fibers.

6. ELASTIC ENERGY INFLECTION POINT: THE WARNING SIGN OF CATASTROPHIC FAILURE

Are there any prior indications of the catastrophic failure (complete failure) of a bundle under stress? In the fiber bundle model, although the elastic energy has a maximum, it appears after the critical extension value, i.e., in the unstable phase of the system. Therefore it can not help us to predict the catastrophic failure point of the system.

However, if we plot $dE^e/d\Delta$, the change of elastic energy with the change of extension value Δ, we see that $dE^e/d\Delta$ has a

maximum and, most importantly, this maximum appears before the critical extension value Δ_c (**Figures 7, 8**). In this section we calculate the particular value of Δ at which $dE^e/d\Delta$ has a maximum. Let us call this Δ value Δ_{max}. We will also see whether there is a relation between Δ_{max} and Δ_c.

6.1. Theoretical Analysis

We recall the expression for the derivative of elastic energy with respect to strain of extension (Equation 45). Taking derivative of the equation, we get:

$$\frac{d^2 E^e(\Delta)}{d\Delta^2} = \frac{N\kappa}{2}\left[2\left(1-P(\Delta)\right) - 4\Delta p(\Delta) - \Delta^2 p'(\Delta)\right]. \quad (49)$$

Setting $d^2 E^e(\Delta)/d\Delta^2 = 0$ at $\Delta = \Delta_{max}$ we get for a general power law type distribution:

$$\Delta_{max} = \left[\frac{2}{(3+\alpha)(2+\alpha)}\right]^{\frac{1}{1+\alpha}} = \Delta_c\left[\frac{2}{3+\alpha}\right]^{\frac{1}{1+\alpha}}. \quad (50)$$

This expression confirms that $\Delta_{max} < \Delta_c$ for $\alpha \geq 0$. For a Weibull distribution with index k, we can write:

$$\frac{d^2 E^e(\Delta)}{d\Delta^2} = \frac{N\kappa}{2}\left[k^2\Delta^{2k} - (k^2+3k)\Delta^k + 2\right]\exp(-\Delta^k). \quad (51)$$

The solution (of $d^2 E^e(\Delta)/d\Delta^2 = 0$) with $(-)$ sign is the acceptable solution for the maximum. Hence,

$$
\begin{aligned}
\Delta_{max} &= \left[\frac{(k+3)-\sqrt{(k+3)^2-8}}{2k}\right]^{\frac{1}{k}} \\
&= \Delta_c\left[\frac{(k+3)-\sqrt{(k+3)^2-8}}{2}\right]^{\frac{1}{k}} \\
&< \Delta_c,
\end{aligned}
\quad (52)
$$

since,

$$\left[\frac{(k+3)-\sqrt{(k+3)^2-8}}{2}\right]^{1/k} < 1 \ \forall \ k > 0. \quad (53)$$

From Equations (50) and (52) we see that the relation between Δ_{max} and Δ_c depends on the threshold distributions and we can express Δ_c in terms of Δ_{max} with a prefactor as:

$$\Delta_c = G(\alpha)\Delta_{max}, \quad (54)$$

for power-law type distributions and

$$\Delta_c = H(k)\Delta_{max}, \quad (55)$$

for Weibull distributions. Now can we find a reasonable approximation for the prefactor that is useful for more than one threshold distributions? An intuitive first choice is the result for the uniform distribution with $\alpha = 0$ gives $\Delta_c = 1.5\Delta_{max}$. This is a good approximation for α close to 0, as expected, but
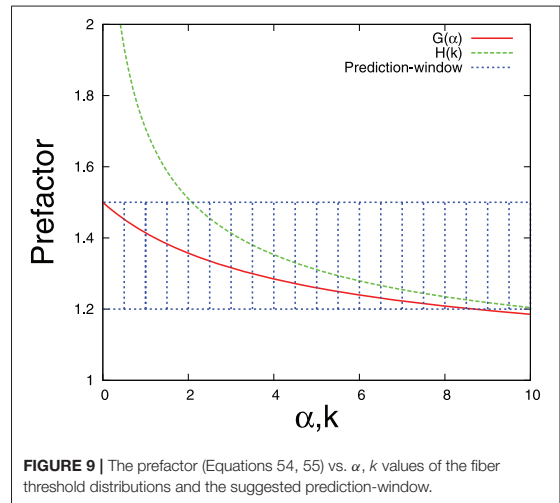
FIGURE 9 | The prefactor (Equations 54, 55) vs. α, k values of the fiber threshold distributions and the suggested prediction-window.

not for very large α values. This prediction is also exact for a Weibull distribution with $k \simeq 2$. If k is noticeably smaller, then the prediction $1.5\Delta_{max}$ is smaller than the true failure point Δ_c. In this case the estimate errs on the side of caution, and the bundle can withstand more than the estimate predicts. A better choice would be to set a prediction-window (1.2 to 1.5) for the prefactor $G(\alpha)$, $H(k)$. Then it can cover a wide range of α and k values (see **Figure 9**). Overall, such a prediction-window for the failure point works well when the threshold distribution does not vary too much with Δ. If we have prior information about the threshold distribution in the system (i.e., range of k or α values), it is possible to narrow down the prediction window and this is consistent with the common philosophy—*extra information helps to develop a better prediction scheme*.
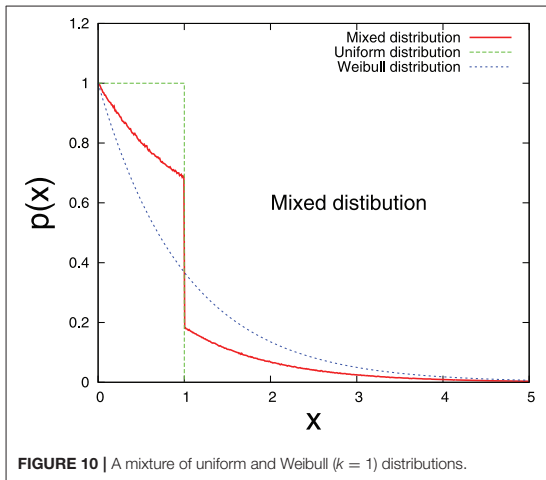
A more general argument is given in **Appendix C** for the relation between Δ_{max} and Δ_c.

6.2. Comparison With Simulation Data

In **Figures 7, 8** we compare the simulation results with the theoretical estimates. The simulations are done for a single bundle with large number ($N = 10^7$) of fibers and the agreement is convincing. We have used Monte Carlo technique to generate uncorrelated fiber thresholds that follow a particular statistical distributions (uniform and Weibull distributions). It is obvious that in simulations we can measure energy values in the stable phase only.

6.3. Simulation Results for a Mixed Threshold Distribution

Now we choose a mixed fiber threshold distribution. Can we see similar signature (maximum of $dE^e/d\Delta$ appears before Δ_c) as we have seen in previous section? The chosen distribution is a mixture of uniform distribution and Weibull distribution ($k = 1$) which is shown in **Figure 10**. We assign strength thresholds to $N/2$ fibers from a uniform distribution and to $N/2$ fibers from
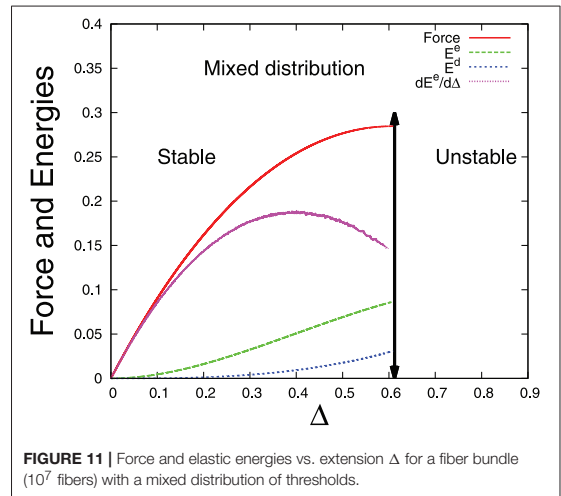
FIGURE 10 | A mixture of uniform and Weibull ($k = 1$) distributions.

FIGURE 11 | Force and elastic energies vs. extension Δ for a fiber bundle (10^7 fibers) with a mixed distribution of thresholds.

a Weibull distribution. The simulation result (**Figure 11**) reveals that $dE^e/d\Delta$ has a maximum which appears before the failure point Δ_c and Δ_{max} is somewhere in between the respective Δ_{max} values for uniform and Weibull threshold distributions—as expected intuitively. If we express the Δ_c value in terms of Δ_{max}, the prefactor is well inside the prediction-window, shown in **Figure 9**.

7. DISCUSSIONS

The Fiber Bundle Model has been used as a standard model for studying stress-induced fracturing in composite materials. In the Equal-Load-Sharing version of the model, all intact fibers share the load equally. In this work we have chosen the ELS models and we have studied the energy budget of the model for the entire failure process, starting from intact bundle up to the catastrophic failure point where the bundle collapses completely. Following the standard definition of elastic and damage energies from continuous damage mechanics framework, we have calculated the energy relations at the failure points for different types of fiber threshold distributions (power law type and Weibull type). At the critical or catastrophic failure point, the elastic energy is always larger than the total damage energy. Another important observation is that the elastic energy variation has a distinct peak before the catastrophic failure point. Also, the energy-release during final catastrophic event is much bigger than the elastic energy stored in the system at the failure point (see section 3 and section 4). Our simulation results on a single bundle with large numbers (10^7) of fibers, show perfect agreement with the theoretical estimates. We have chosen a *single bundle*, keeping in mind that for prediction purposes it is important and necessary that the warning sign can be seen in a single sample.

These observations can form the basis of a prediction scheme by finding the correlation between the position (strain or stretch level) of elastic energy variation peak and the actual failure point. The main concern is to find a direct relation between the elastic energy inflection point (Δ_{max}) and the failure point (Δ_c). We

found that Δ_c and Δ_{max} are related through a prefactor that depends on the exponent of the threshold distribution. Then we tried to find a window of the prefactor (Equations 54 and 55) that can cover a wide range of threshold distributions (**Figure 9**) so that we can express the failure point in terms of energy inflection point, i.e., $\Delta_c = $ prefactor $\cdot \Delta_{max}$ and the approximate prefactor window is 1.2 to 1.5 (**Figure 9**). Moreover, it is also possible to predict the size (energy release) of the final catastrophic event by measuring the stored elastic energy of the system at the failure point.

Our observations in this work have already opened up some scientific questions and challenges: what happens for Local-Load-Sharing (LLS) models [16]? Does the elastic energy variation show similar peaks before the catastrophic failure point? Can we measure and analyze the elastic energy during a rock-fracturing test in terms of the applied strain?

During rock-fracturing experiments [17–20], one can measure axial stress (force), axial and radial strain directly through strain gauges. Amount of damage can be recorded via acoustic emissions (AE) in terms of number of events (micro cracks) and the energy of the events. Clearly, total acoustic energy is the amount of damage energy in the system. It is possible to calculate the amount of work done on the system from applied force and effective strain value. Therefore, the difference between total work done and the damage energy (accumulated acoustic energy) will be the elastic energy of the system. Once we plot the elastic energy vs. strain curve, it is straight forward to estimate the elastic energy growth rate by measuring the slope of the curve at different strain points.

Our next article will resolve some of these issues –we are now working on energy budget of LLS models.

DATA AVAILABILITY

The datasets generated in this study are available on request to the corresponding author.

AUTHOR CONTRIBUTIONS

SP: theory, simulation, data analysis, and plotting. JK: theory (Appendix part). AH: theory. Equal contributions in discussions and writing the article.

ACKNOWLEDGMENTS

REFERENCES

1. Krajcinovic D. *Damage mechanics*. Amsterdam: Elsevier (1996).

2. Henkel M, Hinrichsen H, Lubeck S, Pleimling M. *Non-equilibrium Phase Transitions* vol. 1. Berlin: Springer (2008).

3. Bonamy D, Bouchaud E. Failure of heterogeneous materials: a dynamic phase transition? *Phys Rep.* (2011) 498:1–44. doi: 10.1016/j.physrep.2010.07.006

4. Abaimov SG. *Statistical Physics of Non-thermal Phase Transitions*. Heidelberg: Springer Verlag (2015).

5. Berthier E. *Quasi-brittle failure of heterogeneous materials: damage statistics and localization* (Thesis). Université Pierre et Marie Curie, Paris, France (2015).

6. Chakrabarti BK, Benguigui LG. *Statistical Physics of Fracture and Breakdown in Disordered Solids*. Oxford: Oxford University Press (1997).

7. Biswas S, Ray P, Chakrabarti BK. *Statistical Physics of Fracture, Breakdown, and Earthquake*. Berlin: Wiley-VCH (2015).

8. Villa P, Mahieu E. Breakage patterns of human long bones. *J Hum Evol.* (1991) 21:27–48.

9. Etzion D. Moderating effect of social support on the stress-burnout relationship. *J App Psych.* (1984) 69:615–22.

10. Ramirez AJ, Graham J, Richards MA, Cull A, Gregory WM. Mental health of hospital consultants: the effect of stress and satisfaction at work. *Lancet* (1996) 347:724–28.

11. Peirce FT. Tensile tests for cottom yarns. "The weakest link" theorems on the strength of long and composite specimens. *J Text Ind.* (1926) 17:355.

12. Daniels HE. The statistical theory of the strength of bundles of threads. *Proc Roy Soc Ser A.* (1945) 183:243.

13. Pradhan S, Hansen A, Chakrabarti BK. Failure processes in elastic fiber bundles. *Rev Mod Phys.* (2010) 82:499. doi: 10.1103/RevModPhys.82.499

14. Hansen A, Hemmer PC, Pradhan S. *The fiber bundle model: Modeling Failure in Materials*. Berlin: Wiley-VCH (2015).

15. Pradhan S, Hansen A, Ray P. A renormalization group procedure for fiber bundle models. *Front Phys.* (2018) 6:65. doi: 10.3389/fphy.2018.00065

16. Harlow DG, Phoenix SL. Approximations for the strength distribution and size effects in an idealized lattice model of material breakdown. *J Mech Phys Sol.* (1991) 39:173–200.

17. Pradhan S, Stroisz A, Fjar E, Stenebraten J, Lund H, Sonstebo E. Stress-induced fracturing of reservoir rocks: acoustic monitoring and mCT image analysis. *Rock Mech Rock Eng.* (2015) 48:2529–40. doi: 10.1007/s00603-015-0853-4

18. Baud P, Meredith PG. Damage accumulation during triaxial creep of darley dale sandstone from pore volumetry and acoustic emission. *Int J Rock Mech Min Sci.* (1997) 34:3–4.

19. Holcomb DJ, Stone CM Costin LS. *Combining Acoustic Emission Locations and Microcrack Damage Model to Study Development of Damage in Brittle Materials*. Rotterdam: Rock Mechanics Contributions and Challaenges, Hustrulid and Johnson (1990).

20. Amitrano D. Rupture by damage accumulation in rocks. *Int J Fract.* (2006) 139:369–81. doi: 10.1007/s10704-006-0053-z

APPENDIX

As stated in section 2, the elastic energy in the system at extension Δ is:

$$E^e(\Delta) = \frac{N\kappa}{2}\Delta^2(1 - P(\Delta)), \tag{56}$$

where $P(\Delta)$ is the cumulative probability distribution of the fiber thresholds. The force per fiber $\sigma = F/N$ required to continue the breaking process at a given extension Δ is:

$$\sigma(\Delta) = \kappa\Delta(1 - P(\Delta)) \tag{57}$$

The critical extension Δ_c where the bundle collapses is hence given by:

$$0 = \left.\frac{d\sigma}{d\Delta}\right|_{\Delta_c} = \kappa(1 - P(\Delta_c) - \Delta_c p(\Delta_c)). \tag{58}$$

A. Elastic vs. Damage Energy at the Critical Point

Numerical data seems to suggest that $E^e > E^d$ at the critical point for most threshold distributions. Let us try to prove this analytically by investigating the difference between elastic and damage energy:

$$\begin{aligned}E_{diff}(\Delta) &= E^e(\Delta) - E^d(\Delta)\\ &= \frac{N\kappa}{2}\left[\Delta^2(1 - P(\Delta)) - \int_0^\Delta dx\, x^2 p(x)\right].\end{aligned} \tag{59}$$

The derivative of this energy difference is:

$$\begin{aligned}\frac{dE_{diff}}{d\Delta} &= \frac{N\kappa}{2}\left[2\Delta(1 - P(\Delta)) - \Delta^2 p(\Delta) - \Delta^2 p(\Delta)\right]\\ &= N\kappa\Delta\left[1 - P(\Delta) - \Delta p(\Delta)\right]\\ &= N\Delta\frac{d\sigma}{d\Delta}.\end{aligned} \tag{60}$$

We can now express the energy difference in terms of the forces acting on the fiber bundle. We integrate this expression to find:

$$\begin{aligned}E_{diff}(\Delta) &= \int_0^\Delta dx\,\frac{dE_{diff}}{dx} = N\int_0^\Delta dx\, x\frac{d\sigma}{dx}\\ &= N\left[\Delta\sigma(\Delta) - \int_0^\Delta dx\,\sigma(x)\right]\end{aligned} \tag{61}$$

by partial integration. In particular, this gives the result:

$$E_{diff}(\Delta_c) = N\left[\Delta_c\sigma_c - \int_0^{\Delta_c} dx\,\sigma(x)\right] \tag{62}$$

at the critical point. Since $\sigma_c = \max\sigma(\Delta)$, we see that $E_{diff}(\Delta_c) > 0$ for all threshold distributions. The only exception possible is a threshold distribution with a constant force $\sigma(\Delta) = \sigma_c$. But this results in a lower cut-off $\Delta_0 = \Delta_c > 0$ (for the threshold distribution to be normalizable), and then $E^e(\Delta_c) > E^d(\Delta_c) = 0$.

B. Elastic Energy Maximum Point

First, rewrite (Equation 58) as:

$$1 = g(\Delta_c) \equiv \frac{1 - P(\Delta_c)}{\Delta_c p(\Delta_c)}. \tag{63}$$

This definition of $g(\Delta)$ will be useful in the following derivations. The maximum of the elastic energy is found at an extension Δ_m, which is given by:

$$0 = \left.\frac{dE^e}{d\Delta}\right|_{\Delta_m} \propto 2\Delta_m(1 - P(\Delta_m)) - \Delta_m^2 p(\Delta_m), \tag{64}$$

i.e.,

$$\frac{1}{2} = \frac{1 - P(\Delta_m)}{\Delta_m p(\Delta_m)} = g(\Delta_m). \tag{65}$$

Comparing this expression to Equation (63) allows us to find a relation between Δ_c and Δ_m. We investigate the function $g(\Delta)$:

$$\begin{aligned}g(\Delta) &= \frac{1 - P(\Delta)}{\Delta p(\Delta)} = \frac{1 - P(\Delta)}{1 - P(\Delta) - \frac{d\sigma}{d\Delta}}\\ &= \begin{cases} < 1 & \text{for } \frac{d\sigma}{d\Delta} < 0\\ > 1 & \text{for } \frac{d\sigma}{d\Delta} > 0\end{cases}.\end{aligned} \tag{66}$$

It is clear from Equation (66) that for a threshold distribution with only a single maximum in the load curve, $g(\Delta_m) = 1/2$ must occur in the unstable phase, i.e., $\Delta_m > \Delta_c$.

C. Elastic Energy Inflection Point

The elastic energy maximum occurs after the critical point and is hence unsuitable as a predictor for failure. But what about the maximum of the *derivative* of the elastic energy, the inflection point Δ_{max}? As stated in the section 6:

$$\frac{d^2E^e}{d\Delta^2} \propto 2(1 - P(\Delta)) - 4\Delta p(\Delta) - \Delta^2 p'(\Delta). \tag{67}$$

Setting this second derivative to zero and rearranging terms gives the equation:

$$2(1 - P(\Delta_{max})) - 4\Delta_{max}p(\Delta_{max}) = \Delta_{max}^2 p'(\Delta_{max}). \tag{68}$$

To investigate the relation between Δ_{max} and Δ_c, we combine this with the relations $d\sigma/d\Delta = 1 - P(\Delta) - \Delta p(\Delta)$ and $d^2\sigma/d\Delta^2 = -2p(\Delta) - \Delta p'(\Delta)$ evaluated at Δ_{max} to get:

$$\left.\frac{d\sigma}{d\Delta}\right|_{\Delta_{max}} = -\frac{\Delta_{max}}{2}\left.\frac{d^2\sigma}{d\Delta^2}\right|_{\Delta_{max}}. \tag{69}$$

Let's once again assume that we are working with a threshold distribution that has only a single maximum in its load curve. Then $d\sigma/d\Delta > 0$ corresponds to the stable phase and $d\sigma/d\Delta < 0$ corresponds to the unstable phase. We see that any threshold distribution with $d^2\sigma/d\Delta^2 < -2/\Delta \cdot d\sigma/d\Delta$ everywhere in the unstable phase must have Δ_{max} in the stable phase, i.e., $\Delta_{max} < \Delta_c$.

This is a general (but weak) condition that is sufficient, but not necessary, for $\Delta_{max} < \Delta_c$.

Article II

Burst Distribution for Small Bursts by Asymptotic Expansion in the Fiber Bundle Model

Submitted to Frontiers in Physics

Article II

Article II

Burst Distribution for Small Bursts by Asymptotic Expansion in the Fiber Bundle Model

Jonas T. Kjellstadli*

PoreLab, Department of Physics, NTNU – Norwegian University of Science and Technology, Trondheim, Norway
(Dated: September 6, 2019)

We derive an asymptotic series expansion for the burst size distribution in the equal load sharing fiber bundle model, a predominant model for breakdown in disordered media. Earlier calculations give expressions with correct asymptotic behavior for large bursts, but low accuracy for small bursts, up to an order of magnitude off. The approximations from the expansion we present here give relative errors of only a few percent when compared with results for infinite system sizes. We also solve the burst size distribution exactly for the Weibull threshold distributions.

I. INTRODUCTION

The fiber bundle model [1–4] is a prime example of what Bouchaud calls a metaphorical model [5]; that is, a model which reveals mechanisms that lie hidden beneath layers of complexity in realistic models and are completely lost in phenomenological models. Even in its simplest form, the *equal load sharing model*, the number of papers written on the model may now be counted in the thousands. This is evidence of great richness.

The distribution of bursts, or avalanches, is important in the study of fiber bundle models. Its behavior can signal how close the bundle is to catastrophic failure, even in single samples [6]. Hemmer and Hansen [7] demonstrated in 1992 that the bursts follow a power law with an exponent 5/2 for a wide class of disorder distributions. This work was followed up Pradhan et al. [6, 8], who showed that the power law exponent changes to 3/2 as the bundle is approaching catastrophic failure. By following the development of the crossover burst size — that is, the burst size that constitutes the water shed between bursts following the 5/2 law and the bursts following the 3/2 law — it is possible to quantitatively measure of how far the bundle is from collapse.

However, this approach has the problem that it requires knowledge of large (and hence rare) bursts, which have poor statistics. It would be better to predict failure from the smallest bursts, which happen often and can be measured with higher accuracy. This makes it important to have access to accurate analytic estimates of these values to compare with. Hence, we provide in this article a method to analytically calculate the burst distribution accurately for small bursts.

II. THE EQUAL LOAD SHARING FIBER BUNDLE MODEL

Consider an equal load sharing fiber bundle model with N fibers [1, 2]. The externally applied force (or load) F is distributed identically on all intact fibers, and a fiber acts as Hookean spring until its elongation reaches a certain threshold, where it breaks. Due to the equal load sharing, fibers will always fail in order from smallest to largest threshold as the load is increased.

The thresholds are drawn independently from a probability density $p(t)$, with a corresponding cumulative distribution $P(t) = \int_{-\infty}^{t} p(u)\mathrm{d}u$. Let $\{t_k\}$ be the ordered sequence of thresholds, such that $t_1 \leq t_2 \leq \cdots \leq t_N$. Then the force F_k required to break the kth fiber is

$$F_k = (N + 1 - k)\, t_k. \tag{1}$$

Equation (1) shows that F_k consists of two factors: the decreasing number of intact fibers $N + 1 - k$, and the increasing threshold t_k of the kth fiber. Due to the irregularities of $\{t_k\}$, F_k doesn't increase or decrease smoothly. Instead, it fluctuates up and down around a general increasing trend. (Or decreasing, depending on where in the fracture process we are.)

If the force F is the control parameter during the breaking process, this causes bursts (or avalanches) of several fibers that break under the same load. We have a burst of size Δ beginning with the failure of the kth fiber if $F_k > F_j$ for $j < k$, $F_{k+j} \leq F_k$ for $j < \Delta$, and $F_{k+\Delta} > F_k$. This simply means that when the force reaches F_k, Δ fibers break under that load with no further load increase required, and the burst stops at the $\Delta + 1$th fiber, which is strong enough to withstand the load.

The average of Equation (1) over samples is the load curve [4]

$$\sigma(x) = x\,[1 - P(x)], \tag{2}$$

which is also the limit of equation (1) as $N \to \infty$. Here $\sigma = F/N$ is the applied force per fiber in the bundle, both broken and intact, and x is the elongation of the fiber bundle. For most threshold distributions σ has a single parabolic maximum at elongation x_c, where $1 - P(x_c) = x_c p(x_c)$.

The burst distribution is usually defined as $D(\Delta)$: the expected number of bursts of size Δ during the breaking of a single fiber bundle [3, 4, 7]. This definition makes $D(\Delta) \propto N$ for large systems, and hence it diverges as $N \to \infty$. We will instead use the notation

---

* jonas.kjellstadli@outlook.com

$\bar{D}(\Delta) = D(\Delta)/N$, with the physical interpretation that $\Delta\bar{D}(\Delta)$ is the fraction of fibers broken in bursts of size Δ — which converges to a finite number as $N \to \infty$.

Hemmer and Hansen [7] showed that for continuous load increase, the burst distribution to first order in N has the asymptotic behavior (as $\Delta \to \infty$)

$$\bar{D}(\Delta) \sim C\Delta^{-5/2}, \tag{3}$$

where $C = (2\pi)^{-1/2} x_c p(x_c)^2 [2p(x_c) + x_c p'(x_c)]^{-1}$. This result is universal for threshold distributions where the load curve has a single parabolic maximum.

Pradhan et al. [6, 8] generalized this asymptotic behavior to threshold distributions starting from a lower limit $t_0 \geq 0$, and found that there is a crossover

$$\bar{D}(\Delta) \sim C\Delta^{-5/2}\left(1 - e^{-\Delta/\Delta_c}\right)$$
$$\propto \begin{cases} \Delta^{-3/2} & \text{for } \Delta \ll \Delta_c \\ \Delta^{-5/2} & \text{for } \Delta \gg \Delta_c, \end{cases} \tag{4}$$

with $\Delta_c = 4\pi C^2 p(x_c)^{-2}(t_0 - x_c)^{-2}$ and C as in Equation (3). This crossover to a different exponent as t_0 increases has been proposed as a method to detect imminent failure [3, 6, 8].

Equation (4) is also an asymptotic behavior in the limit $\Delta \to \infty$, and hence it also requires information about large bursts (which are rare events) to predict failure. Our goal is to find a way to calculate the burst distribution accurately for small bursts, which the asymptotic expressions in equations (3,4) cannot do. To this end, we use a threshold distribution with a lower limit $t_0 \geq 0$. The burst distribution is then, to first order in N [4],

$$\bar{D}(\Delta) = \frac{\Delta^{\Delta-1}}{\Delta!} \int_{t_0}^{x_c} \left[a(t)e^{-a(t)}\right]^{\Delta} a(t)^{-1}$$
$$\times [1 - a(t)]\, p(t)\mathrm{d}t \tag{5}$$

for $t_0 < x_c$, where

$$a(t) = \frac{tp(t)}{1 - P(t)}. \tag{6}$$

At x_c, the critical elongation of Equation (2), this function satisfies $a(x_c) = 1$.

III. EXACT BURST DISTRIBUTION

Is it possible to solve the burst distribution exactly? The deciding factor is always the function $a(t)$. Instead of first choosing a threshold distribution and then check whether Equation (5) is solvable, we can instead do it in the opposite order: choose a function $a(t)$ for which the integral can be solved, and then use Equation (6) to find the corresponding threshold distribution.

A. Constant $a(t)$

The simplest expression would be a constant $a(t)$, which implies $a(t) = 1$ because $a(x_c) = 1$. This gives $\bar{D}(\Delta) = 0$ when inserted into Equation (5). To see why, set $a(t) = 1$ in Equation (6), which gives the differential equation

$$\frac{p'(t)}{p(t)} = -\frac{2}{t}, \tag{7}$$

with the normalized solution $P(t) = 1 - t_0/t$ for $t \in [t_0, \infty)$. This makes the load curve in Equation (2) constant: $\sigma(x) = t_0$, i.e., $x_c = t_0$. Thus there is no burst distribution and $\bar{D}(\Delta) = 0$.

B. Power law $a(t)$

Other than $a(t) = 1$, the most intuitive choice for a solvable integral is a power law $a(t) = C(k)t^k$ with $k > 0$. Inserting this into Equation (6) gives the first-order differential equation

$$p(t) + C(k)t^{k-1}P(t) = C(k)t^{k-1} \tag{8}$$

for $P(t)$. It can be solved with the integrating factor method: multiplying the equation with $\mu(t) = \exp\left(\int_{t_0}^{t} \mathrm{d}\tau\, C(k)\tau^{k-1}\right) = \exp\left[C(k)\left(t^k - t_0^k\right)/k\right]$ and integrating from t_0 to t gives the solution

$$P(t) = \frac{C(k)}{k}\left[1 - e^{\frac{C(k)}{k}\left(t_0^k - t^k\right)}\right]. \tag{9}$$

Normalization on the interval $[t_0, \infty)$, i.e., $P(t = \infty) = 1$, yields $C(k)/k = 1$. Thus

$$P(t) = 1 - e^{t_0^k - t^k}, \tag{10}$$

which is a Weibull distribution with shape parameter k and a lower limit t_0. The lower limit corresponds to breaking all fibers with thresholds $t < t_0$ from a fiber bundle with $P(t) = 1 - e^{-t^k}$. Hence the lower limit is equivalent to studying a bunde with $P(t) = 1 - e^{-t^k}$ that has already sustained a damage $d = 1 - e^{-t_0^k}$.

The Weibull distribution in Equation (10) has a critical extension $x_c = k^{-1/k}$, which gives $a(x_c) = 1$, as required for consistency. We can now solve the burst distribution exactly for the Weibull distribution. Inserting $a(t) = kt^k$ and $p(t) = kt^{k-1}e^{t_0^k - t^k}$ into Equation (5) gives

$$\bar{D}(\Delta) = \frac{\Delta^{\Delta-1}}{\Delta!} \int_{t_0}^{k^{-1/k}} \left(kt^k e^{-kt^k}\right)^{\Delta}\left(kt^k\right)^{-1}$$
$$\times \left(1 - kt^k\right)kt^{k-1}e^{t_0^k - t^k}\,\mathrm{d}t. \tag{11}$$

Use the substitution $z = t^k$ to get

$$\bar{D}(\Delta) = \frac{(k\Delta)^{\Delta-1}}{\Delta!}e^{t_0^k}\left[\int\limits_{t_0^k}^{1/k} z^{\Delta-1}e^{-z(k\Delta+1)}dz\right.$$

$$\left. -k\int\limits_{t_0^k}^{1/k} z^{\Delta}e^{-z(k\Delta+1)}dz\right]. \tag{12}$$

Combining integration by parts and induction yields

$$\int\limits_{t_0^k}^{1/k} dz\, z^n e^{-\alpha z} = \frac{n!}{\alpha^{n+1}}\left[e^{-\alpha t_0^k}\sum_{i=0}^{n}\frac{(\alpha t_0^k)^i}{i!}\right.$$

$$\left. -e^{-\alpha/k}\sum_{i=0}^{n}\frac{(\alpha/k)^i}{i!}\right], \tag{13}$$

which gives the exact burst distribution

$$\bar{D}(\Delta) = \frac{\Delta^{\Delta-1}e^{t_0^k}}{\Delta!(k\Delta+1)}\left[e^{-(\Delta+1/k)}\right.$$

$$\left. -\left(kt_0^k\right)^{\Delta}e^{-t_0^k(k\Delta+1)}\right]$$

$$+\frac{(k\Delta)^{\Delta-1}e^{-k\Delta t_0^k}}{\Delta(k\Delta+1)^{\Delta+1}}\sum_{i=0}^{\Delta-1}\frac{\left[(k\Delta+1)t_0^k\right]^i}{i!} \tag{14}$$

$$-\frac{(k\Delta)^{\Delta-1}e^{t_0^k-(\Delta+1/k)}}{\Delta(k\Delta+1)^{\Delta+1}}\sum_{i=0}^{\Delta-1}\frac{(k\Delta+1)^i}{i!k^i}.$$

This expression can easily be evaluated for small bursts, which is what we are interested in. Equation (14) for $k = 2$ and $t_0 = 0$ is shown in Figure 1 together with simulation results. The agreement is excellent, particularly for small Δ where finite size effects from the simulations are negligible.

For the special case $\Delta = 1$, Equation (14) becomes

$$\bar{D}(\Delta = 1) = \frac{e^{t_0^k}}{(k+1)^2}\left[ke^{-(1+1/k)}\right.$$

$$\left. +\left(1-(k+1)kt_0^k\right)e^{-(k+1)t_0^k}\right]. \tag{15}$$

For large bursts Equation (14) is impractical to use, but for $\Delta \gg \Delta_c$ the first term is dominant. The equation then simplifies to

$$\bar{D}(\Delta) \simeq \frac{\Delta^{\Delta-1}e^{-\Delta}}{\Delta!(k\Delta+1)}e^{t_0^k-1/k} \simeq \frac{e^{t_0^k-1/k}}{\sqrt{2\pi}k}\Delta^{-5/2}, \tag{16}$$

via Stirling's approximation, $\Delta! \simeq \sqrt{2\pi\Delta}\Delta^{\Delta}e^{-\Delta}$. This is the expected asymptotic power law from Equation (3) for the Weibull distribution from Equation (10).
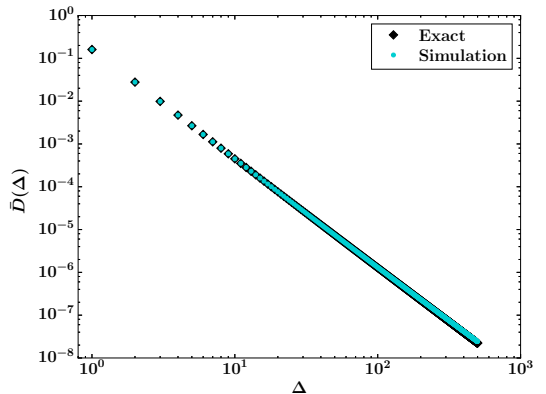

FIG. 1. Burst distribution $\bar{D}(\Delta)$ for a Weibull threshold distribution with $k = 2$ and $t_0 = 0$. The exact result (black) is Equation (14), and the simulation results (turquoise) were done with $N = 1024^2$ and 10^6 samples.

IV. ASYMPTOTIC SERIES EXPANSION

The simplicity of the Weibull threshold distribution is an exception, and for other threshold distributions we cannot expect to find an exact result for the burst distribution. We therefore return to Equation (5) to make an asymptotic series expansion, and note that the equation has the form of a Laplace integral [9]

$$I(\Delta) = \int\limits_{t_0}^{x_c} f(t)e^{\Delta\phi(t)}dt, \tag{17}$$

with

$$f(t) = p(t)\frac{1-a(t)}{a(t)} \tag{18}$$

$$\phi(t) = -a(t) + \ln(a(t)). \tag{19}$$

For large Δ the integral is dominated by a small interval around the maximum of $\phi(t)$ in the interval $[t_0, x_c]$. In our case ϕ has its maximum at $a(t) = 1$, i.e., at the critical extension x_c, the upper limit of integration. Hence the asymptotic behaviour of Equation (17) as $\Delta \to \infty$ is

$$I(\Delta) \sim \int\limits_{x_c-\epsilon}^{x_c} f(t)e^{\Delta\phi(t)}dt \tag{20}$$

where ϵ is a small number. In the small interval $[x_c - \epsilon, x_c]$ we can Taylor expand $f(t)$ and $\phi(t)$ around x_c,

$$f(t) = f_1(t - x_c) + f_2(t - x_c)^2$$
$$+ f_3(t - x_c)^3 + \cdots$$
$$\phi(t) = \phi_0 + \phi_2(t - x_c)^2 + \phi_3(t - x_c)^3 \tag{21}$$
$$+ \phi_4(t - x_c)^4 + \cdots$$

Note that f_n and ϕ_n are not identical to the nth derivatives of $f(t)$ and $\phi(t)$ evaluated at x_c, only proportional to them. The exact expressions for these coefficients in terms of $a(t)$ are shown in Equations (34,36). Also note that the vanishing terms $f_0 = f(x_c) = 0$ and $\phi_1 \propto \phi'(x_c) = 0$ (ϕ has its maximum at x_c) are not included here.

In the limit $\Delta \to \infty$, when the interval $[x_c - \epsilon, x_c]$ can be chosen arbitrarily small, the two first terms in the expansion of ϕ will dominate the others. We therefore separate these terms by factorizing the exponential in the integrand of Equation (20) as

$$
\begin{aligned}
\mathrm{e}^{\Delta \phi(t)} = {} & \exp\left(\Delta\phi_0 + \Delta\phi_2(t - x_c)^2\right) \\
& \times \exp\left(\Delta\left[\phi_3(t - x_c)^3 + \phi_4(t - x_c)^4 + \cdots\right]\right),
\end{aligned}
\tag{22}
$$

and then Taylor expand the second factor

$$
\begin{aligned}
\exp\left(\Delta\left[\phi_3(t - x_c)^3 + \phi_4(t - x_c)^4 + \cdots\right]\right) = {} & 1 \\
+ \Delta\left[\xi_{1,3}(t - x_c)^3 + \xi_{1,4}(t - x_c)^4 + \cdots\right] & \\
+ \Delta^2\left[\xi_{2,6}(t - x_c)^6 + \xi_{2,7}(t - x_c)^7 + \cdots\right] & \\
+ \cdots, &
\end{aligned}
\tag{23}
$$

which defines $\xi_{n,m}$. Inserting these expansions into Equation (20) and extending the lower integration limit back down to t_0 gives

$$
\begin{aligned}
I(\Delta) \sim {} & \mathrm{e}^{\Delta\phi_0} \int_{t_0}^{x_c} \mathrm{e}^{\Delta\phi_2(t - x_c)^2} \\
& \times \left[f_1(t - x_c) + f_2(t - x_c)^2 + \cdots\right] \\
& \times \left\{1 + \Delta\left[\xi_{1,3}(t - x_c)^3 + \cdots\right]\right. \\
& \left. + \Delta^2\left[\xi_{2,6}(t - x_c)^6 + \cdots\right] + \cdots\right\} \mathrm{d}t.
\end{aligned}
\tag{24}
$$

The standard approach is to extend the lower limit of integration to $-\infty$ because the integral over $[-\infty, x_c - \epsilon]$ is subdominant to the integral over $[x_c - \epsilon, x_c]$ in the limit $\Delta \to \infty$ [9]. But our goal is to use the asymptotic series to calculate an approximation for $\bar{D}(\Delta)$ for small Δ, and we know that the lower limit t_0 is important for small bursts [6].

To solve this integral, multiply the Taylor expansions and separate terms with even and odd powers of $t - x_c$ into $I_{\mathrm{even}}(\Delta)$ and $I_{\mathrm{odd}}(\Delta)$, respectively. The odd terms are

$$
\begin{aligned}
I_{\mathrm{odd}}(\Delta) = {} & \mathrm{e}^{\Delta\phi_0} \int_{t_0}^{x_c} \mathrm{e}^{\Delta\phi_2(t - x_c)^2} \\
& \times \left\{\left[f_1(t - x_c) + f_3(t - x_c)^3 + \cdots\right]\right. \\
& + \Delta\left[\omega_{1,5}(t - x_c)^5 + \omega_{1,7}(t - x_c)^7 + \cdots\right] \\
& + \Delta^2\left[\omega_{2,7}(t - x_c)^5 + \omega_{2,9}(t - x_c)^9 + \cdots\right] \\
& \left. + \cdots\right\} \mathrm{d}t,
\end{aligned}
\tag{25}
$$

where $\omega_{n,m}$ is defined in Equation (38). Then choose $u = \Delta\phi_2(t - x_c)^2$, which yields

$$
\begin{aligned}
I_{\mathrm{odd}}(\Delta) = {} & \frac{\mathrm{e}^{\Delta\phi_0}}{2\Delta\phi_2} \int_{\Delta\phi_2(t_0 - x_c)^2}^{0} \mathrm{e}^{u} \\
& \times \left\{\left[f_1 + f_3\frac{u}{\Delta\phi_2} + \cdots\right]\right. \\
& + \Delta\left[\omega_{1,5}\left(\frac{u}{\Delta\phi_2}\right)^2 + \omega_{1,7}\left(\frac{u}{\Delta\phi_2}\right)^3 + \cdots\right] \\
& + \Delta^2\left[\omega_{2,7}\left(\frac{u}{\Delta\phi_2}\right)^3 + \omega_{2,9}\left(\frac{u}{\Delta\phi_2}\right)^4 + \cdots\right] \\
& \left. + \cdots\right\} \mathrm{d}u,
\end{aligned}
\tag{26}
$$

We can now group these terms by the integrands' dependence on Δ:

$$
\begin{aligned}
I_{\mathrm{odd}}(\Delta) = {} & \frac{\mathrm{e}^{\Delta\phi_0}}{2\Delta\phi_2}\left(\Omega_0(\Delta) + \Omega_1(\Delta)\Delta^{-1}\right. \\
& \left. + \Omega_2(\Delta)\Delta^{-2} + \cdots\right),
\end{aligned}
\tag{27}
$$

where Ω_n — see Equation (40) — depends on Δ due to the lower limit of integration.

The even terms in $t - x_c$ are

$$
\begin{aligned}
I_{\mathrm{even}}(\Delta) = {} & \mathrm{e}^{\Delta\phi_0} \int_{t_0}^{x_c} \mathrm{e}^{\Delta\phi_2(t - x_c)^2} \\
& \times \left\{\left[f_2(t - x_c)^2 + f_4(t - x_c)^4 + \cdots\right]\right. \\
& + \Delta\left[\omega_{1,4}(t - x_c)^4 + \omega_{1,6}(t - x_c)^6 + \cdots\right] \\
& + \Delta^2\left[\omega_{2,8}(t - x_c)^8 + \omega_{2,10}(t - x_c)^{10} + \cdots\right] \\
& \left. + \cdots\right\} \mathrm{d}t.
\end{aligned}
\tag{28}
$$

Since $\phi_2 < 0$, choose $u = \sqrt{-\Delta\phi_2}(t - x_c)$. Then

$$
\begin{aligned}
I_{\mathrm{even}}(\Delta) = {} & \frac{\mathrm{e}^{\Delta\phi_0}}{\sqrt{-\Delta\phi_2}} \int_{\sqrt{-\Delta\phi_2}(t_0 - x_c)}^{0} \mathrm{e}^{-u^2} \\
& \times \left\{\left[f_2\left(\frac{u}{\sqrt{-\Delta\phi_2}}\right)^2 + f_4\left(\frac{u}{\sqrt{-\Delta\phi_2}}\right)^4 + \cdots\right]\right. \\
& + \Delta\left[\omega_{1,4}\left(\frac{u}{\sqrt{-\Delta\phi_2}}\right)^4 + \omega_{1,6}\left(\frac{u}{\sqrt{-\Delta\phi_2}}\right)^6 + \cdots\right] \\
& + \Delta^2\left[\omega_{2,8}\left(\frac{u}{\sqrt{-\Delta\phi_2}}\right)^8 + \omega_{2,10}\left(\frac{u}{\sqrt{-\Delta\phi_2}}\right)^{10} + \cdots\right] \\
& \left. + \cdots\right\} \mathrm{d}u.
\end{aligned}
\tag{29}
$$

Grouping these terms by the integrands' dependence on Δ yields

$$I_{\text{even}}(\Delta) = \frac{e^{\Delta\phi_0}}{\sqrt{-\Delta\phi_2}} \left(\Theta_1(\Delta)\Delta^{-1} + \Theta_2(\Delta)\Delta^{-2} + \Theta_3(\Delta)\Delta^{-3} + \cdots\right), \tag{30}$$

with Θ_n as shown in Equation (39).

Combining Equations (27,30) with $\phi_0 = -1$ (from Equation (36)) and Equation (5) gives the full asymptotic series for the burst size distribution as

$$
\begin{aligned}
\bar{D}(\Delta) &\sim \frac{\Delta^{\Delta-1}e^{-\Delta}}{\Delta!} \left[\frac{1}{2\Delta\phi_2}\left(\Omega_0(\Delta) + \Omega_1(\Delta)\Delta^{-1} + \cdots\right)\right. \\
&\left. + \frac{1}{\sqrt{-\Delta\phi_2}}\left(\Theta_1(\Delta)\Delta^{-1} + \Theta_2(\Delta)\Delta^{-2} + \cdots\right)\right] \\
&= \frac{\Delta^{\Delta-2}e^{-\Delta}}{\Delta!}\left(C_1(\Delta) + C_2(\Delta)\Delta^{-1/2}\right. \\
&\left. + C_3(\Delta)\Delta^{-1} + C_4(\Delta)\Delta^{-3/2} + \cdots\right).
\end{aligned}
\tag{31}
$$

Unfortunately, the "coefficients" C_n depend on Δ, and the terms in the asymptotic series must therefore be evaluated separately for each value of Δ. To do this evaluation, the relations between the various coefficients that have been introduced in the series expansions are needed.

A. Coefficient expressions

To define the coefficients from the asymptotic series expansion, use

$$
\begin{aligned}
A_n(\Delta, t_0) &\equiv \int_{\Delta\phi_2(t_0-x_c)^2}^{0} du\ e^u u^n \\
B_n(\Delta, t_0) &\equiv \int_{\sqrt{-\Delta\phi_2}(t_0-x_c)}^{0} du\ e^{-u^2} u^{2n}
\end{aligned}
\tag{32}
$$

for the integrals that will show up in the expressions.

1. Definition of f

To determine the coefficients f_n, expand Equation (18) around $a = 1$:

$$f(t) = p(t)\left[(1-a) + (1-a)^2 + (1-a)^3 + \cdots\right]. \tag{33}$$

Then Taylor expand $a(t)$ and $p(t)$ around x_c as $a(t) = 1 + a_1(t - x_c) + a_2(t - x_c)^2/2 + \cdots$ and $p(t) = p_0 + p_1(t - x_c) + p_2(t - x_c)^2/2 + \cdots$, where $a_n \equiv a^{(n)}(x_c)$ and $p_n \equiv p^{(n)}(x_c)$ are the nth derivatives of $a(t)$ and $p(t)$ evaluated at x_c. Comparison with Equation (21) gives

the relation

$$
\begin{aligned}
f_n &= \sum_{m=0}^{n-1} \frac{p_m}{m!} \sum_{l=1}^{n-m} (-1)^l l! \\
&\times \sum_{\substack{\sum_{i=1}^{\infty} k_i = l \\ \sum_{i=1}^{\infty} i k_i = n-m}} \prod_{i=1}^{n-m-l+1} \frac{1}{k_i!}\left(\frac{a_i}{i!}\right)^{k_i},
\end{aligned}
\tag{34}
$$

where $n \geq 1$ since $f_0 = 0$, and $k_i \in \mathbb{N}$.

2. Definition of ϕ

To determine ϕ_n, expand Equation (19) around $a = 1$:

$$\phi(t) = -1 - \frac{(1-a)^2}{2} - \frac{(1-a)^3}{3} - \frac{(1-a)^5}{4} - \cdots. \tag{35}$$

Then expand $a(t) = 1 + a_1(t - x_c) + a_2(t - x_c)^2/2 + \cdots$ in the above equation. Comparison with Equation (21) gives

$$
\begin{aligned}
\phi_0 &= -1 \\
\phi_1 &= 0 \\
\phi_n &= -\sum_{m=2}^{n} \frac{(-1)^m}{m} \sum_{\substack{\sum_{i=1}^{\infty} k_i = m \\ \sum_{i=1}^{\infty} i k_i = n}} m! \\
&\times \prod_{i=1}^{n-m+1} \frac{1}{k_i!}\left(\frac{a_{(i)}}{i!}\right)^{k_i},
\end{aligned}
\tag{36}
$$

where $n \geq 2$ and $k_i \in \mathbb{N}$.

3. Definition of ξ

From Equation (23) we get

$$\xi_{n,m} = \sum_{\substack{\sum_{i=3}^{\infty} k_i = n \\ \sum_{i=3}^{\infty} i k_i = m}} \prod_{i=3}^{m-3n+3} \frac{\phi_i^{k_i}}{k_i!}, \tag{37}$$

where $n \geq 1$, $m \geq 3n$, and $k_i \in \mathbb{N}$.

4. Definition of ω

Comparing Equation (24) with Equations (25,28) yields

$$\omega_{n,m} = \sum_{i=3n}^{m-1} f_{m-i}\xi_{n,i}, \tag{38}$$

where $n \geq 1$ and $m \geq 3n + 1$.

By examining the expressions in Equations (29,30) we see that the coefficients $\Theta_n(\Delta)$ are

$$\Theta_n(\Delta) = \frac{f_{2n}B_n(\Delta, t_0)}{(-\phi_2)^n} + \sum_{i=1}^{2n-1} \frac{B_{n+i}(\Delta, t_0)}{(-\phi_2)^{n+i}}\omega_{i,2(n+i)}, \tag{39}$$

with $n \geq 1$ and B_n from Equation (32). Similarly, from Equations (26,27) we get

$$\Omega_n(\Delta) = \frac{f_{2n+1}A_n(\Delta, t_0)}{\phi_2^n} + \sum_{i=1}^{2n} \frac{A_{n+i}(\Delta, t_0)}{\phi_2^{n+i}}\omega_{i,2(n+i)+1}, \tag{40}$$

with $n \geq 0$ and A_n from Equation (32).

6. Definition of C

From Equation (31), we get

$$C_{2n-1}(\Delta) = \frac{\Omega_{n-1}(\Delta)}{2\phi_2}$$
$$C_{2n}(\Delta) = \frac{\Theta_n(\Delta)}{\sqrt{-\phi_2}}, \tag{41}$$

where $n \geq 1$.

B. Crossover

We know from Equation (4) that around Δ_c, the burst distribution contains a crossover from $\Delta^{-3/2}$ to $\Delta^{-5/2}$ behavior. Does Equation (31) reproduce this? The first term in the series is

$$C_1(\Delta)\frac{\Delta^{\Delta-2}e^{-\Delta}}{\Delta!} \approx \frac{\Omega_0(\Delta)}{2\sqrt{2\pi}\phi_2}\Delta^{-5/2}$$
$$= \frac{f_1 A_0(\Delta, t_0)}{2\sqrt{2\pi}\phi_2}\Delta^{-5/2}. \tag{42}$$

Using the Stirling approximation $\Delta! \approx \sqrt{2\pi}\Delta^{\Delta+1/2}e^{-\Delta}$ and inserting for f_1, $A_0(\Delta, t_0)$, and ϕ_2 from Equations (32,34,36) gives

$$C_1(\Delta)\frac{\Delta^{\Delta-2}e^{-\Delta}}{\Delta!} \approx \frac{-p_0 a_1}{2\sqrt{2\pi}\phi_2}\Delta^{-5/2}\int\limits_{\Delta\phi_2(t_0-x_c)^2}^{0} e^u du$$
$$= C\Delta^{-5/2}\left(1 - \exp\left[-\Delta/\Delta_c\right]\right),$$
$$(43)$$

where $C = (2\pi)^{-1/2}x_c p_0(2p_0 + x_c p_1)^{-1}$ is the same as in Equation (3) and $\Delta_c = 2a_1^{-2}(x_c - t_0)^{-2} = 4\pi C^2 p_0^2(x_c - t_0)^{-2}$ is the same as in Equation (4).

The first term of the asymptotic series is exactly Equation (4), and the asymptotic series therefore reproduces the known crossover behavior in the limit $\Delta \to \infty$.

V. APPROXIMATION FOR SMALL BURSTS

The asymptotic expansion in Equation (31) is done in the limit of infinitely large bursts, and one should not expect the series to give a perfect approximation of $\bar{D}(\Delta)$ when Δ is finite. In general, the infinite series might not converge for finite Δ. However, one can still use the asymptotic series to find an approximation for $\bar{D}(\Delta)$ for small Δ.

A. Optimal approximation for finite burst size

For a finite Δ we use the general procedure outlined by Bender and Orzag [9]:

First chose a fixed value of Δ. Then locate the smallest term (in absolute value) of the asymptotic series in Equation (31), $C_m(\Delta)\Delta^{\Delta-2-(m-1)/2}e^{-\Delta}/\Delta!$. When summing the series up to (but not including) a certain term, then that term gives a measure of the error from the exact result [9]. Hence, we sum the asymptotic series up to (but not including) the smallest term, so that we get the smallest possible error estimate. If term number m is the smallest one, the optimal approximation is

$$\bar{D}(\Delta) \approx \sum_{i=1}^{m-1} C_i(\Delta)\frac{\Delta^{\Delta-2-(i-1)/2}e^{-\Delta}}{\Delta!}. \tag{44}$$

Note that this method is applicable even when the infinite asymptotic series does not converge. The caveat is that it has to be done separately for each value of Δ where we wish to approximate the burst distribution.

There is a practical limit to how many terms from Equation (31) one can calculate. The smallest term m must be chosen among the terms that are calculated. Hence we cannot guarantee that the smallest term we find is the smallest one in the entire infinite series. If it is not, then the accuracy of the approximation will be reduced.

Truncating the series at the smallest term does not necessarily give the best approximation. For certain values of Δ there will exist better choices of truncation. However, Equation (44) provides the method with the best *guaranteed* error without a priori knowledge of the burst distribution.

B. Comparison with exact result

To test the accuracy of Equation (44) we compare it with the exact result from Equation (14) for the Weibull distribution. This is easier than relying on simulatons, as both expressions are derived in the limit $N \to \infty$ where there are no finite size effects.

We have calculated the first 13 terms of Equation (31) for $\Delta \leq 400$. With this limitation of 13 terms, we use Equation (44) to calculate the optimal approximation. For a Weibull distribution with $k = 1$ and $t_0 = 0$, Figure 2 shows this approximation and the exact result from Equation (14), with the corresponding relative error in Figure (3).
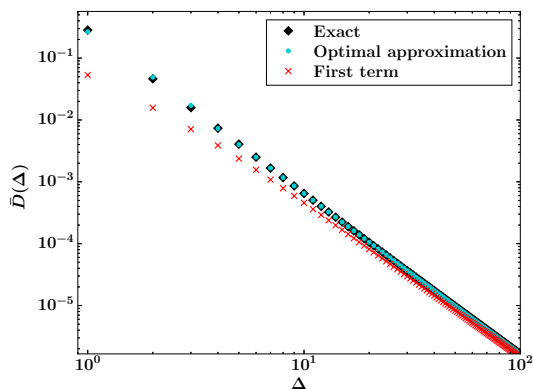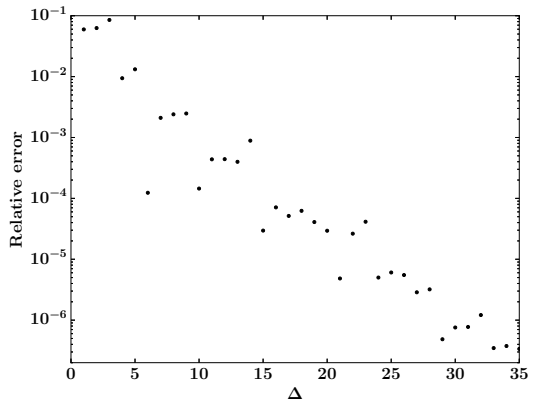

FIG. 3. Relative error for the optimal approximation from Equation (44) (with 13 available terms) for a Weibull threshold distribution with $k = 1$ and $t_0 = 0$.
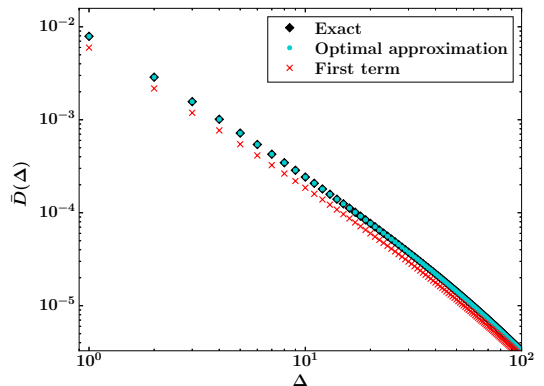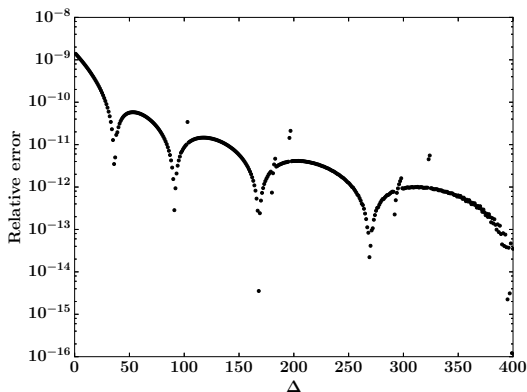

FIG. 2. Optimal approximation from Equation (44) with 13 available terms (turquoise) and exact result (black) for the burst distribution. The first term of the asymptotic series (red) is shown for comparison. The threshold distribution is Weibull with $k = 1$ and $t_0 = 0$.

FIG. 4. Optimal approximation from Equation (44) with 13 available terms (turquoise) and exact result (black) for the burst distribution. The first term of the asymptotic series (red) is shown for comparison. The threshold distribution is Weibull with $k = 1$ and $t_0 = 0.8$.

The first term, which corresponds to Equation (4), is almost an order of magnitude off for $\Delta = 1$, whereas the optimal approximation gives a relative error smaller than 10%. For most burst sizes, the relative error of the optimal approximation is smaller than 1%. These errors are mainly because 13 terms is not sufficient to give high accuracy for the smallest values of Δ for this threshold distribution.

With 13 terms, we can achieve higher accuracy with other parameters. For a Weibull distribution with $k = 1$ and $t_0 = 0.8$ we show the exact solution and optimal approximation in Figure 4, and the corresponding relative error in Figure 5. The optimal approximation is again noticeably better than Equation (4); the accuracy is excellent, with relative error smaller than 10^{-8} even for $\Delta = 1$. In this case, the small relative error indicates that 13 terms is sufficient to find the smallest term in the asymptotic series.

VI. DISCUSSION AND CONCLUSION

In the equal load sharing fiber bundle model, we have solved the burst size distribution analytically for all Weibull threshold distributions, Equation (14). This is a significant improvement over previous results, which described the asymptotic behavior for infinite burst size.

The exact result is impractical to use for large burst sizes Δ, but can easily be evaluated for small Δ. In this sense it complements the existing asymptotic result; Equation (14) can be used for small Δ, and for suffi-

FIG. 5. Relative error for the optimal approximation from Equation (44) (with 13 available terms) for a Weibull threshold distribution with $k = 1$ and $t_0 = 0.8$.

ciently large Δ we can use Equation (4) instead. Together, these results provide a highly accurate way to calculate the burst size distribution for Weibull threshold distributions.

For other threshold distributions where the burst distribution cannot be solved exactly, another method is needed to calculate the burst distribution for small Δ. We have therefore derived the full asymptotic series expansion for the burst size distribution, Equation (31). Even if the full infinite series is valid only in the limit $\Delta \to \infty$, it can still be used to find approximations for small Δ through Equation (44).

The accuracy of this optimal asymptotic approximation depends on the threshold distribution and the number of calculated terms used for the optimal approximation. With 13 terms, the relative error ranges from several percent to $\sim 10^{-9}$ for the smallest bursts, but even the worst case gives much better approximations than Equation (4).

ACKNOWLEDGMENTS

[1] Peirce FT. 32—X.—Tensile tests for cotton yarns v.—"The Weakest Link" Theorems on the strength of long and of composite specimens. *J Text Inst.* (1926) **17**:T355–68. doi: 10.1080/19447027.1926.10599953

[2] Daniels HE. The statistical theory of the strength of bundles of threads. I. *Proc Roy Soc A.* (1945) **183**:405–35. doi: 10.1098/rspa.1945.0011

[3] Pradhan S, Hansen A, Chakrabarti BK. Failure processes in elastic fiber bundles. *Rev Mod Phys.* (2010) **82**:499–555. doi: 10.1103/RevModPhys.82.499

[4] Hansen A, Hemmer PC, Pradhan S. *The Fiber Bundle Model.* Berlin: Wiley-VCH (2015).

[5] Bouchaud JP. Econophysics: still fringe after 30 years? *Europhysics News.* (2019) **50**:24–7. doi: 10.1051/epn/2019103

[6] Pradhan S, Hansen A, Hemmer PC. Crossover behavior in burst avalanches: signature of imminent failure. *Phys Rev Lett.* (2005) **95**:125501. doi: 10.1103/PhysRevLett.95.125501

[7] Hemmer PC, Hansen A. The distribution of simultaneous fiber failures in fiber bundles. *J Appl Mech.* (1992) **59**:909–14. doi: 10.1115/1.2894060

[8] Pradhan S, Hansen A, Hemmer PC. Crossover behavior in failure avalanches. *Phys Rev E.* (2006) **74**:016122. doi: 10.1103/PhysRevE.74.016122

[9] Bender CM, Orszag SA. *Advanced Mathematical Methods for Scientists and Engineers: Asymptotic Methods and Perturbation Theory.* New York: Springer (1999).

Article III

Can Local Stress Enhancement Induce Stability in Fracture Processes?
Part I: Apparent Stability

Article III

Article III

Can Local Stress Enhancement Induce Stability in Fracture Processes? Part I: Apparent Stability

Jonas T. Kjellstadli*, Eivind Bering, Martin Hendrick, Srutarshi Pradhan and Alex Hansen

PoreLab, Department of Physics, NTNU – Norwegian University of Science and Technology, Trondheim, Norway

By comparing the evolution of the local and equal load sharing fiber bundle models, we point out the paradoxical result that stresses seem to make the local load sharing model stable when the equal load sharing model is not. We explain this behavior by demonstrating that it is only an *apparent stability* in the local load sharing model, which originates from a statistical effect due to sample averaging. Even though we use the fiber bundle model to demonstrate the apparent stability, we argue that it is a more general feature of fracture processes.

Keywords: fiber bundle model, material failure, crack growth, local load sharing, fracture localization

1. INTRODUCTION

The stability of materials against fracture is essential for our civilization. We need to be able to trust that buildings, bridges, airplanes, ships, etc. do not collapse. To prevent the collapse of structures, one needs to understand the processes that constitute fracture. Fracture has been studied by the engineering and materials science communities for a very long time [1]. Only over the last 30 years, it has also entered physics [2]. Within the physics approach to fracture, there has been an emphasis on the role of disorder and fluctuations [3, 4].

We may summarize the physics of fracture in a heterogeneous brittle materials as follows: The material heterogeneity implies that both the local strength of the material and the stress field it is experiencing are themselves heterogeneous. Fractures may occur and develop as a result of either the material being locally weak or locally under high stress. Applying a sufficiently large load to a material, the fracture process will start by the material failing where it is weakest. The ensuing microcracks will induce high stresses at the crack tips. If these are sufficiently high, the microcracks will grow. Hence, a competition between stress enhancement due to developing microcracks and local material weakness breaks out [3–5]. At some point, the stress intensity at the crack tips has become so large that the local material weakness is no longer able to compete and catastrophic failure sets in: a macroscopic crack develops.

Essential in this summary is the opposite roles played by heterogeneity and stress enhancement: the heterogeneity stabilizes the fracture process whereas the stress enhancement destabilizes it. In this paper we demonstrate that stress enhancement may seemingly have the *opposite* effect, i.e., it stabilizes the fracture process. This is a situation which essentially turns upside down common wisdom within the physics community on how fracture processes proceed.

It turns out, however, that this paradoxical behavior is an apparent effect caused by the fluctuations that occur during the fracture process. We use the fiber bundle model [6–8] to demonstrate the *apparent stability* and its explanation. We consider two variants of the model: the *equal load sharing* (ELS) model [9] where there is local heterogeneity but no local stress

enhancement, and the *local load sharing* (LLS) model [10] where there is a competition between local stress enhancement and local heterogeneity. Even though we use the fiber bundle model as a tool to demonstrate the apparent stability, we argue that the effect is more general. The lesson to be learned is the following: even though the average stress vs. strain curve may have a positive slope, seemingly indicating stability, the positive slope is not necessarily caused by stability, but by the evolution of the fluctuations biasing the average in a way that makes the slope positive.

However, there also exists a real effect where the local stress enhancement of the LLS model can make it more stable than the ELS model. This shielding effect—its origins and consequences—is the subject of Part II [11].

There are two main sources of fluctuations in dynamical systems such as materials failing under stress [12, 13]: one comes from statistical fluctuations of the probability distributions that define intrinsic properties of the system elements. Another type of fluctuations arises as a result of the system dynamics depending on the spatial structures. The first type of fluctuation has a direct relation with the system size and it normally disappears as the system size diverges due to self averaging. One can minimize the effect of these fluctuations either by making the system size larger or by increasing the number of samples. On the other hand, the dynamics-dependent fluctuations do not disappear with increasing size. It is therefore crucial to know the nature of this second type of fluctuations and its role during the entire evolution dynamics. It is this second type of fluctuations that is the cause of the apparent stability.

2. THE FIBER BUNDLE MODEL

A fiber bundle consists of N fibers placed between two clamps. The fibers act as Hookean springs with identical spring constants κ up to an extension threshold t_i, individual for each fiber i, where they fail and cannot carry a load any more. Hence the connection between the extension x of a fiber i and the force f_i it carries is

$$f_i = \begin{cases} \kappa x & \text{if } x < t_i, \\ 0 & \text{if } x \geq t_i. \end{cases} \tag{1}$$

The thresholds t_i are drawn from a probability density $p(t)$, with corresponding cumulative probability $P(t) = \int_0^t p(u)\mathrm{d}u$.

2.1. Equal Load Sharing

In the ELS model an externally applied force F is distributed equally on all the intact fibers. This means that fibers fail in order of increasing thresholds as the force F increases. The force per fiber $\sigma = F/N$ required to give the bundle an extension x is on average [8]

$$\sigma(x) = \kappa \left(1 - P(x)\right) x. \tag{2}$$

Equivalently,

$$\sigma(k) = \kappa \left(1 - \frac{k}{N}\right) P^{-1} \left(\frac{k}{N}\right), \tag{3}$$

since $P(x)$ is the fraction of broken fibers k/N—also called the damage d—at extension x [14]. The fluctuations around this average are of the first type, and disappear as $N^{-1/2}$ when $N \to \infty$ [8].

The *load curve* is the smallest force per fiber σ required to break the next fiber. Hence, we plot either this minimum σ as a function of the extension x or the fraction of broken fibers k/N (see **Figure 1**). When plotted against the extension x, the load curve is the stress-strain curve. Equations (2) and (3) give the average load curve for ELS. We will use the terminology that a fiber bundle is *locally stable* if the load σ must be increased to continue breaking more fibers, i.e., if the load curve is increasing. From Equation (2) we determine the critical extension x_c at which the ELS model becomes unstable by setting $\mathrm{d}\sigma/\mathrm{d}x|_{x_c} = 0$. For a general Weibull threshold distribution

$$P(t) = 1 - \exp(-t^\beta + t_0^\beta) \tag{4}$$

with shape parameter β and lower cut-off t_0 ($t \geq t_0$), this gives $x_c = \beta^{-1/\beta}$. This means that the ELS model is unstable from the beginning of the failure process when $t_0 \geq \beta^{-1/\beta}$.

2.2. Local Load Sharing

In the LLS model, the loads originally carried by broken fibers are carried by their nearest intact neighbors only. Hence there is a spatially dependent stress field. A *hole* is a cluster (in the percolation sense) of h failed fibers joined through nearest neighbor connections. The *perimeter* of a hole is the set of p intact fibers that are nearest neighbors of the hole. With these definitions the force acting on an intact fiber i with the LLS model is given by

$$f_i = \sigma \left(1 + \sum_j \frac{h_j}{p_j}\right), \tag{5}$$

where j runs over the set of holes that neighbor fiber i. The first term is the force originally applied to every fiber, while the second is the redistribution of forces due to failed fibers. Equation (5) is completely general, and can be used for any lattice and dimensionality, or even for random graphs.

To determine which fiber breaks next under an external load we define the *effective threshold* $t_{\mathrm{eff},i}$ of fiber i as

$$t_{\mathrm{eff},i} = \frac{t_i}{1 + \sum_j \frac{h_j}{p_j}}. \tag{6}$$

The breaking criterion of fiber i is then $\sigma = \kappa t_{\mathrm{eff},i}$, and the fiber with the smallest effective threshold will fail under the smallest applied load σ.

3. DETERMINING STABILITY

The LLS model contains stress enhancement in that fibers belonging to the perimeters of holes carry more load than corresponding fibers in the ELS model. Therefore, the results in **Figure 1**—where we show the load curves (σ vs. k/N) of the

ELS and LLS model based on the Weibull threshold distribution from Equation (4) with $\beta = t_0 = 1$—are surprising. The ELS load curve is unstable for all values of k/N (as indicated by the negative slope) because $t_0 = x_c$, but there is a region for which the sample averaged LLS load curve has a positive slope, which seems to indicate local stability. This was first pointed out by Sinha et al. [15].

Our explanation of this paradoxical behavior lies in the difference between single samples and sample averages. Stability is a property of individual samples, not the average behavior. In the ELS model there is no difference between the two, since fluctuations around the sample averaged load curve are of the first type and disappear as $N \to \infty$. But the LLS model has fluctuations of the second type—they persist in the limit of infinitely large systems—and we must therefore study individual samples to determine when systems are stable.

We argue that in the LLS model, the stability of single samples, both global and local, is determined by the upper bounding curve of the force fluctuations. We show in **Figure 1** how the density ρ of these fluctuations are distributed around the averaged load curve for the LLS model. In any finite, but small, damage interval $[k/N, k/N + \Delta]$ there will be at least one strong fiber that requires a load σ close to the upper bounding curve to break. For a system to be locally stable, consecutive intervals must require higher loads to break, i.e., the bounding curve of the fluctuations must increase. We see in **Figure 1** that it does not. Hence, there is no local stability for the LLS model either, as expected.

Are other averages than the arithmetic mean more representative of individual samples? In the field of Anderson localization [16], the average conductance differs vastly between different averaging procedures [17], and the arithmetic mean is

not representative of typical single samples. We therefore show both the arithmetic, geometric, and harmonic mean of the LLS model in **Figure 1**. The three means all give qualitatively similar behavior, and all of them fail to represent the behavior of single samples. Hence we will from now on use $\langle \sigma \rangle$ for the arithmetic mean $\langle \sigma \rangle_A$, which is a suitable representative for the three means when computing sample averages.

4. APPARENT STABILITY

The *apparent* local stability in **Figure 1** is caused by the sharp decline in fluctuations smaller than the average in a damage region around the site percolation threshold $p_c \approx 0.59$ [18] of the square lattice.

The fluctuations are initially heavily biased with a large concentration below the average. Around the percolation threshold, the bias in the fluctuations begins to shift rapidly from small values of σ to the upper bounding curve, and this shift is enough to make the average load curve increase even though the upper bounding curve is decreasing. This is supported by **Figure 2**, which shows the averaged LLS load curve and its standard deviation.

We now consider a uniform threshold distribution on $[t_0, 1]$:

$$P(t) = \frac{t - t_0}{1 - t_0}, \quad (7)$$

which gives a critical extension $x_c = 1/2$. The ELS model with this distribution is hence unstable from the beginning of the breaking process if $t_0 \geq 1/2$. We choose $t_0 = 1/2$ for a comparable situation to the Weibull distribution studied earlier.
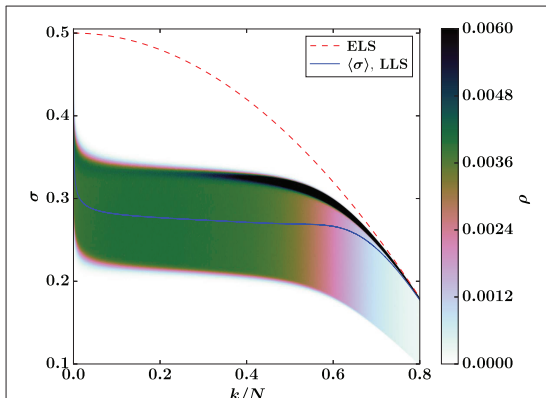
The averaged load curves for LLS and ELS with the threshold distribution from Equation (7) are shown in **Figure 3**, together with the density of fluctuations around the LLS load curve. The upper bounding curve of the LLS force fluctuations
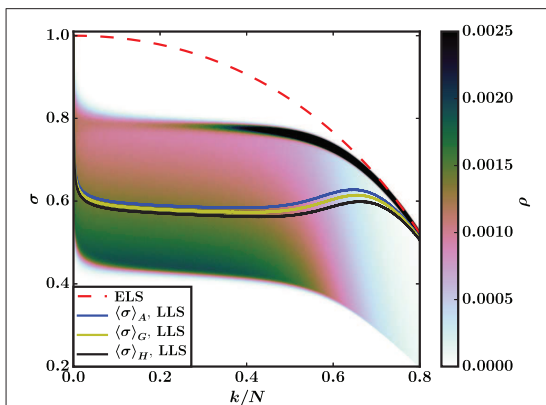
FIGURE 1 | Load curves for the ELS and LLS models with a Weibull threshold distribution $P(t) = 1 - \exp(-t + 1)$, Equation (4) with $\beta = t_0 = 1$. The ELS curve is Equation (3), whereas the LLS curves are sample averages—arithmetic mean $\langle \sigma \rangle_A$, geometric mean $\langle \sigma \rangle_G$, and harmonic mean $\langle \sigma \rangle_H$—from simulations on a square lattice ($N = 128^2$). The background is a color map that shows the density ρ of single sample LLS load curves for the 1.5×10^5 samples that the averages are based on. The color bar is capped at $\rho = 0.0025$ to highlight the fluctuations with the smallest values of σ.
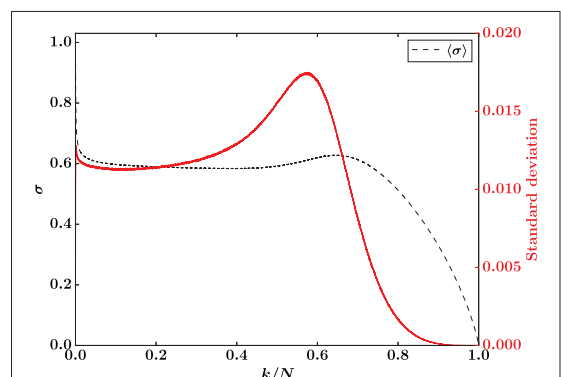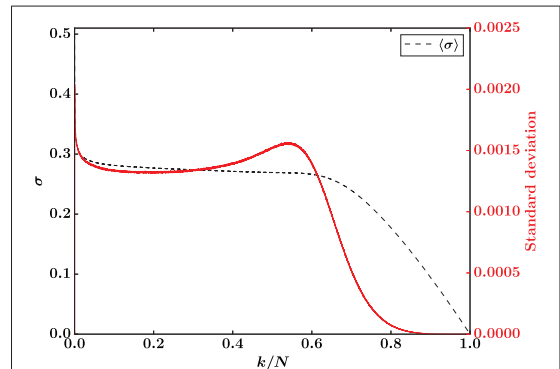

FIGURE 2 | Sample averaged load curve for the LLS model (black, left axis) and corresponding standard deviation (red, right axis) for a Weibull threshold distribution with $\beta = t_0 = 1$. Results are from simulations on a square lattice ($N = 128^2$) with 1.5×10^5 samples.

FIGURE 3 | Load curves for the ELS and LLS models with a uniform threshold distribution on [0.5, 1), Equation (7) with $t_0 = 1/2$. The ELS curve is Equation (3), whereas the LLS curve is a sample average from simulations on a square lattice ($N = 128^2$). The background is a color map that shows the density ρ of single sample LLS load curves for the 1.5×10^5 samples that the average is based on. The color bar is capped at $\rho = 0.006$ to highlight the fluctuations with the smallest values of σ.

FIGURE 4 | Sample averaged load curve for the LLS model (black, left axis) and corresponding standard deviation (red, right axis) for a uniform threshold distribution on [0.5, 1). Results are from simulations on a square lattice ($N = 128^2$) with 1.5×10^5 samples.

decreases for all damages k/N, indicating that the system is unstable throughout the breaking process also for this uniform threshold distribution.

In **Figure 3** there is a region around the percolation threshold where the fluctuations shift—similarly to how they change in **Figure 1** for the Weibull threshold distribution—corroborated by the standard deviation in **Figure 4**. In this case the fluctuations are not very biased to begin with, but distributed almost uniformly around the average. This—and the fact that the fluctuations span a smaller range of forces σ, as demonstrated by a standard deviation an order of magnitude smaller in **Figure 4** than in **Figure 2**—makes the shift of the fluctuations smaller than for the Weibull threshold distribution, and it is not enough to make the averaged load curve increase as a function of damage.

The averaged LLS load curve does not show any apparent stability for the uniform distribution, but the underlying effect—that the distribution of the force fluctuations changes rapidly in a region around the percolation threshold—that causes the apparent stability for the Weibull distribution is still present, as shown by the color map in **Figure 3**.

The changing fluctuations around the percolation threshold can be understood by examining the hole structure of the LLS fiber bundle as the damage increases. When only a few fibers have broken the breaking process localizes around a single hole, which starts expanding and keeps growing until the entire fiber bundle has broken [19]. This growth process is illustrated in **Figure 5** for the Weibull threshold distribution and **Figure 6** for the uniform threshold distribution.

Fibers that break after the localization sets in are in the perimeter of the growing hole. Since there are almost no other holes, (nearly all) perimeter fibers get the same contribution

to effective threshold from the hole structure (Equation 6), and therefore the fiber that breaks next is the perimeter fiber with the smallest threshold. This results in a breaking process that is similar to invasion percolation where the weakest neighboring fiber is "invaded" by the hole every time a fiber breaks.

Hole and perimeter sizes of the growing hole are similar in different samples. Hence the force fluctuations in **Figures 1**, **3** mainly represent the distribution (over samples) of the smallest threshold in the perimeter of the hole. It follows that the lower end of the fluctuations are due to the hole encountering new fibers with small thresholds as it expands. These fibers break quickly—they are likely to have the smallest threshold among the perimeter fibers—while the stronger fibers in the perimeter survive.

The lower end of the fluctuations disappear rapidly around the percolation threshold because the growing hole has permeated most of the lattice, and therefore has few new areas to expand into, as shown in **Figures 5**, **6**. As a result, there are few new neighborhoods to expand into to find new neighbors with small thresholds. This mechanism radically changes the distribution of force fluctuations, so that the sample averaged load curve increases in **Figure 1** even though individual samples are all locally unstable.

4.1. The Effect of the Lattice

The above reasoning does not hinge on the lattice being square, and should be valid for any lattice. We therefore expect that the same Weibull threshold distribution will give similar results for the LLS model on other lattices: the sample averaged load curve should increase around the site percolation threshold due to the shift in bias as the lower end of the fluctuations disappear. We show averaged LLS load curves for four lattices in 2D, 3D, and 4D for the Weibull threshold distribution in **Figure 7**. The figure shows positive slopes of the load curves for
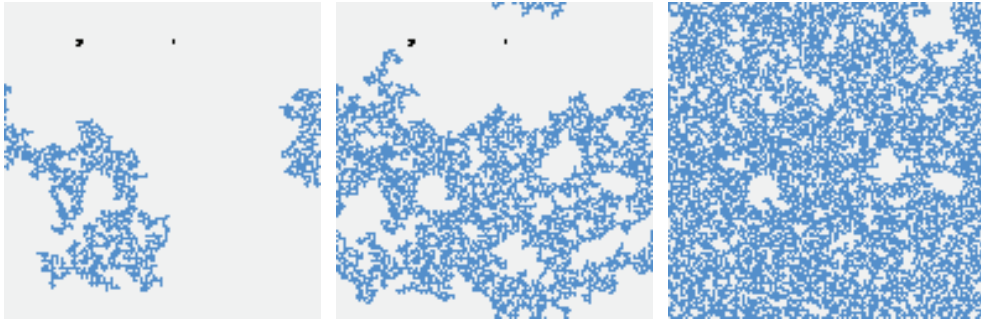
FIGURE 5 | Hole structure of a square lattice ($N = 128^2$) LLS fiber bundle with the Weibull threshold distribution $P(x) = 1 - \exp{(-x + 1)}$ at three different damages: $k/N = 0.1$ (left), $k/N = 0.3$ (middle), and $k/N = 0.59$ (right). Intact fibers are light gray, the largest hole is blue, and other broken fibers are black. From early on in the breaking process a single hole is growing continually.
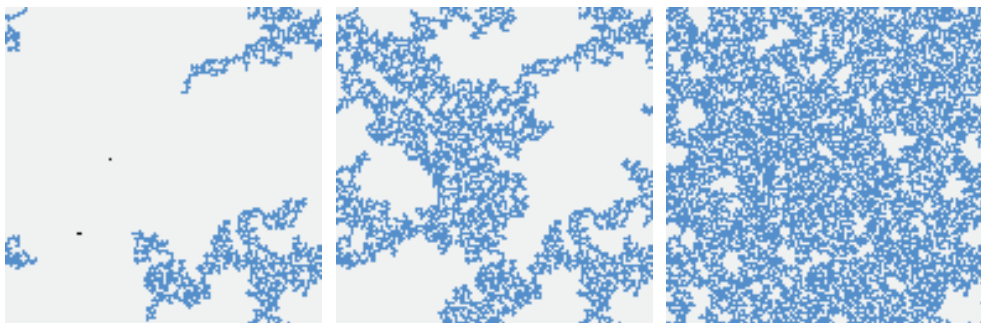
FIGURE 6 | Hole structure of a square lattice ($N = 128^2$) LLS fiber bundle with a uniform threshold distribution on [0.5, 1] at three different damages: $k/N = 0.1$ (left), $k/N = 0.3$ (middle), and $k/N = 0.59$ (right). Intact fibers are light gray, the largest hole is blue, and other broken fibers are black. From early on in the breaking process a single hole is growing continually.

all four lattices in a region around the corresponding percolation threshold, in accordance with the above argument. In all of these cases, individual samples are locally unstable, showing that the sample averaged load curve cannot be trusted as an indicator of local stability.

4.2. Apparent Stability in Globally Stable Systems

From the examples presented so far, it could be argued that the effect we describe is less relevant because it occurs in systems that are unstable once the breaking process starts. Let us therefore investigate a common threshold distribution where the systems are stable to begin with: the uniform distribution on [0, 1].

Figure 8 shows the density ρ of force fluctuations and the corresponding sample averaged load curve for this uniform threshold distribution with LLS on a square lattice. Again the lower end of the fluctuations disappear in a region around the percolation threshold, which makes the sample average increase.
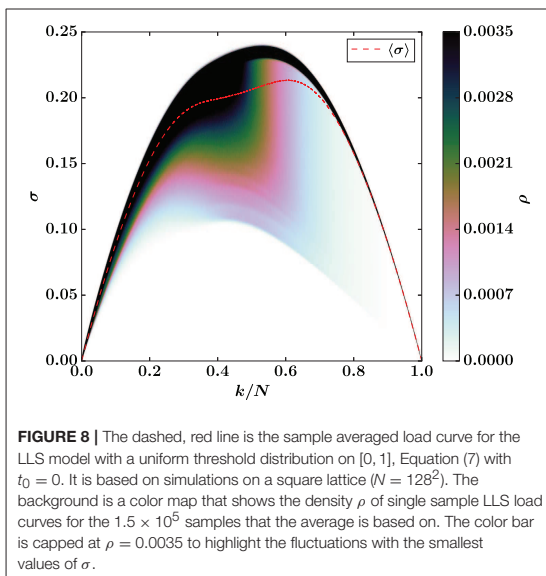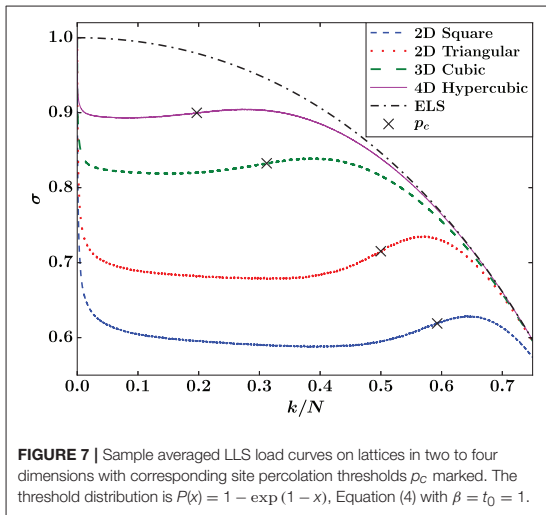
Due to this effect, the averaged load curve has its maximum at $k/N \simeq 0.607$, whereas the maxima of individual load curves are distributed around a median damage $k/N \simeq 0.533$. The difference between these two maxima is clearly seen in **Figure 8**.

In the intermediate region, the sample averaged load curve indicates stability—via its positive slope—when the fiber bundles are actually unstable. Hence, it cannot be trusted as an indicator of global stability. In general, stability—both local and global—is a property of individual samples that cannot be inferred from sample averages.

4.3. The Shielding Effect

Note that the ELS model becomes unstable at $k/N = 1/2$ for the uniform threshold distribution on [0, 1], which means that the LLS model, surprisingly, collapses later than the ELS model. This is due to a shielding effect that also has its origins in the geometry of the underlying lattice, but is otherwise unrelated to the statistical effect we have presented here. We discuss this at length in Part II [11].

FIGURE 7 | Sample averaged LLS load curves on lattices in two to four dimensions with corresponding site percolation thresholds p_c marked. The threshold distribution is $P(x) = 1 - \exp(1 - x)$, Equation (4) with $\beta = t_0 = 1$.

FIGURE 8 | The dashed, red line is the sample averaged load curve for the LLS model with a uniform threshold distribution on $[0, 1]$, Equation (7) with $t_0 = 0$. It is based on simulations on a square lattice ($N = 128^2$). The background is a color map that shows the density ρ of single sample LLS load curves for the 1.5×10^5 samples that the average is based on. The color bar is capped at $\rho = 0.0035$ to highlight the fluctuations with the smallest values of σ.

5. IMPLICATIONS FOR OTHER MODELS

The ELS and LLS models are the two extremes of load sharing, and other models, like the γ-model [20] or the soft clamp fiber bundle model [21], should exhibit behavior and phenomena somewhere between ELS and LLS. Intermediate load sharing rules can have infinite interaction ranges, but they should have finite *effective* ranges of interaction. The longer this interaction range, the more the model resembles ELS, and conversely, the shorter it is, the more the model resembles LLS.

With an effective range of interaction significantly smaller than the system size, a model is expected to contain the apparent stability and its underlying cause. Instead of a narrow perimeter where fibers break, there will be a *boundary layer* where fibers break, with width equal to the effective interaction range. Our argument for the disappearance of the lower end of the force fluctuations remains the same for such a model, except that it no longer happens around the percolation threshold. Instead, this effect occurs when the boundary layer permeates most of the lattice, and cannot expand into new areas to find weak fibers.

Note that for intermediate effective interaction ranges, this effect may be less pronounced than in the LLS model, but it should still be present. Therefore, the apparent stability presented here and its explanation should be considered a general feature of brittle fracture processes in disordered materials.

6. CONCLUSION

We have demonstrated a general mechanism resulting in the average force not being a reliable indicator of stability during fracture processes with local stress enhancement due to bias in the fluctuations around the average. We find that for several threshold distributions in the fiber bundle model, this mechanism gives an apparent stability, the illusion of stability due to an increasing average force even though individual systems are not stable. This apparent stability occurs around the site percolation threshold of the lattice for the systems we have studied in two to four dimensions.

DATA AVAILABILITY

The datasets generated for this study are available on request to the corresponding author.

AUTHOR CONTRIBUTIONS

The idea and interpretation of the results were a collaborative effort of all the authors. JK did the simulations, data analysis, and wrote the first draft of the manuscript. All authors contributed to further manuscript editing and review.

REFERENCES

1. Lawn B. *Fracture of Brittle Solids*. Cambridge: Cambridge University Press (1993).

2. Herrmann HJ, Roux S. *Statistical Models for the Fracture of Disordered Media*. Amsterdam: North-Holland (1990).

3. Roux S, Hansen A. Early stages of rupture of disordered materials. *EuroPhys Lett.* (1990) **11**:37–42. doi: 10.1209/0295-5075/11/1/007

4. Chakrabarti BK, Benguigui LG. *Statistical Physics of Fracture and Breakdown in Disordered Solids*. Oxford: Oxford University Press (1997).

5. Bonamy D, Bouchaud E. Failure of heterogeneous materials: a dynamic phase transition? *Phys Rep.* (2011) **498**:1–44. doi: 10.1016/j.physrep.2010.07.006

6. Daniels HE. The statistical theory of the strength of bundles of threads. I. *Proc R Soc A.* (1945) **183**:405–35. doi: 10.1098/rspa.1945.0011

7. Pradhan S, Hansen A, Chakrabarti BK. Failure processes in elastic fiber bundles. *Rev Mod Phys.* (2010) **82**:499–555. doi: 10.1103/RevModPhys.82.499

8. Hansen A, Hemmer PC, Pradhan S. *The Fiber Bundle Model*. Berlin: Wiley-VCH (2015).

9. Peirce FT. 32—X.—Tensile tests for cotton yarns v.—"The Weakest Link" Theorems on the strength of long and of composite specimens. *J Text Inst.* (1926) **17**:T355–68. doi: 10.1080/19447027.1926.10599953

10. Harlow DG, Phoenix SL. The chain-of-bundles probability model for the strength of fibrous materials I: analysis and conjectures. *J Comp Mater.* (1978) **12**:195–214. doi: 10.1177/002199837801200207

11. Kjellstadli JT, Bering E, Pradhan S, Hansen A. Can local stress enhancement induce stability in fracture processes? Part II: the shielding effect. *arXiv[Preprint].arXiv:1904.11774* (2019). Available at: https://arxiv.org/abs/1904.11774 (accessed June 25, 2019).

12. Freidlin MI, Wentzell AD. *Random Perturbations of Dynamical Systems*. Berlin: Springer (2012).

13. Abaimov SG. *Statistical Physics of Non-Thermal Phase Transitions*. Berlin: Springer (2015).

14. Gumbel EJ. *Statistics of Extremes*. Mineola, NY: Dover (2004).

15. Sinha S, Kjellstadli JT, Hansen A. Local load-sharing fiber bundle model in higher dimensions. *Phys Rev E.* (2015) **92**:020401. doi: 10.1103/PhysRevE.92.020401

16. Anderson PW. Absence of diffusion in certain random lattices. *Phys Rev.* (1958) **109**:1492–505. doi: 10.1103/PhysRev.109.1492

17. Slevin K, Markoš P, Ohtsuki T. Reconciling conductance fluctuations and the scaling theory of localization. *Phys Rev Lett.* (2001) **86**:3594–7. doi: 10.1103/PhysRevLett.86.3594

18. Stauffer D, Aharony A. *Introduction to Percolation Theory*. London: Taylor and Francis (1992).

19. Bering E. *On the stability of the local load sharing fiber bundle model* (Masters thesis). Norwegian University of Science and Technology, Trondheim (2016).

20. Hidalgo RC, Moreno Y, Kun F, Herrmann HJ. Fracture model with variable range of interaction. *Phys Rev E.* (2002) **65**:046148. doi: 10.1103/PhysRevE.65.046148

21. Batrouni GG, Hansen A, Schmittbuhl J. Heterogeneous interfacial failure between two elastic blocks. *Phys Rev E.* (2002) **65**:036126. doi: 10.1103/PhysRevE.65.036126

Article IV

Can Local Stress Enhancement Induce Stability in Fracture Processes?
Part II: The Shielding Effect

Article IV

Can Local Stress Enhancement Induce Stability in Fracture Processes? Part II: The Shielding Effect

Jonas T. Kjellstadli,[*] Eivind Bering,[†] Srutarshi Pradhan,[‡] and Alex Hansen[§]

PoreLab, Department of Physics, NTNU – Norwegian University of Science and Technology, Trondheim, Norway
(Dated: September 3, 2019)

We use the local load sharing fiber bundle model to demonstrate a shielding effect where strong fibers protect weaker ones. This effect exists due to the local stress enhancement around broken fibers in the local load sharing model, and it is therefore not present in the equal load sharing model. The shielding effect is prominent only after the initial disorder-driven part of the fracture process has finished, and if the fiber bundle has not reached catastrophic failure by this point, then the shielding increases the critical damage of the system, compared to equal load sharing. In this sense, the local stress enhancement may make the fracture process more stable, but at the cost of reduced critical force.

I. INTRODUCTION

When brittle materials fail mechanically under loading, the failure is the end point of a competition between local stress and local strength in the material. They pull in opposite directions [1]. When there is a local failure somewhere in the material, stresses increase at that location, which increases the likelihood that the subsequent failure happens in that neighborhood. One may say that stresses make local failures attract each other. Disorder in the strength of the material on the other hand, has the opposite effect. This is a purely statistical effect: the further away from the failure, the weaker the weakest spot in the material will be. Hence, the disorder drives local failures apart; they induce repulsion between the local failures.

When the damaged zones grow, the stresses at their edges increase and at some point, the repulsion induced by the disorder in the local strength is no longer able to counter this effect. When this occurs, catastrophic failure ensues. But this picture is not the whole story. We show in Figure 1 the stress σ as a function of the damage d for two fracture models: The equal load sharing (ELS) fiber bundle model (FBM) and the local load sharing (LLS) FBM [2, 3], to be described in Section II. The LLS model contains stress enhancement at the edge of the damaged zones, i.e., clusters of broken fibers, whereas the ELS model does not. As expected we see that the ELS model is stronger than the LLS model since the maximum value of σ is larger for this model than for the LLS model. However, one curious feature stands out in this figure: *The LLS model reaches its maximum value of σ for a higher damage d than the ELS model.* In other words, the LLS model where there is stress enhancement may sustain higher damage than the ELS model where there is no stress enhancement. We will show that this effect is due to *shielding* [4] of weak areas by strong areas.

———

[*] jonas.kjellstadli@outlook.com
[†] eivind.bering@ntnu.no
[‡] srutarshi.pradhan@ntnu.no
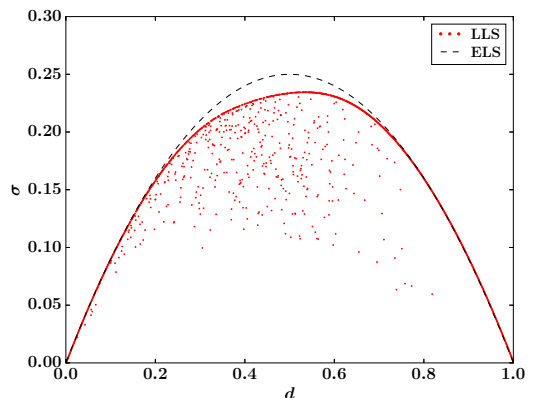[§] alex.hansen@ntnu.no

FIG. 1. Stress σ vs. damage d in the equal load sharing (ELS) fiber bundle model and the local load sharing (LLS) fiber bundle model on a square lattice. The ELS curve has been calculated analytically via equation (1), and the LLS result is a simulation of a single sample ($N = 2048^2$). For clarity, the LLS result shows only every 2500th data point. The threshold distribution is uniform on the unit interval for both models.

We discussed in Part I [5] a different mechanism that would lead to an *apparent* stability of the LLS model when the ELS model is unstable. This turned out to be a purely statistical effect coming from averaging over many samples. In Figure 1, we show only a single sample for the LLS model; there is no averaging. Hence, the shielding effect is a real effect that can be observed in single samples.

In Section II we describe the ELS and LLS fiber bundle models. We then go on in Section III to give a detailed explanation of the shielding effect in terms of the LLS model in one dimension. In Section IV we demonstrate that the shielding effect is sufficiently common to produce the effect already seen in Figure 1. In Section V we demonstrate two effects in the LLS model compared to the ELS model that we attribute to the shielding effect,

and Section VI deals with determining when the shielding effect is relevant. We end by summarizing and discussing our results in Section VII.

II. THE FIBER BUNDLE MODEL

We start by defining the Fiber Bundle Model [2, 3]. N elastic fibers with identical spring constants κ are placed between two clamps. In the simulations and results we will use $\kappa = 1$ for simplicity. The only effect of changing κ is to rescale the forces. A fiber i acts like Hookean spring, the force it carries given by $f_i = \kappa x$, for an elongation x smaller than its threshold t_i, which is individual for each fiber. When the elongation reaches the threshold, the fiber breaks irreversibly and cannot carry a force anymore. The thresholds are drawn from a probability distribution, denoted by the cumulative distribution $P(t)$, which is a parameter of the model. The number of broken fibers is denoted by k. Thus k/N is the fraction of broken fibers, also called the damage d. We use quasistatic loading of the model, where the load is increased until it is sufficient to break a single fiber, and then immediately lowered.

A. Equal Load Sharing

To determine what happens when fibers break, a load sharing rule is required. The simplest one is the ELS scheme [6, 7], also known as global load sharing, where every intact fiber shares the applied load equally. It corresponds to the clamps being infinitely stiff (as long as the spring constant κ is identical for the fibers). This means that there is no stress enhancement around the fibers that fail. A further consequence is that the fibers break in order of increasing thresholds as the applied force is increased, regardless of whether quasistatic loading is used.

With $k = NP(x)$ broken fibers at elongation x [8] and a total external force $F = N\sigma$, ELS results in the relation

$$\sigma = \kappa x \left(1 - P(x)\right) = \kappa P^{-1}(d)\left(1 - d\right) \qquad (1)$$

between the force per fiber σ required to break the next fiber and the elongation x (or the damage d) of the fiber bundle. Note that equation (1) is exact in the limit $N \to \infty$, but for finite system sizes there are fluctuations around this average behavior [3].

For nearly all choices of threshold distribution $P(t)$, equation (1) has a single maximum σ_c, the critical strength of the bundle, at which the fiber bundle collapses. There is a corresponding critical elongation x_c and critical damage $d_c = P(x_c)$. These quantities are also defined for local load sharing, which we will discuss next, but there they are not available from simple analytical expressions.

B. Local Load Sharing

A different load sharing rule is the LLS one [9], where the extra load from broken fibers is distributed equally onto the nearest intact neighbors in the lattice the fibers are placed on. As a consequence, LLS behaves differently when the underlying lattice changes. This is different from ELS, where fiber placement is irrelevant, since the load is assumed to be evenly distributed.

For LLS one must choose a lattice for fiber placement. A *hole* is then defined as a cluster of h broken fibers connected by nearest neighbor connections. The *perimeter* of a hole is the p intact fibers that are nearest neighbours of the hole. With an applied force per fiber $\sigma = F/N$, the force acting on an intact fiber i can then be expressed as

$$f_i = \sigma \left(1 + \sum_j \frac{h_j}{p_j}\right). \qquad (2)$$

Here j runs over holes neighboring the fiber. The two terms can be interpreted as respectively the force originally applied to every fiber, and the redistribution of forces due to broken fibers.

LLS was originally defined for a one-dimensional lattice with periodic boundary conditions [9], but the formulation in equation (2) is a generalization applicable to any lattice. We mainly study LLS on a two-dimensional square lattice in this paper. We also use periodic boundary conditions for the lattices we study.

Equation (2) is *history independent*: the breaking order of fibers does not affect the load redistribution. This is the way LLS was defined originally [9], but some later implementations have been history dependent, where the load a fiber carries is simply divided among its nearest neighbors when it breaks [10] making it impossible to determine the load a fiber carries without knowing the order in which the fibers up to that point have failed. In 1D this approach does not give very different results from the history independent model, since 1D LLS has zero critical damage and collapses due to extreme loads on fibers that neighbor large holes. However, in dimensions $D > 1$, the history dependent model gives very different results [11] from the history independent model [12].

To determine a failure criterion for individual fibers we define the *effective threshold* $t_{\text{eff},i}$ of fiber i as

$$t_{\text{eff},i} = \frac{t_i}{1 + \sum_j \frac{h_j}{p_j}}. \qquad (3)$$

The effective thresholds depend both on the original thresholds t_i of the fibers and the hole structure of the bundle, meaning that they change as the fiber bundle breaks down. By combining this expression with equation (2) we find the breaking criterion $\sigma = \kappa t_{\text{eff},i}$ where the fiber with the smallest effective threshold fails under the smallest external load σ.

Hence quasistatic loading results in a fracture process where the next fiber to break is always the one with the smallest effective threshold, given by equation (3). When a fiber is broken, effective thresholds must be updated to determine which fiber breaks next.

III.   DEFINING SHIELDING

Let us investigate a simple example in 1D to demonstrate what we mean by shielding. Consider $N = 10$ fibers with thresholds $\{t_i\} = \{0.1, 0.2, ..., 1.0\}$ arranged as follows:

$$1.0 \quad 0.1 \quad 0.2 \quad 0.9 \quad 0.8 \quad 0.3 \quad 0.7 \quad 0.5 \quad 0.6 \quad 0.4. \quad (4)$$

With ELS we find a critical strength $\sigma_{c,\text{ELS}} = 0.3\kappa$, but what about LLS?

When all fibers are intact the effective thresholds are identical to the original thresholds in equation (4). The first fiber to break with LLS is the one with threshold $t = 0.1$, which happens at $\sigma = 0.1\kappa$. If we let $\times$ represent a broken fiber, then the effective thresholds after breaking the first fiber are

$$\frac{2}{3} \quad \times \quad \frac{2}{15} \quad 0.9 \quad 0.8 \quad 0.3 \quad 0.7 \quad 0.5 \quad 0.6 \quad 0.4.$$

The broken fiber constitutes a hole of size $h = 1$, with $p = 2$ fibers in its perimeter. These two fibers are the only ones whose effective thresholds change when the first fiber breaks. From equation (3) we see that their new effective thresholds are their original thresholds divided by $1 + 1/2$.

The effectively weakest fiber now breaks at $\sigma = 2\kappa/15$, and the effective thresholds afterward are

$$0.5 \quad \times \quad \times \quad 0.45 \quad 0.8 \quad 0.3 \quad 0.7 \quad 0.5 \quad 0.6 \quad 0.4,$$

since there is a single hole with $h = p = 2$. The third fiber breaks at $\sigma = 0.3\kappa = \sigma_{c,\text{ELS}}$, which results in the effective thresholds

$$0.5 \quad \times \quad \times \quad 0.45 \quad \frac{8}{15} \quad \times \quad \frac{7}{15} \quad 0.5 \quad 0.6 \quad 0.4.$$

The smallest effective threshold is 0.4, and once this fiber breaks, the fiber bundle collapses. Hence the critical strength is $\sigma_{c,\text{LLS}} = 0.4\kappa > \sigma_{c,\text{ELS}}$.

With ELS, 0.3κ is the critical strength because the fibers with thresholds 0.4 and 0.5 receive some of the redistributed load from the broken fibers. They break at $\sigma = 0.28\kappa$ and $\sigma = 0.3\kappa$, respectively.

With LLS, the four strongest fibers happen to neighbor the three broken ones and receive all redistributed load. In this sense, the other three intact fibers (the three rightmost ones) are *shielded* from this additional load, and their effective thresholds are unchanged from the fully intact fiber bundle. In our example the result is an increased critical strength and critical damage compared to ELS, because the four strong fibers that receive additional loads don't have their effective thresholds lowered below 0.3.

But this example is contrived. A large system ($N \rightarrow \infty$) *will* contain strong configurations like the one in our example, but it will also contain weak configurations with many adjacent fibers that all have small thresholds. In 1D, a hole can never have a larger perimeter than $p = 2$. Therefore a sufficiently large hole (that originates at a particularly weak configuration) will reduce the effective thresholds of its neighboring fibers enough that they also break, inducing a fatal rupture that opens the fiber bundle like a ziplock. Strong configurations, where shielding is important, are ripped open by this expanding hole.

The result is that in 1D, as $N \rightarrow \infty$, the critical damage of LLS goes to zero and the critical strength goes to the lower limit of the threshold distribution [3]. Both of which are much smaller than their corresponding ELS values.

Still, our example highlights an interesting effect: with localized force distribution, strong fibers can shield weaker ones from some of the applied load. The question of interest is whether there is a noticeable shielding effect in the LLS model on lattices in $D > 1$, and, if so, with what consequences?

IV.   EVIDENCE OF SHIELDING

Let w be the intact fiber with the smallest threshold, i.e., the weakest intact fiber. We then study be the probability p_w that w is the first fiber to break when the applied load σ is increased.

With ELS we get $p_w = 1$, since all intact fibers share the same load. With LLS this is not the case, because the fiber with the smallest *effective* threshold breaks. Equation (3) shows that a small effective threshold results from a combination of small threshold and large force redistribution.

Figure 2 shows p_w as a function of the damage d for the LLS model with $P(t) = t$ on a square lattice for different system sizes N. Throughout most of the fracture process p_w is small, i.e., it is unlikely that w will break at any given step. This indicates that load redistribution dominates the effective thresholds, and that at least some of the fibers with small thresholds are partially shielded from the applied load.

There are significant finite size effects for p_w in Figure 2. Finite size scaling indicates that in the thermodynamic limit $N \rightarrow \infty$, there is a sharp transition from $p_w = 0$ to $p_w = 1$ around $d \approx 0.98$. When all intact fibers neighbor a single hole, then $p_w = 1$, and the damage at which the transition happens should therefore be expected to change with the lattice.

To study shielding further we define a *load sharing factor* σ/f_i, the ratio between the applied load σ and the force f_i acting on fiber i. For ELS the force $f_{i,\text{ELS}}$ is iden-
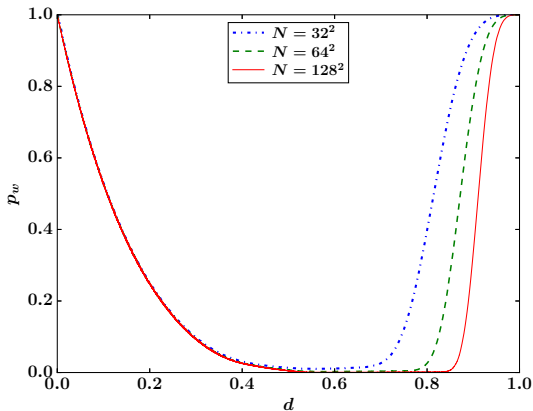
FIG. 2. Probability p_w to break the intact fiber with the smallest threshold in LLS simulations on a square lattice. The threshold distribution is uniform: $P(t) = t$. The number of samples is 8×10^5, 2×10^5, and 10^5 for system sizes $N = 32^2$, 64^2, and 128^2, respectively.
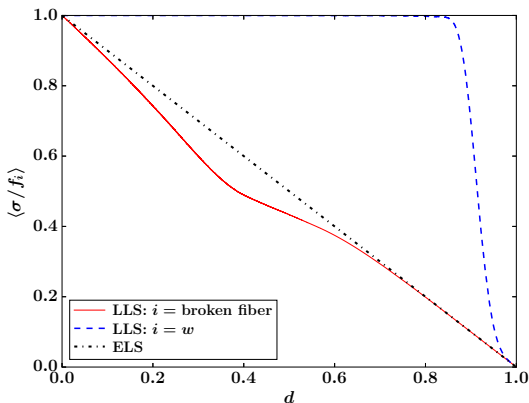

FIG. 3. Sample averaged load sharing factor $\langle \sigma/f_i \rangle$ for LLS with $i = w$ and i being the broken fiber, and for ELS (equation (5)). The threshold distribution is uniform ($P(t) = t$) and the LLS results are from simulations on a square lattice ($N = 128^2$) averaged over 10^5 samples.

tical for all intact fibers, and there is an exact expression

$$\frac{\sigma}{f_{i,\text{ELS}}} = 1 - d \qquad (5)$$

in the limit $N \to \infty$. For LLS the load sharing factor depends on which fibers we follow through the breaking process.

Figure 3 contrasts the load sharing factor for ELS and LLS. The broken fibers in the LLS model are on average

more loaded than in the ELS model, which is expected; highly loaded fibers are more likely to break since their effective thresholds are reduced significantly from the original thresholds.

It is more interesting that w, the intact fiber with the smallest threshold, on average recieves almost no extra load from redistribution throughout most of the breaking process. In particular, the average fraction of the load it receives is much smaller than fibers in the ELS model. While one cannot in general trust averages in the LLS model blindly [5], this does indicate that these weak fibers are shielded from some of the applied load, and that fibers with higher thresholds (but smaller effective thresholds due to being highly loaded) break instead of them.

That the average load sharing factor of the fiber w decreases rapidly from 1 (Figure 3) around the same damage that p_w increases quickly (Figure 2) is not a coincidence. When the intact fiber with the smallest threshold becomes more highly loaded, it is very likely to have the smallest effective threshold, and hence the probability that it breaks increases. The finite size effects of the load sharing factor in Figure 3 for w therefore mirror the ones for p_w in Figure 2.

V. EFFECTS OF SHIELDING

Since the shielding effect protects the weakest intact fibers, we intuitively expect that LLS will have more intact weak fibers than ELS. To investigate this hypothesis, Figure 4 shows the cumulative probability distribution $P(t_{\text{intact}})$ of fiber thresholds of intact fibers for a single sample with $N = 1024^2$ fibers. The thresholds were drawn from a uniform distribution $P(t) = t$.

With a damage of $d = 0.2$, there are some intact fibers in LLS that have smaller threshold than the intact fibers in ELS, but the difference between the two load sharing rules is not large. This is because the LLS model behaves similarly to ELS in the early stages of the breaking process. The disorder of the threshold distribution dominates. Hence fibers fail because they have small thresholds, rather than because they are highly loaded [12]. In this regime there is little room for the shielding, which is an effect of the LLS rule, to affect the fiber bundle significantly.

This changes when the damage increases, as Figure 2 shows. When $k/N = 0.5$, slightly below the critical damage of the sample for both LLS and ELS, there is a significant difference between the threshold distributions of intact fibers for the two load sharing rules. With LLS, the weakest intact fibers have thresholds $t < 0.25$, while with ELS the lower limit for thresholds is $t = 0.5$. Approximately 8.2% of intact fibers in LLS have thresholds smaller than the lower limit for ELS. Thus the shielding effect that emerges from LLS protects some fibers with small thresholds, which survive longer than they would have with ELS.
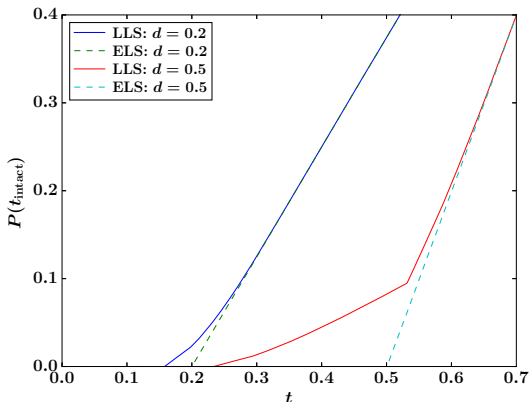
FIG. 4. Cumulative distribution $P(t_{\text{intact}})$ of fiber thresholds of intact fibers at two different damages d for a single sample ($N = 1024^2$). LLS results are from a simulation on a square lattice, ELS results are calculated using the same thresholds as in the LLS simulation. The threshold distribution of all fibers is uniform: $P(t) = t$.

FIG. 5. Cumulative distribution of critical damage $P(d_c)$ for LLS on a square lattice. The number of samples is 8×10^5, 2×10^5, 10^5, and 3×10^4 for system sizes $N = 32^2$, 64^2, 128^2, and 256^2, respectively. The threshold distribution is uniform: $P(t) = t$.

FIG. 6. Cumulative distribution of critical strength $P(\sigma_c)$ for LLS on a square lattice. The number of samples is 8×10^5, 2×10^5, 10^5, and 3×10^4 for system sizes $N = 32^2$, 64^2, 128^2, and 256^2, respectively. The threshold distribution is uniform: $P(t) = t$.

Note that only a small fraction of the weak fibers are shielded by this effect. Out of the $523,690$ fibers with thresholds smaller than 0.5 in the analyzed sample, only approximately 8.2% are intact at damage $d = 0.5$.

Another effect of shielding is an increase in the critical damage d_c, the fraction of fibers broken when the fiber bundle collapses, compared to ELS. For a uniform threshold distribution $P(t) = t$, ELS has $d_c = 1/2$. Figure 5 shows the cumulative probability distribution of d_c for LLS on a square lattice, also for a uniform threshold distribution. As $N \to \infty$, the critical damage converges to a value that is roughly 5% larger than the ELS value.

This means that shielding has the surprising effect of making LLS *more stable* than ELS. An LLS fiber bundle reaches catastrophic failure at a higher damage than a corresponding ELS fiber bundle, and there is a region with d slightly larger than $1/2$ where ELS is unstable (it has passed the greatest force it can sustain before breaking), while LLS is not (it has yet to reach this point).

However, this increased stability comes at the cost of a reduced critical strength σ_c. ELS has $\sigma_c = 1/4$ for $P(t) = t$, and Figure 6 shows the corresponding values for LLS on a square lattice. As $N \to \infty$ the LLS critical strength converges toward $\sigma_c \approx 0.233$, approximately 7% smaller than the ELS value.

So far we have investigated LLS on a square lattice only, but effects of the proposed shielding mechanism should be present in all other lattices (except for 1D, as explained earlier). Nothing about the proposed shielding effect is specific to the square lattice, but we should expect that the effects become smaller as the connectivity of the lattice increases; it is less likely that a weak
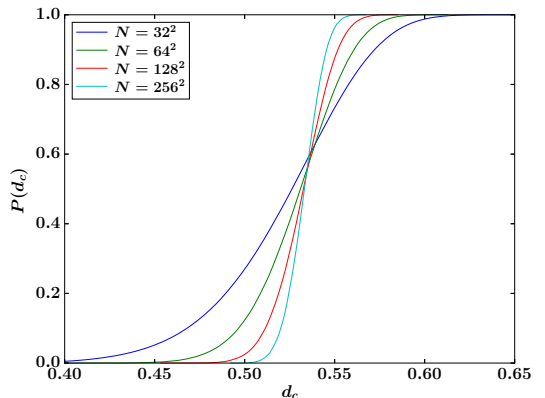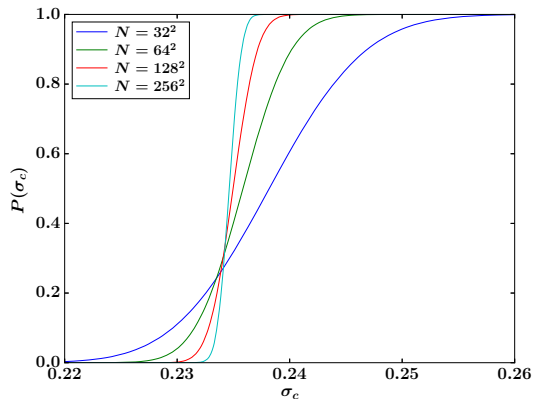
fiber is surrounded (and hence shielded) by strong fibers in a higher-dimensional lattice or a lattice with higher connectivity. To test this hypothesis, Figure 7 shows the distribution of critical damage for LLS on four different lattices.

As expected, the critical damage is highest for the square lattice, because the shielding effect is the most pronounced there. The square lattice has the lowest connectivity and dimension of the four lattices that is tested
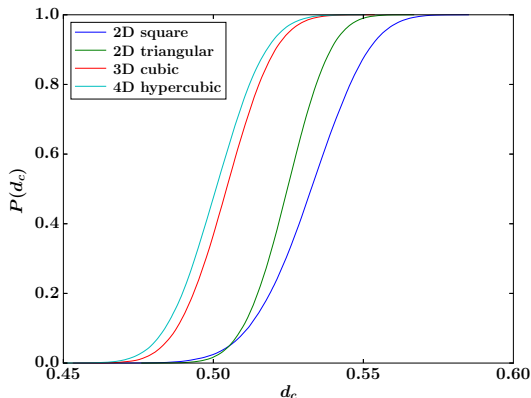
FIG. 7. Cumulative distribution of critical damage $P(d_c)$ for LLS on four lattices with similar number of fibers: square ($N = 128^2$), triangular ($N = 128^2$), cubic ($N = 25^3$), and 4D hypercubic ($N = 11^4$), all simulated with 10^5 samples. The threshold distribution is uniform: $P(t) = t$.
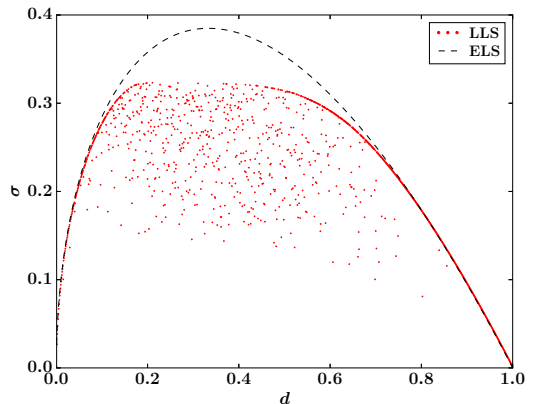

FIG. 8. Stress σ vs. damage d in the ELS model and the LLS model on a square lattice. The ELS curve has been calculated analytically via equation (1), and the LLS result is a simulation of a single sample ($N = 1024^2$). For clarity, the LLS result shows only every 800th data point. The threshold distribution is $P(t) = t^2$ for both models.

here.

The triangular lattice has a smaller critical damage, but still significantly greater than ELS. This is consistent with a somewhat less pronounced shielding effect, which is expected for a lattice that is also two-dimensional, but with higher connectivity than the square lattice.

The cubic and 4D hypercubic lattices have much smaller critical damages than the two-dimensional lattices, and are comparable to ELS. This is consistent with the proposed shielding effect, which should become much weaker as the dimension increases; there are many more possible paths for a hole to gain access to the inside of a shielded region in higher dimensions, and shielding is therefore much rarer.

VI. WHEN IS SHIELDING RELEVANT?

Early in the breaking process the LLS model behaves ELS-like, as corroborated by Figures 1, 2, 3, and 4. The disorder of the threshold distribution dominates the process, i.e., the effective thresholds from equation (3) are dominated by the original thresholds in the numerator, not the hole structure in the denominator. What happens when the fiber bundle has a critical damage in this disorder-dominated regime? If the increased critical damage of LLS compared to ELS for the uniform distribution is indeed an effect of shielding, one would expect that for threshold distributions where the critical damage d_c is in the disorder-dominated regime, LLS has a smaller critical damage than ELS due to the local stress enhancement.

To demonstrate this, we choose the threshold distribu-

tion $P(t) = t^2$. The ELS model then has a critical damage $d_c = 1/3$, close to the disorder-dominated regime. What about the LLS model? Figure 8 compares the stress σ vs. damage d for the ELS model and the LLS model on a square lattice. As in Figure 1 for the uniform distribution, the LLS model has a smaller critical strength σ_c than the ELS model, but in this case the critical damage d_c also seems to be smaller, approximately $d_c \approx 0.2$.

To determine the critical damage of the LLS model more accurately we plot its cumulative probability distribution for different system sizes in Figure 9, like we did in Figure 5 for the uniform distribution. It indicates that, in the limit $N \to \infty$, the critical damage is $d_c < 0.2$, i.e., much smaller than for the ELS model.

This is consistent with the expanation that the shielding effect is responsible for the increased critical damage of the LLS model for the uniform threshold distribution. When catastrophic failure occurs early in the breaking process, i.e., in the disorder-dominated regime, the shielding effect hardly influences the fiber bundle in the stable phase; shielding is stronger the more the hole structure of the fiber bundle dominates the effective thresholds, and it is therefore weak in the disorder-dominated regime, as corroborated by the results for $d = 0.2$ in Figure 4. Hence, for this kind of threshold distribution, the local stress enhancement of LLS leads to decreases in both critical strength σ_c and critical damage d_c compared to the ELS model, since shielding is not relevant in the stable phase. However, if catastrophic failure occurs late enough for the shielding effect to be relevant in the stable phase — exactly what damages count as
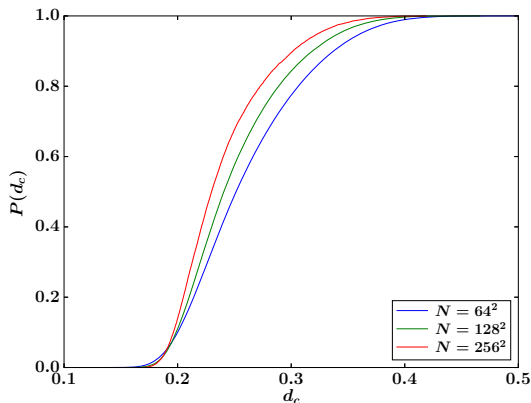
FIG. 9. Cumulative distribution of critical damage $P(d_c)$ for LLS on a square lattice. The number of samples is 10^6, 1.5×10^5, and 1.5×10^4 for system sizes $N = 64^2$, 128^2, and 256^2, respectively. The threshold distribution is $P(t) = t^2$.
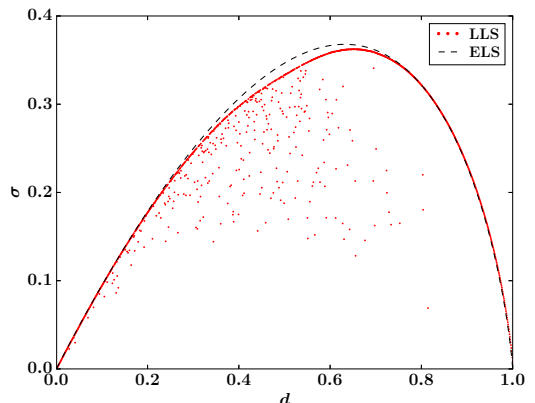

FIG. 10. Stress σ vs. damage d in the ELS model and the LLS model on a square lattice. The ELS curve has been calculated analytically via equation (1), and the LLS result is a simulation of a single sample ($N = 1024^2$). For clarity, the LLS result shows only every 800th data point. The threshold distribution is $P(t) = 1 - e^{-t}$ for both models.

"late enough" will depend on the lattice — then it leads to the LLS model having a higher critical damage than the ELS model.

An example of a threshold distribution where the shielding effect is relevant is the Weibull distribution $P(t) = 1 - e^{-t}$. Figure 10 shows the stress σ vs. the damage d for this threshold distribution with LLS on a square lattice and ELS. For the ELS model, $d_c = 1 - e^{-1} \approx 0.632$, which is smaller than the critical damage for the LLS model, as evidenced by the cumulative distributions of the critical damage in Figure 11.

VII. DISCUSSION

We have shown that the LLS fiber bundle model contains a shielding effect where some of the fibers with the smallest thresholds (i.e., the weakest fibers) among the intact fibers are shielded from some of the applied load, compared to ELS. Increased connectivity and dimension of the lattice makes shielding less probable, and hence the effects decrease as the dimension or connectivity increases. The exception to this behavior is that the effect is not noticeable in 1D, where LLS has zero critical damage and strength. It is not clear if the shielding effect is important for applications where a three-dimensional model is appropriate. But for cases where a two-dimensional model is correct, the shielding effect can be expected to give important contributions to the behavior of the fracture process.

Shielding has two major effects. The first is that two-dimensional LLS models can be more stable than corresponding ELS models, in the sense that catastrophic failure occurs at a higher damage. This is, however, ac-
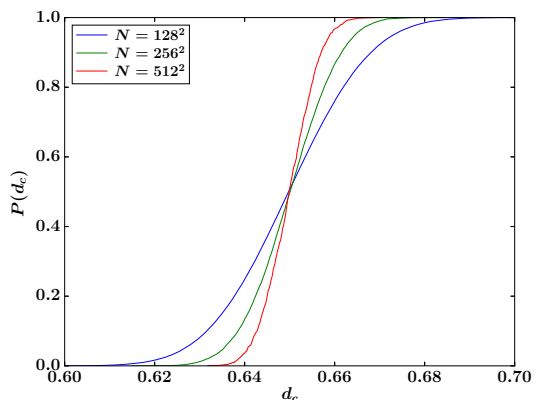

FIG. 11. Cumulative distribution of critical damage $P(d_c)$ for LLS on a square lattice. The number of samples is 1.5×10^5, 1.5×10^4, and 1.5×10^3 for system sizes $N = 128^2$, 256^2, and 512^2, respectively. The threshold distribution is $P(t) = 1 - e^{-t}$.

companied by a reduced critical strength. In total, LLS can, surprisingly, be preferable to ELS in two dimensions when stability is more important than strength for the application in question.

The second effect is that weak fibers are better protected and survive longer in LLS than in ELS. This is in some ways similar to how cars are built to protect the people inside at the expense of the sturdiness of the car

itself. Potential applications where it is more important to have weak fibers survive than that the strength of the entire fiber bundle is high will be better off using LLS instead of ELS.

We have mainly studied the uniform threshold distribution $P(t) = t$, but also shown that shielding is an important effect for other threshold distributions — like the Weibull distribution $P(t) = 1 - \mathrm{e}^{-t}$ — where catastrophic failure occurs after the initial disorder-dominated regime. However, if failure does occur in the disorder-dominated regime, before the shielding effect is strong enough, shielding will not give significant contributions to the behavior in the stable phase of the fracture process. We therefore expect that the shielding effect is universal in the sense that for the class of threshold distributions where catastrophic failure happens sufficiently late, the shielding effect will give significant contributions to the behavior in the stable phase, including an increased crit-

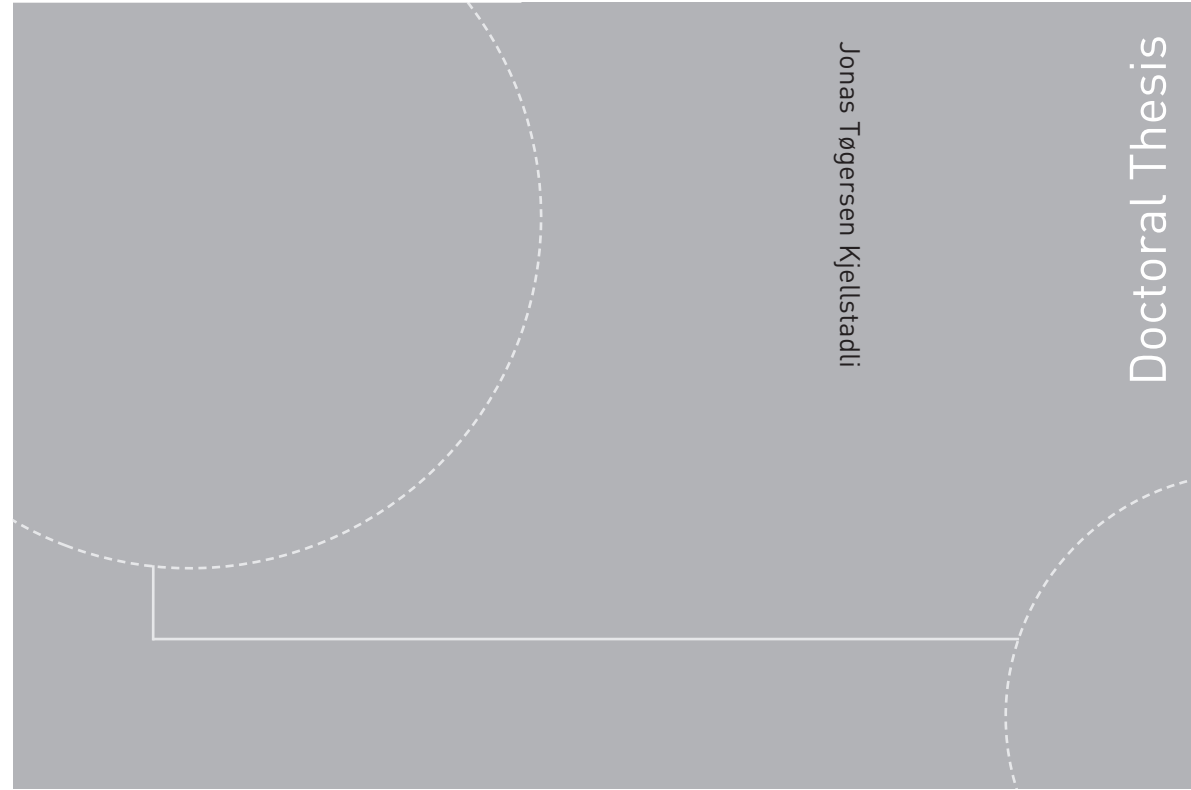ical damage when compared with ELS.

What happens in more realistic scenarios with intermediate interaction ranges, like in e.g. the γ-model [13] or soft clamp model [14], is still an open question. One could speculate that such models should be somewhere between the ELS and LLS models, and that they might contain a weaker shielding effect than in the LLS model, but a thorough analysis would be required to give definite answers.

[1] Roux S, Hansen A. Early stages of rupture of disordered materials. *EPL*. (1990) **11**:37–42. doi: 10.1209/0295-5075/11/1/007

[2] Pradhan S, Hansen A, Chakrabarti BK. Failure processes in elastic fiber bundles. *Rev Mod Phys*. (2010) **82**:499–555. doi: 10.1103/RevModPhys.82.499

[3] Hansen A, Hemmer PC, Pradhan S. *The Fiber Bundle Model*. Berlin: Wiley-VCH (2015).

[4] Bering E. *On the stability of the local load sharing fiber bundle model* (Masters thesis). Norwegian University of Science and Technology, Trondeim (2016).

[5] Kjellstadli JT, Bering E, Hendrick M, Pradhan S, Hansen A. Can local stress enhancement induce stability in fracture processes? Part I: apparent stability. *Front Phys*. (2019) **7**:105. doi: 10.3389/fphy.2019.00105

[6] Peirce FT. 32—X.—Tensile tests for cotton yarns v.—"The Weakest Link" Theorems on the strength of long and of composite specimens. *J Text Inst*. (1926) **17**:T355–68. doi: 10.1080/19447027.1926.10599953

[7] Daniels HE. The statistical theory of the strength of bundles of threads. I. *Proc Roy Soc A*. (1945) **183**:405–35. doi: 10.1098/rspa.1945.0011

[8] Gumbel EJ. *Statistics of Extremes*. Mineola: Dover (2004).

[9] Harlow DG, Phoenix SL. The chain-of-bundles probability model for the strength of fibrous materials I: analysis and conjectures. *J Comp Mater*. (1978) **12**:195–214. doi: 10.1177/002199837801200207

[10] Kun F, Zapperi S, Herrmann HJ. Damage in fiber bundle models. *EJPB*. (2000) **17**:269–79. doi: 10.1007/PL00011084

[11] Danku Z, Ódor G, Kun F. Avalanche dynamics in higher-dimensional fiber bundle models. *Phys Rev E*. (2018) **98**:042126. doi: 10.1103/PhysRevE.98.042126

[12] Sinha S, Kjellstadli JT, Hansen A. Local load-sharing fiber bundle model in higher dimensions. *Phys Rev E*. (2015) **92**:020401. doi: 10.1103/PhysRevE.92.020401

[13] Hidalgo RC, Moreno Y, Kun F, Herrmann HJ. Fracture model with variable range of interaction. *Phys Rev E*. (2002) **65**:046148. doi: 10.1103/PhysRevE.65.046148

[14] Batrouni GG, Hansen A, Schmittbuhl J. Heterogeneous interfacial failure between two elastic blocks. *Phys Rev E*. (2002) **65**:036126. doi: 10.1103/PhysRevE.65.036126

Jonas Tøgersen Kjellstadli

Local versus Equal Load Sharing in the Fiber Bundle Model

Jonas Tøgersen Kjellstadli

Doctoral Thesis

NTNU
Norwegian University of
Science and Technology
Faculty of Natural Sciences
Department of Physics

NTNU
Norwegian University of
Science and Technology

NTNU

NTNU
Norwegian University of
Science and Technology